PROPOSAL FOR A HIGH-ENERGY NEUTRINO EXPERIMENT

IN THE NAL 30 m^3 H$_2$, D$_2$ BUBBLE CHAMBER

University of Hawaii (R. Cence, F. Harris, M. Peters, V. Peterson,
D. Yount)

Northwestern University (S. Meyer)

University of California, Lawrence Radiation Laboratory (M. Alston-Garnjost, R. Birge, G. Goldhaber, J. Kadyk, S. Parker, M.L. Stevenson, G. Trilling)

ABSTRACT

We propose to study high-energy neutrino interactions in the NAL 30 m^3 bubble chamber. A slight alteration of the chamber design will allow a large-solid-angle quantameter to be placed just outside the thin (1/2 inch steel) wall of the bubble chamber. A detector, designed to identify the muon of the interaction is placed outside the vacuum tank. With this hybrid system we can reconstruct the neutrino's energy, the lepton momentum transfer squared, Q^2, the lepton energy transfer ($\nu = E-E'$), and measure many features of the final hadron state. This sytem detects with high efficiency over the entire range of variables and is well suited to making a detailed general survey of neutrino interactions in the neutrino energy range 15 to 80 GeV. A million-picture exposure would yield tens of thousands of neutrino interactions with circulating protons at 200 GeV. A similar number of events should be obtained with protons at 500 GeV. Table I summarizes the preliminary cost estimates.

PROPOSAL FOR A HIGH-ENERGY NEUTRINO EXPERIMENT
IN THE NAL 30 m^3 H$_2$, D$_2$ BUBBLE CHAMBER

University of Hawaii, Northwestern University,

Lawrence Radiation Laboratory

I.   INTRODUCTION

II. HIGH-ENERGY NEUTRINO INTERACTIONS

A. Kinematics

B. Dynamics

   1. Differential Cross Section

   2. "Spin-$\frac{1}{2}$-Parton" Model

   3. Pomeranchukon - Exchange Model
   4. Fireball Model (upper limit for hadron multiplicity)

C. Event Rate

D. Measurement of $\dfrac{d\,N_{\nu,\bar{\nu}}}{d\,E_{\nu,\bar{\nu}}}$

   1. Neutrino Energy Spectrum

   2. Measurement of Meson Production by Protons

   3. Meson Focusing System

   4. Neutrino Flux Monitor

E. Measurement of the Neutrino Energy

   1. Curvature and Total Energy of Charged Hadrons

   2. Total Energy of π^0's via Proportional Calorimeter

   3. Total Energy of Hadrons via Proportional Calorimeter

   4. Lepton Total Energy

F. Measurement of Structure of Hadronic State

G. Hadronic Decay Modes of the Intermediate Vector Boson (if it

   exists)

III. EXPERIMENTAL EQUIPMENT

A. Neutrino Beam

   1. Targets

I. INTRODUCTION

We propose an experimental program for studying the interactions
of neutrinos on hydrogen and deuterium for neutrino energies above
15 GeV. This program includes measurements of:

a. the total cross section to see if it saturates or remains linear
   in neutrino energy,

b. distributions in the deep-inelastic region to test scale invariance
   and various models such as Pomeron exchange and the parton hypothesis,

c. the elastic differential cross section to learn more about nucleon
   form factors,

d. interactions involving W mesons, if they exist.

A detector similar to the 14-foot BNL bubble chamber, suitably altered
to detect π^0's neutrons, and muons electronically, seems ideal for
neutrino energies up to 80 GeV.

The proposal parallels experiments on elastic and "deep-inelastic"
electron scattering: the neutrino provides an independent probe of
nuclear structure with, we believe, comparable sensitivity to the
electron, while the bubble-chamber technique makes possible a detailed
analysis of the final-state hadrons.

In the case of neutrinos, only the direction of the incident lepton
is known, and it is necessary to determine its energy E. This can be
done by measuring the energies of all final π^0's, charged hadrons,
neutrons, and leptons (muons). Provided we identify which of the
final particles is the outgoing lepton (energy E'), we can make the
same analysis as in deep-inelastic electron scattering. The total
and the "elastic scattering" cross sections will also be measured.

Bubble-chamber detection of neutrino events provides precise information on the location of the interaction vertex as well as the momenta of all charged outgoing particles. Photons from π^O's are detected with essentially 100 $^O/_O$ efficiency by a proportional quantameter (lead plates with wire coordinate planes in the gas gaps), and spatial information as well as the total electromagnetic energy is obtained. A proportional hadrometer (copper or concrete plates with wire coordinate planes in the gas gaps) determines the energy in nuclear cascades and traces individual hadron tracks. Neutrons are also detected in the hadrometer, while muons are identified when they penetrate this hadron absorber. Backgrounds are suppressed by the time resolution of the trigger logic, by the energy discrimination of the quantameter and hadrometer, and by detailed track analysis in the bubble chamber, quantameter, and hadrometer.

There are several major advantages of the hybrid system consisting of the bubble chamber and electronic detectors. First, the bubble chamber permits an accurate (to $\pm$ 3 $^O/_O$) determination of the charged-hadron and lepton energies through track curvature, while the quantameter determines the total electromagnetic energy to about the same precision. The energy appearing in the form of neutrons is detected with the hadrometer to somewhat less accuracy, but this component is normally a small fraction of the total. Detailed vertex information is a second advantage, as already mentioned. Third, the angular acceptance is large, and a wide range of lepton-momentum and lepton-energy transfers is sampled with good efficiency. Finally, since the muon energy is determined in the bubble chamber, the thickness of the muon detector

is much less than the muon range.

In Section II we discuss some of the measurements that might be made in the neutrino energy range from 15 to 80 GeV. We use these considerations as the basis for designing detectors. Section II also contains specifications required for the neutrino beam and a summary of the components of the neutrino facility that participants in this proposal could help to develop. Technical design considerations are discussed in Section III. Finally, in Section IV we suggest a possible schedule for obtaining one million events during both 200-GeV and 500-GeV phases of the accelerator operation.

II. HIGH-ENERGY NEUTRINO INTERACTIONS

A. Kinematics of ν + N → lepton + hadrons

We adopt the notation of Bjorken and Paschos.[1] Fig. 1 then summarizes much of the kinematics where Q^2 is the square of the momentum transfer to the leptons, and ν is the difference in initial and final lepton energies. The solid parallel lines are the loci of equal invariant hadron mass W, given in terms of the nucleon mass M by the following equations:

$$Q^2 = 2M + M^2 - W^2, \tag{1}$$

$$= E - E', \tag{2}$$

$$\gamma_W = (E_H = M + \nu)/W, \tag{3}$$

$$\sin^2 \frac{\theta}{2} = \frac{Q^2}{4EE'}, \tag{4}$$

$$\sin^2 \theta_H = \left[\frac{E'}{E} \frac{\cos^2 \frac{\theta}{2}}{1 + \frac{\nu}{Q^2} 2} \right]^{\frac{1}{2}}, \tag{5}$$

where θ and θ_H are the laboratory angles of the final lepton and hadron systems, E is the neutrino energy and E' the final lepton energy.

The loci of equal values of γ_W, the Lorentz-contraction factor, are indicated by the dashed parabolic curves in Fig. 1. The straight lines radiating from the point ($Q^2=0$, $\nu = 50$ GeV) are loci of equal lepton angles for E=50 GeV. Fig. 2 is the corresponding graph for E=20 GeV.

If all the final hadrons are in thermal equilibrium, we can estimate the pion multiplicity $<n\pi>$, which depends only on W. The opening angle for the hadron jet is of order γ_W^{-1}. The rising parallel lines in Figs. 1 and 2 correspond to different values of $<n\pi>$. We believe this model provides an upper limit to the multiplicity and serves to emphasize the scope of the experimental task in detecting neutral pions.

B. Dynamics

1. Differential Cross Section

The differential cross section for the interaction of neutrinos on hadrons can be written in terms of the quantities just defined as

$$\frac{d^2\sigma}{dQ^2 d\nu} = \frac{G^2}{2\pi} \frac{E'}{E} \beta \left\{ 1 - \frac{Q^2}{4EE'} + \frac{\nu^2 + Q^2}{2\,EE'} \left[(R) + (L) \right] + \frac{E + E'}{2\,EE'} \sqrt{\nu^2 + q^2} \left[(L) - (R) \right] \right\} \tag{6}$$

where

$$\beta = W_2 = \frac{1}{2\pi} \frac{Q^2}{\nu} \frac{1}{(1 + \frac{Q^2}{\nu^2})} (1 - \frac{Q^2}{2M\nu})(2\sigma_S + \sigma_R + \sigma_L) \tag{7}$$

$$(R) \equiv \frac{\sigma_R}{2\sigma_S + \sigma_R + \sigma_L} , \qquad (L) \equiv \frac{\sigma_L}{2\sigma_S + \sigma_R + \sigma_L} \tag{8}$$

where σ_R, σ_L and σ_S are cross sections for the appropriate helicity states.

For $Q^2 << \nu^2$, Eq. (6) becomes

$$\frac{d^2\sigma}{dQ^2\,d\nu} = \frac{G^2}{2\pi}\,\frac{E'}{E}\,\beta\left[1 + \frac{\nu}{E'}\,(L) - \frac{\nu}{E}\,(R)\right] \qquad (9)$$

or

$$\frac{d^2\sigma}{dx\,dy} = \frac{G^2\,M\,E}{\pi}\nu\beta\left[(1-y) + \frac{y^2}{2}\,((R)+(L)) + y\left(1-\frac{y}{2}\right)\{(L)-(R)\}\right] (10)$$

where

$$\beta = \frac{Q^2}{2\pi}\,(1-x)\,(2\sigma_S + \sigma_R + \sigma_L) \qquad (11)$$

and

$$x \equiv \frac{Q^2}{2M\nu} \quad , \quad y \equiv \frac{\nu}{E} , \qquad (12)$$

$$0 \le x \le 1, \; 0 \le y \le 1 .$$

Some motivation for the use of the variable x can be seen if one supposes that the neutrino might scatter off only a fraction, x, of the nucleon. The kinematics of quasi-elastic scattering is obtained by replacing M by xM. It would be represented in Fig. 1 by a radial line from the origin with a slope x times that of the one for $Q^2 = 2M\nu$. Bjorken has shown that at high incident energies if the parts are point-like the σ_R, σ_L, and σ_S are functions of x only (scale invariance). Consequently, when one integrates equation (10) over x and y one obtains $\sigma = $ (constant) E, a relation that we can test experimentally provided we detect all final states.

2. "Spin-$\frac{1}{2}$-Parton" Model

To obtain a feeling for where events would lie in the $Q^2 - vs - \nu$ plane for the "spin-$\frac{1}{2}$-parton" model, we have set $\nu\beta = $ (constant) $\cdot$ (1-x) and $\sigma_R = \sigma_S = 0$. Fig. 3 shows how 1000 50-GeV neutrino interactions would be distributed under these assumptions. The important point is that all sectors contain statistically significant populations.

3. Pomeranchukon-Exchange Model

Predictions for the Pomeranchukon-exchange model can be obtained by setting $\nu\beta$ = (constant) $(1-X)$ and $\sigma_L = \sigma_R$, $\sigma_S = 0$. The distribution of 1000 events at 50 GeV for these assumptions are shown in Fig. 4.

We propose to make our detection efficiency high in all sectors of the Q^2 -vs-ν plot and consequently, to be able to measure the total cross section.

4. Fireball Model

We introduce the notion of the hadron system being in thermal equilibrium to obtain a crude idea as to what the pion multiplicity might be and how this fireball will emit its products in the lab system. It can be shown that half of the products will be emitted into a cone of half angle,

$$\theta_{cone} \approx \gamma_W^{-1} \approx \sqrt{\left(\frac{2M}{E}\right)\frac{(1-X)}{y}} \quad . \tag{13}$$

The laboratory angle for the final lepton is

$$\theta_\mu \approx \sqrt{\left(\frac{2M}{E}\right)\frac{Xy}{(1-y)}} \tag{14}$$

and for the laboratory direction of the hadron system is,

$$\theta_H \quad \sqrt{\left(\frac{2M}{E}\right)\frac{X}{y}(1-y)} \quad . \tag{15}$$

In order to summarize the production and decay processes, we distort the triangular sectors of Fig. 5 ab into rectangular ones. Within the rectangular sectors we draw pictures of how the events might look. The kinematics of the outgoing hadron system and final lepton are shown for some of the sectorS. Most hadrons will be obtained within the shaded cones; the vector is the outgoing lepton momentum. Fig. 5b summarizes the corresponding information at E=20 GeV. The hadron

ꞌc ones are constructed with pessimistic (it predicts too many π^0's with cone angles too large) assumptions, namely, those of a fireball model for the hadron system. The Pomeranchukon-exchange model would predict cones with smaller opening angles and smaller meson multiplicity.

Bjorken and Paschos[1] point out that the difference, $\sigma_\nu - \sigma_{\bar\nu}$, is very model dependent. We wish to expose the chamber to both ν and $\bar\nu$.

C. Event Rate

In estimating the event rate, we assume the radial distribution for the neutrino beam at the detector obtained from the spectra of D. Carey, et al.[2], (reproduced here as Fig. 6c). We then integrate Eq. (10) over X and y, assuming σ_R, σ_L, and σ_S are functions only of X. The resulting total cross section is proportional to the neutrino energy E. The event rates are calculated for two assumptions: a.) the linear relation, $\sigma = 0.8$ E GeV $\times 10^{-38}$ cm^2, holds for all energies; and b.) the cross section saturates at E = 10 GeV and remains constant at 8×10^{-38} cm^2, for higher energies.

The lower set of curves in Fig. 6a indicates the number of neutrino interactions per GeV per 10^6 beam pulses (at 2×10^{13} protons/pulse) per 10^{-38} cm^2. The upper set of curves in Fig. 6a is for assumption a, $\sigma = 0.8$ E (GeV) $\times 10^{-38}$ cm^2, while curves for assumption b with a saturated cross section at 8×10^{-38} cm^2 are shown in Fig. 6b. Also shown in Figs. 6a, b are histograms for the number of interactions per 10^6 pulses that lie within 1 meter of the beam axis. Because there is so much uncertainty about K$^-$ yields and hence $\bar\nu$

flux, we show no corresponding curves for antineutrinos.

D. Measurement of $\dfrac{d\ N\nu,\bar{\nu}}{d\ E\nu,\bar{\nu}}$

    1. Neutrino Energy Spectrum

In determining cross sections, one must first find the energy spectrum of the incident neutrinos. This spectrum, normalized with the data obtained from the neutrino flux monitor, gives the number of neutrinos incident in each energy interval during the course of the experiment. Neutrino events occurring in the bubble chamber can then be assigned to the appropriate intervals once the total energy of the final-state particles has been measured.

    2. Measurement of Meson Production by Protons

As part of an initial beam survey, measurements should be made of meson production by protons of 200 GeV from targets of H_2, D_2, Li, Be, and Al. Data are needed for pion momenta above 20 GeV/c and laboratory angles between zero and 20 milliradians. Similar studies should be carried out at 500 GeV as soon as protons of this energy become available.

We feel that our understanding of the production mechanism would be significantly enhanced if a bubble chamber of modest size were exposed to primary protons at 200 and 500 GeV. Attention would be focused on low-energy charged kaons and pions corresponding to the backward jet in the center-of-mass system. We therefore endorse, and some of us would like to participate in, the bubble-chamber survey proposed by G. Snow.[3] We suggest that NAL investigate the possibility of making the bending magnets of area 2 capable of bending 500 GeV protons. Exposure of only 10 to 20 protons per pulse are needed.

The quadrupoles could remain at their 200 GeV values.

3. Meson-Focusing System

The meson-focusing device should maximize the neutrino flux at 35 GeV with incident protons of 200 GeV. To reduce systematic errors in the cross sections resulting from uncertainties in the neutrino energy and thus the neutrino flux, the meson-focusing device should simultaneously minimize the logarithmic derivative, $\left| d \ln \frac{d N_\nu}{d E_\nu} \middle/ d \ln E_\nu \right|$. This can be accomplished by eliminating those mesons that produce low-energy neutrinos ($E < 16$ GeV) and by focusing those mesons that produce neutrinos near 35 GeV. The low-power, high-band-pass devices proposed by Frisch and Kang[4] and by Palmer[5] appear to be well suited to the neutrino energy selection required. For our hybrid system a one-millisecond beam spill would be ideal, that is, short enough for the bubble chamber and long enough for the electronic devices. (We anticipate of order 1 neutrino interaction per pulse in the quantameter and of order 100 per pulse in the hadrometer. The "deadtime" of these instruments is less than 1 μ sec.)

4. Neutrino Flux Monitor

Wachsmuth[6] has described a monitoring system for the neutrino flux which measures essentially the longitudinal and radial distributions of muons within the muon shield in front of the bubble chamber. We believe such a system is necessary for reliable operation of the neutrino beam, as well as for the flux determinations required in obtaining cross sections.

D. Measurement of the Neutrino Energy

1. Curvature and Total Energy of Charged Hadrons

The neutrino energy, E or E_ν, $\bar\nu$, is determined for each event

by measuring the energies of all outgoing particles. The energy of the charged-hadron component is given most precisely by track curvature in the 30-KG field of the bubble chamber, while a less-precise check is obtained from the hadron calorimeter associated with muon identification. The hadrometer is limited primarily by the statistics of hadron cascades in which, unlike electromagnetic cascades, a significant and variable fraction of the energy is lost to secondary neutrinos, slow neutrons, and nuclear binding energy.[7] Fluctuations in these losses are characteristic of all hadron calorimeters, and they point up one of the major advantages of the bubble chamber as a tool for doing neutrino physics. Curvature should give the charged-hadron energy to $\pm 3\ ^{\circ}/_{\circ}$, while the hadrometer resolution and precision for single events may be about $\pm 10^{\circ}/_{\circ}$ at 35 GeV.[7]

2. Total Energy of π°'s via Proportional Calorimeter

Considerable thought has been given to ways in which neutrals could be detected in the large H_2, D_2 bubble chambers.[8] For chambers of volume exceeding 100 m^3, it is possible to place track-sensitive inserts of H_2 or D_2 into mixtures of H_2-N_e and obtain effective volumes* of order 30 m^3 for neutrino physics. NAL has proposed a chamber smaller than 100 m^3, namely 30 m^3, similar to the proposed BNL 14-foot chamber. The effective volume of inserts into this 12-foot-diameter sphere are less than 3 m^3, a volume that would yield too few events in the high-energy region.

*"Effective volume" is the volume of the insert multiplied by the efficiency for detecting all of the photons from neutral pions in the H_2-N_e mixture.

To permit the necessary determination of the neutral pion energy, we propose to take advantage of a special feature of the NAL 15-foot (30 m^3) bubble chamber design -- namely the thin exit wall of 1/2" steel, less than one radiation length. The thin wall implies that protons from π^o decay can be detected efficiently and the total shower energy measured precisely by a cylindrical π^o quantameter[9] at the downstream end of the chamber. A possible arrangement is shown schematically in Figs. 7 and 8. The quantameter itself is described in more detail in Section III. The total-energy resolution should be better than ± 3 $^o/_o$ for events in which the total energy into neutral pions is above a few GeV. Precise calibration would then permit an obsolute determination of the π^o component in a single event to about the resolution limit.

We propose to install the quantameter in a special reentrant well constructed in the vacuum tank downstream of the hydrogen volume. This location, shown in Fig. 8 requires that the coil diameter be extended about 1/2 meter. These modifications, in addition to permitting a quantameter of 15 to 20 radiation lengths thickness, would preserve the entire useful volume of the bubble chamber. The volume assumed in calculating the yield histograms of Figs. 6a, b is a cylinder of 1-m radius, intercepting a sphere 3.6 m in diameter, and yielding a fiducial volume of 10 m^3. The volume outside this cylinder could be used as a blanket of H-N$_e$ mixture to detect wide-angle photons.

3. Total Energy of Hadrons via Proportional Calorimeter

The total energy of the hadrons (charged hadrons and neutrons)

can be obtained from a hadrometer. This device is analogous to the quantameter except that the plates would be made of copper, non-magnetic steel, or concrete instead of lead (for operation near the bubble chamber), and the plate thicknesses would total 10-15 collision lengths rather than 15-20 radiation lengths. Thus the hadrometer serves three purposes: it stops hadrons permitting muon identification, it measures hadron energy, including the energy of any neutrons emitted from the neutrino vertex, and/ it follows tracks spatially.

The hadrometer would be located just outside the bubble-chamber magnet as close to the magnet as practical. It's configuration might approximate a vertical half-cylinder, similar to the quantameter, although rectangular modules, such as those shown in Fig. 8, appear to be more practical. As in the case of the quantameter, a portional-calorimeter design with wire readout will be used. This is discussed in more detail in Section III.

4. Lepton Total Energy

The momentum of the final lepton is measured by curvature. Like the curvature measurements of the charged-hadron energy, this possibility is a major advantage of the bubble-chamber approach: peripheral equipment is required only to identify escaping muons, not to stop them or otherwise determine their energy. Final electrons are identified in the quantameter. Thus the hadrometer or absorber used with the bubble chamber is much thinner than the full muon range. This, in turn, permits much larger solid-angle detection for muons at an acceptable cost -- a feature well matched to intrinsically large solid angle of the bubble chamber.

Any particle penetrating 10-15 collision lengths of hadrometer is almost certainly a muon. Proportional (Charpak) chambers[10] or wire chambers can be used to locate the muon path with high spatial resolution. The muon may be identified by projecting each track from the vertex through the quantameter and hadrometer and testing whether its location at the final muon detector is consistent with location at the observed track. We propose to build into the quantameter and hadrometer a number of coordinate-sensitive planes to follow each track in detail, tracing each detected muon backwards into the bubble chamber.

F.   Measurement of Structure of Hadronic State

The bubble chamber is ideally suited to studies of the final hadronic system. Hadrons, like muons, trapped in the magnetic field can usually be identified by their interactions in the hydrogen of the chamber. A much larger class of events can be studied in detail by tracing individual tracks through the quantameter and into the hadrometer where energetic nucleons in the final state may possibly be identified.[11]

Similarly, detailed information on individual π^o's and η^o's can be obtained from a knowledge of the vertex location and the origins of correlated γ showers. In many cases, for example, the π^o energy can be determined from the photon opening angle, and in some cases a separation of π^o and η^o decays should be possible.

A procedure of the type just discussed requires extensive use of coordinate-sensitive planes. The proportional-calorimeter design described in Section III permits several planes per gap or per

plate without interfering in any way with the determinations of neutral pion or hadron energy. This option is a major advantage of the proportional (Charpak) chamber.[10]

G. Possible Hadronic Decay Modes of the Intermediate Vector Boson (IVB)

If the mass of the IVB is large many decay modes are possible.[8] Again the high measurement accuracy of the bubble chamber makes it an ideal instrument for detecting these modes. Provided the mass of the IVB is not too large, its width is likely to be much smaller than the experimental resolution function of the bubble chamber. Thus the signal/noise will be improved with increased measurement accuracy.

We list below in diagramatic form some examples of the possible hadronic decay modes of the IVB.

Baryon-Antibaryon

$$W^{\pm} \to \overline{H}_8 (\tfrac{1}{2}^+) + H_8 (\tfrac{1}{2}^+)$$
$$\to \overline{H}_8 (\tfrac{1}{2}^+) + H_{10} (\tfrac{3}{2}^+)$$

Boson-Antiboson

$$W^{\pm} \to \overline{H}_8 (0^-) + H_8 (1^-)$$

The symbol $\overline{H}_8 (\tfrac{1}{2}^+)$ represents an antibaryon of the $\tfrac{1}{2}+$ octet, etc.

Only those pairs of final particle-antiparticle states that are nearest neighbors in the Y —vs— T plot of Fig. 9 are allowed under the $\Delta S=0$ and $\Delta S=\Delta Q$ rules. For neutral IVB's (if neutral lepton currents exist) the nearest neighbors joined by the dashed lines would be possible decay products.

For low-momentum-transfer production the IVB would receive most of the energy of the incident neutrino. Consequently, the decay fragments would be thrown into a forward cone of half angle $MW/2E$.

The quantameter would easily detect the π^{o}'s that might be among the decay products.

III. EXPERIMENTAL EQUIPMENT

    A. Neutrino Beam

        1. Targets

The enhancement of the high-energy portion of the neutrino spectrum requires thin targets consisting of light nuclei. Fig. 10 (Fig. 4a of TM 218)[12] summarizes how the number of neutrinos above a certain energy depends upon the target thickness. Our requirement is for q > 2, thus the optimum target thickness is about 1 mfp. The detrimental effects on the high-energy neutrino spectrum of multiple interactions of the incident nucleon within a complex nucleus provide strong motivation for developing targets of very light nuclei. Experimentation and design studies for the neutrino target should begin as soon as possible.

        2. Meson-Focusing System

We wish to participate in the design and testing of a meson-focusing device[4,5] to produce those special qualities in the neutrino beam alluded in Section II D.3.

        3. Neutrino Flux Monitor

The CERN neutrino spectrum was measured by placing emulsions and ionization chambers at various depths and radial positrons in the muon shield to determine the muon flux at these points. Wachsmuth[6] asserts that if the pion and kaon spectra are known and the shield measurements taken, $\dfrac{d\ \tilde{N}_{\nu}}{d\ E_{\nu}}$ at the bubble chamber can be determined to about 5 $^{o}/_{o}$. The importance of determining $\dfrac{d\ N_{\nu}}{d\ E_{\nu}}$ is

so great for this experiment that some of us would like to partici-
pate in these measurements.

While the equipment relating to the neutrino beam would be
part of the NAL facility, members of this proposal are prepared
to participate in the design and development of this apparatus.

B.   Hybrid Detector System

1.   30 m^3 H$_2$, D$_2$ Bubble Chamber

The detector has already been discussed briefly in Section II,
dealing with the type of measurements one might make. The hybrid
system shown in Fig. 8 is built around the NAL bubble chamber and
offers these advantages:

a.   precision on $E_\nu = E_\pi o + E_H + E_\mu$ to $\pm 3~{}^o/_o$,

b.   vertex information of the bubble chamber,

c.   absorber (hadrometer) thickness much less, than the muon
     range

d.   large solid angle,

e.   simplicity.

Of these, the first four follow immediately from the use of the bub-
ble chamber itself, particularly its ability to measure E_H and E_μ,
once the muon has been identified. Supplementary information on E_H,
including identification of baryons, is provided by the hadrometer,
while $E_\pi o$ is given solely by the quantameter. The advantage of
                                                          the
simplicity follows partly from relatively/thin absorber required
(since the bubble chamber measures E_μ) and partly from the use of
porportional calorimeters to be described.

The reentrant cylindrical tank housing the quantameter is an

important change in the preliminary bubble-chamber design and
necessitates an increase in the coil diameter of about 1/2 meter;
this change will greatly increase the effectiveness of the bubble
chamber for both strong and weak interaction physics, particularly
in reactions involving final π^o's.

2. Ionization and Proportional Calorimeters

Parallel-plate ionization calorimeters, such as the quanta-
meters[9] widely used in monitoring photon beams, have several intrin-
sic properties that are essential in determining $E_\pi o$ and E_H accurately.
First, the response depends only upon the relative ionization in the
gas gaps as compared to the ionization in the plates; tolerances of
a few percent in these parameters are easily met and insure a uni-
form response to the same level. Second, since the ratio of gap to
plate is independent of track angle in a parallel plate chamber,
such a device is intrinsically isotropic. Third, the output of an
ionization calorimeter is linear in the energy absorbed over a wide
range. Fourth, an ion chamber is operated as a one-parameter device;
there is one high-voltage setting and one output signal proportional
to the total energy deposited in the chamber as sampled periodically
via the ionization in the gas gaps. This last feature greatly simpli-
fies the operation of the calorimeter and results in a high repro-
ducible instrument.

In the case of electromagnetic showers $(E_\pi o)$, virtually all
of the energy appears ultimately in the form of ions, which are
sampled directly in the ionization calorimeter thereby avoiding
such questions as the response of scintillation or Cerenkov counters.

In the case of hadronic cascades, a certain portion of the energy is lost to neutrinos, slow neutrons, and nuclear binding, as mentioned previously.[7] A typical loss might be 20-30 $^o/_o$ at 35 GeV, although for some events the loss may be catastrophically large. Within the statistical uncertainties of this process, the response is similar for all hadrons, including high-energy neutrons, providing the absorber thickness is sufficient to contain the cascade. The actual gain can be determined by calibration with hadrons of various energy.

The only serious limitation of ionization calorimeters, as far as the present application is concerned, is their relatively low gain, typically[9] $4x10^3$ ions per GeV absorbed with 1-atm of A-CO_2. This small signal appears across the relatively large capacity of the parallel plate structure and is not easily detected.

A much higher gain is possible by using the high electric fields surrounding small-diameter (20-100μ) wires to induce proportional avalanche multiplication. Proportional calorimeters[10] retain the uniformity, isotropy, and linearity of ion chambers, and if the signals from the high-voltage plates are added, there is one high-voltage setting and one output signal. The gain of a proportional chamber, unlike an ion chamber, varies exponentially with the high voltage, but good reproducibility can be obtained.

Proportional, chambers cease to be linear when the space charge in single avlanches appreciably distorts the electric field near the wires. This occurs typically at $5x10^6$ ions, and the high voltage is normally set low enough so that this condition is not

exceeded.

A crucial point in our application is that the primary
ionization of the shower, consisting of some 4000 ions/GeV, in
the gas, is distributed over several hundred tracks in perhaps
10 gaps. As many as 10^3 avalanches may be thus involved so that
an output of 5×10^9 ions or more can be obtained without exceeding
the linear response region. This largely compensates for the greater
capacity of a pair of plates or of an entire chamber, as compared
with the capacity of a single wire, and it yields an output voltage
within one or two orders of magnitude of that normally obtained on
a single wire of a multiwire proportional chamber. Such a net
signal can easily be measured, and if necessary, one can afford
sensitive amplifiers since only a small number of total-energy
outputs are involved. (The situation is quite different when one
must read 10^3 to 10^4 separate wires.)

3. Proportional Quantameter

We presently envision the proportional quantameter to consist
of 10 lead plates and a similar number of gas gaps totaling 20
radiation lengths of lead, about 11.6 cm. A sector $90^\circ \times 90^\circ$ measured
from the center of the bubble chamber would be about 4 meters high
with a 3-m arc and would weigh about 16 tons. Each double gap would
consist of a single wire plane centered between two lead plates and
defining a total gap of $2 \times .5$ cm = 1.0cm. Ten of these gaps would
add an additional 10 cm to the quantameter thickness. Allowing an
additional 5 cm for flanges and windows, we obtain a total quanta-
meter thickness of about 30 cm. A 35-cm-wide reentrant tank would

allow, in addition, the installation of a couple of scintillation counters or possibly a two-gap spark chamber. Some reduction in quantameter thickness could be obtained by using tungsten plates, fewer gaps, or somewhat less than 20 radiation lengths of material. Note that the steel walls of the bubble chamber and the reentrant wall will amount to 1-2 radiation lengths and may be considered as the first plate of the quantameter, while the quantameter at 1 collision length may be considered the first plate of the hadrometer. The quantameter itself might then begin with a sensitive gap followed by the first lead plate.

The wires of the proportional quantameter will be read out to provide spatial resolution. A wire diameter of 50μ and a spacing of 2mm is probably convenient[10] although 1mm seems feasible if one is willing to try hard enough. Vertical wires are straight forward in the cylindrical configurations, but horizontal wires may force a modular quantameter design with flat parallel plates.

4. Proportional Hadrometer

The hadrometer consists of perhaps 15 plates of copper each 10 cm thick and separated by gaps of 1.2 cm. A less-expensive plate material may be practical, giving the same thickness in collision lengths. The 12-cm lead of the quantameter is equivalent to about 1 collision length for hadrons while the 150 cm of copper adds an additional 13 collision lengths. The copper coils of the bubble chamber magnet amount to several collision lengths but do not seriously limit the accuracy of the hadron-energy determination for most event types.

We presently envision a proportional hadrometer design, with
copper plates and wire readout, subtending vertical and horizontal
angles of about 90° by 90° as measured at the center of the bubble
chamber. The volume of copper would then be 8mx8xm1.5m and the weight
about 800 tons.

As indicated in Table I, the cost of such a hadrometer is more
than half the total for the experiment. Further, whereas the quanta-
meter is essential to the experiment in providing a unique determina-
tion of $E_\pi o$, the measurement of E_H is best done by the bubble chamber
itself. If one abandons the measurements of E_H in the hadrometer and
reduces the track following requirements, a number of cost-saving
options are then possible including: reducing the hadrometer accept-
ance to 45° x 45°, using optical spark chambers instead of proportional
chambers, reducing the number of plates, and using cheaper plate
materials, for example a single wall of concrete shielding blocks.
These options would not optimize the physics but might help to ensure
that the essential physics is done.

5. Range Detector for Muons Leaving the Bubble Chamber

Highly peripheral events produce muons at large angles and at
sufficiently low momenta that the muons can be trapped in the
bubble-chamber magnetic field. Muons of a few GeV and more pass
through the 14 collision lengths of photon and hadron absorber and
can be identified in that way. A single plane of scintillators down-
stream of the hadrometer might suffice, while the last several gaps
of the hadrometer could provide the spatial resolution necessary to
permit muon tracks to be traced back to the bubble chamber. Events
with muons in an intermediate energy range, for example the range from 1 to

3 GeV, may frequently remain ambiguous, as far as muon identification is concerned unless the hadrometer subtends a very large solid angle and unless individual tracks are followed through each plane of the hadrometer until they stop.

6. Triggering Options

Signals should be available from the quantameter and hadrometer

within 100 ns of the occurence of an event and with a time jitter
of less than 50 ns.[10]. These signals, in coincidence with scintil-
lator planes, could be used to develop a trigger requiring an inter-
action having total energy above, for example, 10 GeV. Four
scintillator planes might suffice: an anticounter in front of the
bubble chamber, a yes-counter in front of the quantameter and another
in front of the hadrometer, and finally the muon counter plane
already mentioned. The trigger could be used to flash the bubble
chamber illumination or fire peripheral spark chambers, or it
could simply be recorded for use in analyzing the bubble-chamber
film. We presently favor the last option, at least during the
early stages of the experiment.

IV. SCHEDULES AND PARTICIPATION

A. Design and Development of Equipment

We shall explore ways in which the participating groups, and
particularly LRL as a service to other users, can participate in
the design and development of the neutrino beam, quantameter, hadro-
meter, counters and modifications of the bubble chamber. Arrange-
ments for sharing the cost could be negotiated between our groups
and NAL.

B. LRL Development

Work should begin immediately on some of the special items
just mentioned. Among these is the design of the reentrant tank
for the quantameter, which could be carried out by LRL mechanical
engineers skilled in cryogenic equipment. The design could proceed
at Berkeley in close collaboration with W. Fowler and his group at

NAL. In addition, the shop and experimental facilities of LRL could be made available to the University of Hawaii group and others involved in developing the quantameter and hadrometer.

C. Participation of Our Personnel at NAL.

The development of the neutrino beam equipment would best be done at NAL. We would hope to make the experience of graduate students stationed at NAL as broad as possible. Thus, while a major fraction of their time would be devoted to development of the neutrino facility and bubble chamber, their direct participation in construction and other activities of the accelerator should be encouraged.

D. Beam Survey Experiment

The meson production measurements should start as soon as the survey beam (10^{10} proton/pulse) is available in Area 2. Here, we could provide experienced personnel and some equipment to aid groups that have made specific survey proposals involving major hardware commitments.

A survey bubble chamber of the type suggested by Snow[3] should be available at the turn-on date of Area 2. The present film and data-analysis equipment at our participating institutions is adequate to handle exposure of several hundred thousand pictures on both hydrogen and deuterium. The information from the yield measurements could be used to up-date the operating parameters of the meson-focusing device. Early exposures to 500-GeV protons would be very useful in designing the focusing for the 500-GeV phase. Since only ten or twenty protons per pulse are required, one might consider

designing the bending magnets of Area 2 (super conducting?) to bend 500-GeV protons, allowing the quadrupoles to remain set at their 200-GeV design values. At the low intensities required, no radiation damage would result to the beam transport equipment, and no additional shielding would be required. Reliable, fail-safe intensity-control equipment would, however, be necessary.

E. Million-Picture Exposure at 200 GeV

The experimental program of preparing the neutrino beam for this application could easily occupy the first year or more after beam turn-on. The accelerator operation in its second and third years is likely to be more reliable, and the bubble chamber will be better understood. We therefore propose that a one-million picture exposure to hydrogen of both neutrinos and anti-neutrinos of high energy be made in the second or third year of operation at NAL. Similar exposures to deuterium would come later.

F. Million-Picture Exposure at 500 GeV

Our reason for requesting an exposure at higher accelerator energy is to allow the energy at which we have a low value of $\left| d \ln \dfrac{d N_\nu}{d E_\nu} \middle/ d \ln E_\nu \right|$ to be increased significantly. This, in turn, would raise the central neutrino energy from 35 GeV to 70 GeV for an acceptable uncertainty in the number of neutrinos incident. The 500-GeV exposure would occur at a much later date.

V. PRELIMINARY COST ESTIMATE

A preliminary cost estimate is given in Table I. The principal assumptions are:

A. Geometry shown in Fig. 8,

B. $1.00/pound for copper plates (container negligible),

C. $.50/pound for lead plates (container 18K),

D. all wires readout, 2-mm wire spacing, 10 planes/chamber,
    $5/wire to readout, $1.50/wire to fabricate the quantameter,
    $2.50/wire to fabricate the hadrometer.

As already mentioned, the cost is clearly dominated by the
copper plates of the hadrometer,[13] $1600K out of $2600K total.
If one reduces the hadrometer to an angular acceptance of $45°x45°$
(4mx4m), keeping other parameters fixed, the hadrometer cost is
reduced from $1900K to $550K and the experiment from $2600K to
$1250K, about a factor of two. Other savings could be made by
using optical spark chambers or hadrometer plates of concrete
shielding blocks. The quantameter and necessary modifications
of the bubble chamber seem to us essential if one is to carry
out a neutrino program of the type proposed here.

TABLE I

Preliminary Cost Estimates (All Wires Read Out)

			Cost K$	Cost K$
1.	Modifications of Bubble Chamber Coils and Vacuum Tank		300	300
2.	Quantameter:	Lead Plates and Container	50	
		10 Wire Planes	30	
		10x4m/2mm=20,000 Readouts x $5/wire	100	180
3.	Hadrometer:	Copper Plates and Container	1600	
		10 Wire Planes	100	
		10x8m/2mm=40,000 Readouts x $5/wire	200	1900
4.	Counter Planes:	4mx4m Anti (8scintillators 16 PMS)	20	
		4mx4m Yes at Quantameter In	20	
		8xm8x Yes at Hadrometer In (16 scintillators, 32 PMS)	40	
		8mx8m Yest at Hadrometer Out	40	120
5.	Computer Interfacing		50	50
6.	Fast Logic, Slow Logic, etc.		50	50

TOTAL = $ 2600K   (90°x90° Hadrometer)

If the plate area of the hadrometer is reduced from 8mx8m to 4mx4m, the estimated cost of the experiment is

TOTAL = $1250K   (45°x45° Hadrometer)

REFERENCES

1. J.D. Bjorken and E.A. Paschos, SLAC-PUB-678, December, 1969 (Lectures by Bjorken at 1969 Summer Study).

2. D. Carey, Y.W. Kang, F.A. Nezrick, and R. Stefanski, TM-222 "A Note on the 200-GeV Neutrino Design."

3. G.A. Snow (correspondent) "Preliminary Proposal to Study Multiparticle p-p and π-p Interactions from 75 to 200 GeV/c (and higher momenta as soon as they become available), April 23, 1970. University of Maryland High Energy Physics Group.

4. D. Frisch and Y.W. Kang, "D.C. Horn for Very-High-Energy Spark-Chamber Neutrino Experiments," 1969 NAL Summer Study $\underline{1}$, 389.

5. R.B. Palmer, "The Design of Long-Pulse Monopole Focusing Elements," 1969 NAL Summer Study $\underline{1}$, 383.

6. H. Wachsmuth, "Neutrino Spectrum Determination from Muon Flux Measurements," 1969 NAL Summer Study $\underline{1}$, 367.

7. V.S. Murzin, Progress in Elementary-Particle and Cosmic-Ray and Cosmic-Ray Physics, (North-Holland Publishing Company, Amsterdam, The Netherlands, 1967), Vol. IX, p. 245.

8. See for example M.L. Stevenson, "High-Energy Neutrino Physics $< E_\nu > 20$ GeV and the Constraints Placed on Detectors," 1969, NAL Summer Study $\underline{2}$, 121.

9. R.R. Wilson, Nucl. Instr. $\underline{1}$, 101 (1957). A high-energy (multi-GeV) quantameter is described by D. Yount, Nucl. Instr. Methods $\underline{52}$, 1 (1957).

10. G. Charpak, D. Rahm, and H. Steiner, "Some Developments in the Operation of Multiwire Proportional Chambers," CERN Preprint.

11. A. Pais, "Weak Interactions at High Energies," Presented at the Conference on "Expectations for Particle Reactions at the New Accelerators," University of Wisconsin, 1970; S.D. Drell and Tung-Mow Yan, "Final Particle Correlations in Deep Inelastic Lepton Processes," Phys. Rev. Letters $\underline{24}$, 855 (1970).

12. M.L. Stevenson, "Targets for the Neutrino Beam: Concepts," NAL Report TM 218.

13. D.D. Jovanovic, R. Palmer, and B. Roe, "Muon Detectors after the 25-foot Chamber" Aspen 1969 Summer Study, $\underline{2}$, 207.

Fig 1

FIG2.
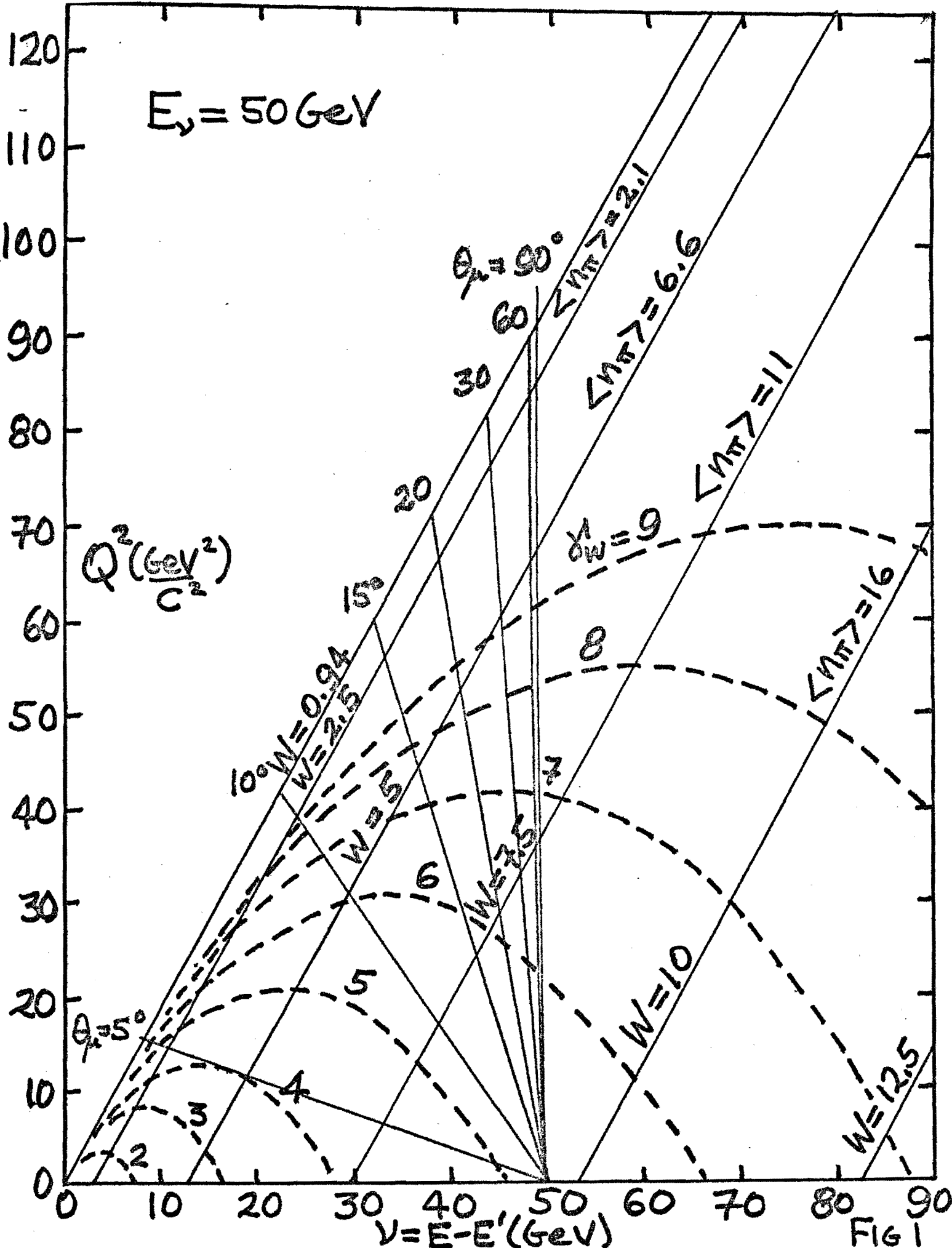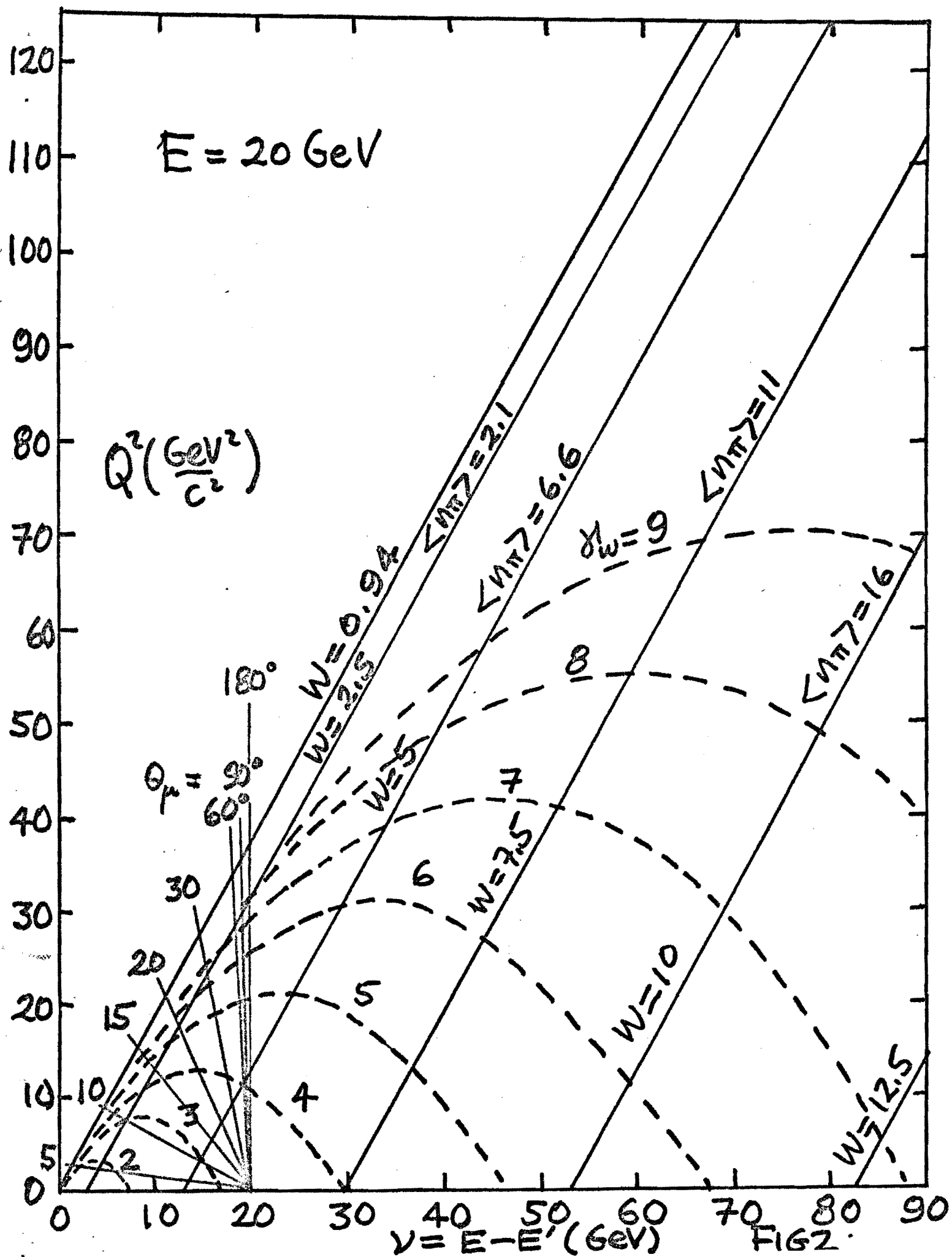
Distribution of 1000 Events

$E_\nu = 50 \text{GeV}$

for $y_f = K(1-x)$
$c_R = c_3 = 0$
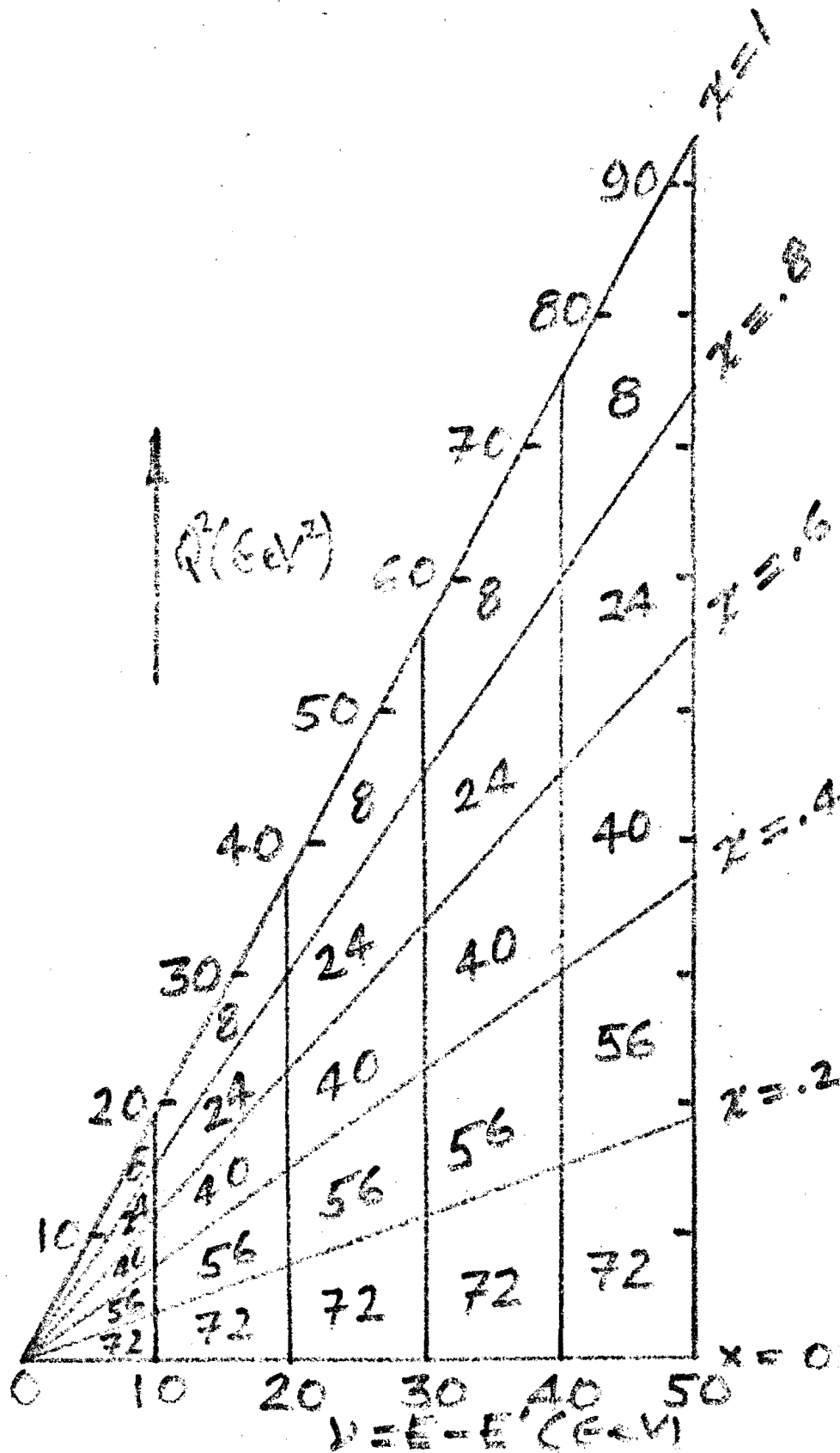
SPIN $\frac{1}{2}$ PARTONS

$M_W = \infty$

FIG 3

Distribution of 1000 Events
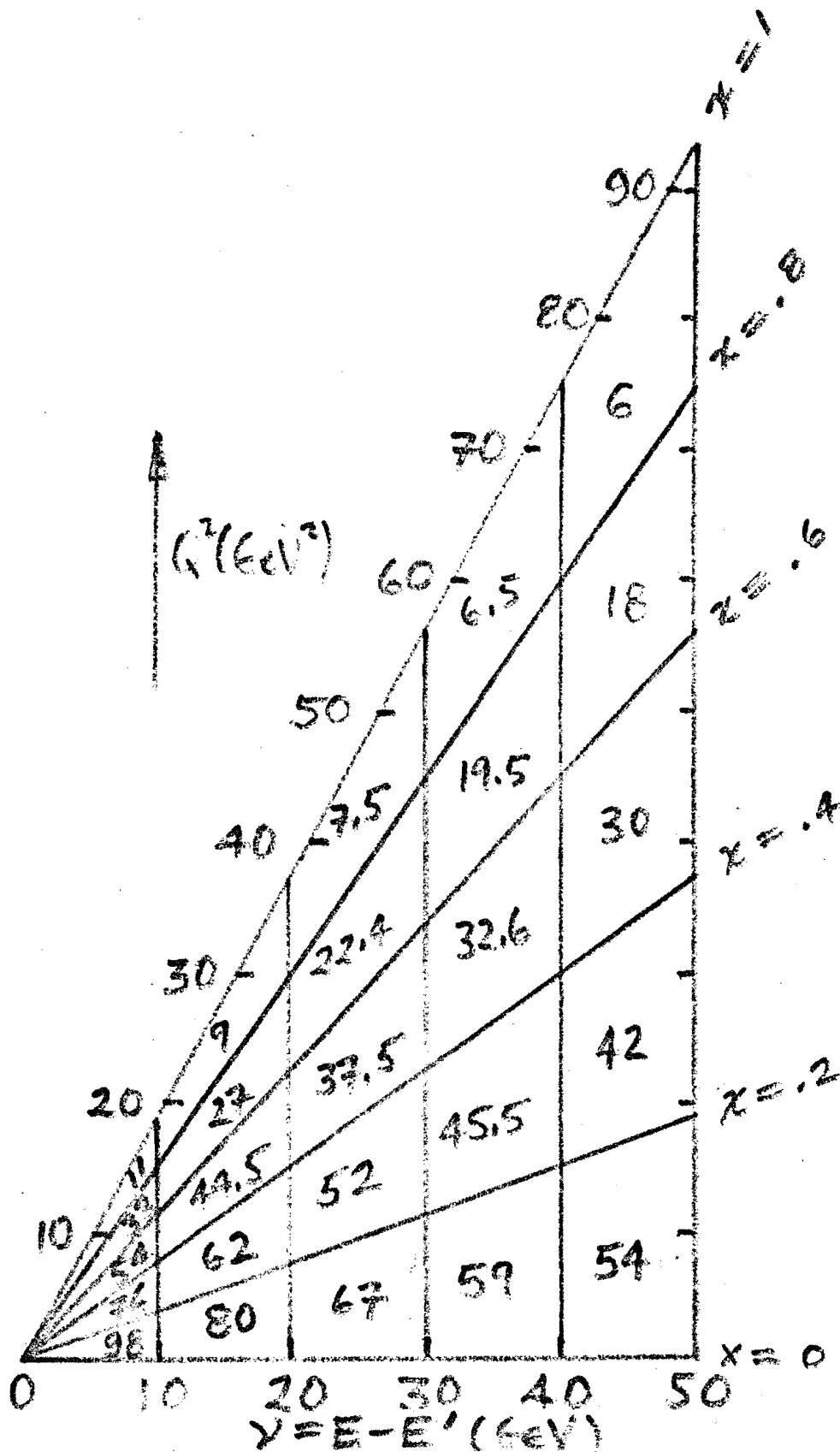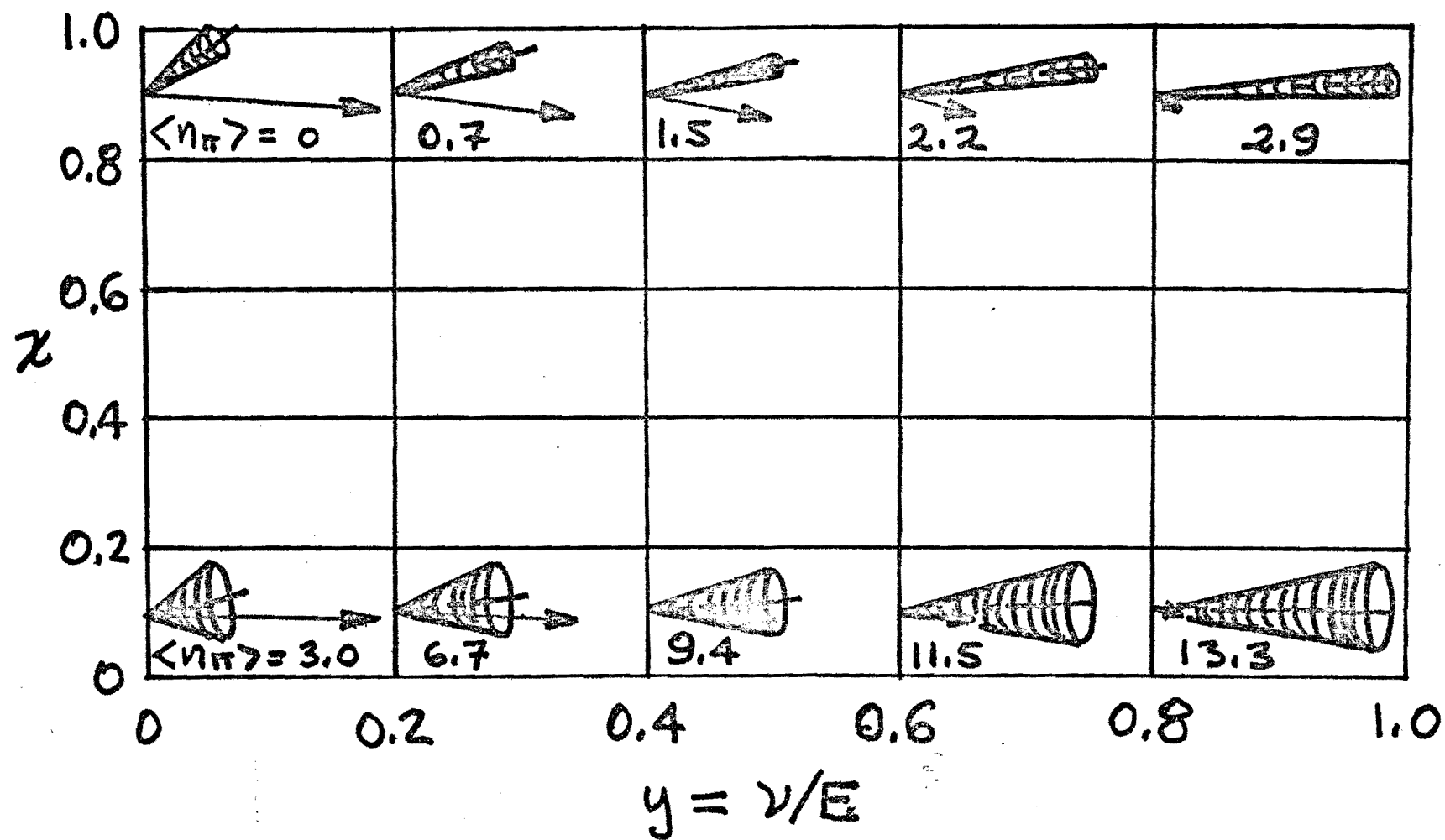
FIG 4

FIG 5a

E = 20 GeV

x (vertical axis)

$y = \nu/E$ (horizontal axis)

FIG. 5b

Yields in NAL 12' spherical H₂ Bubble Chamber using neutrino flux calc of Carey et al. TM222 (FANC model at 200 GeV)

Fig 6a
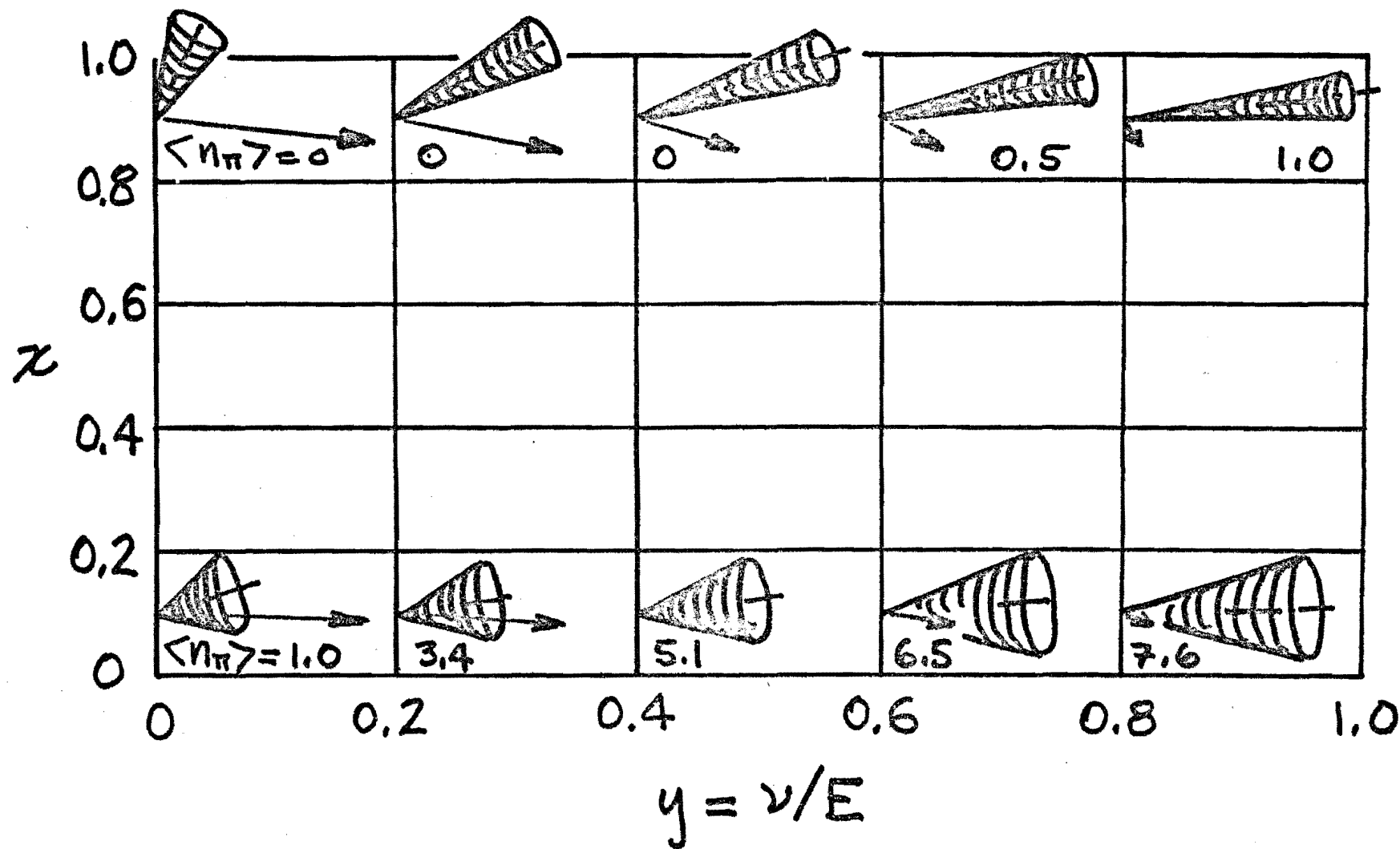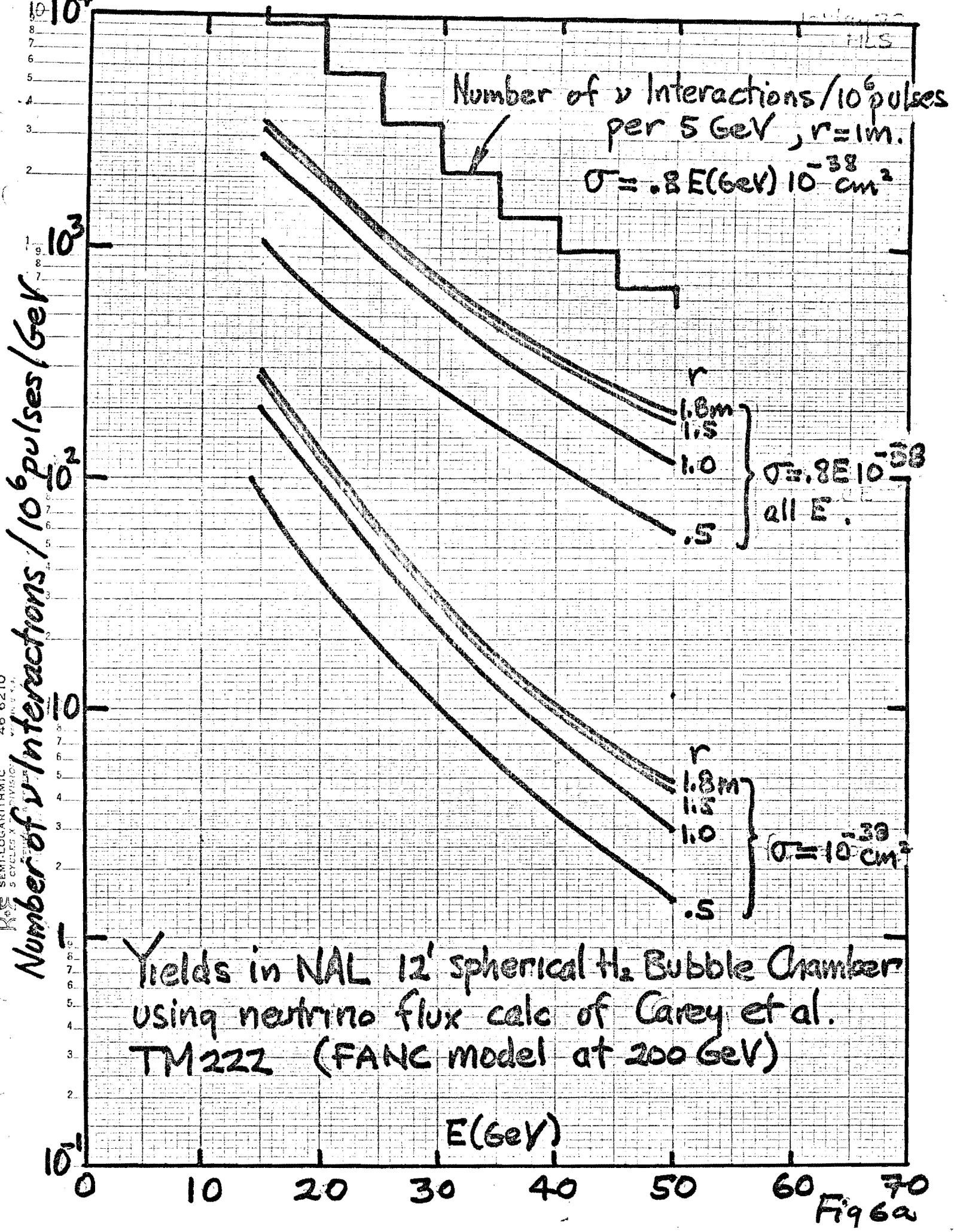
Number of ν Interactions/10^6pulses per 5 GeV

for $\sigma = 8 \times 10^{-30}$ cm^2
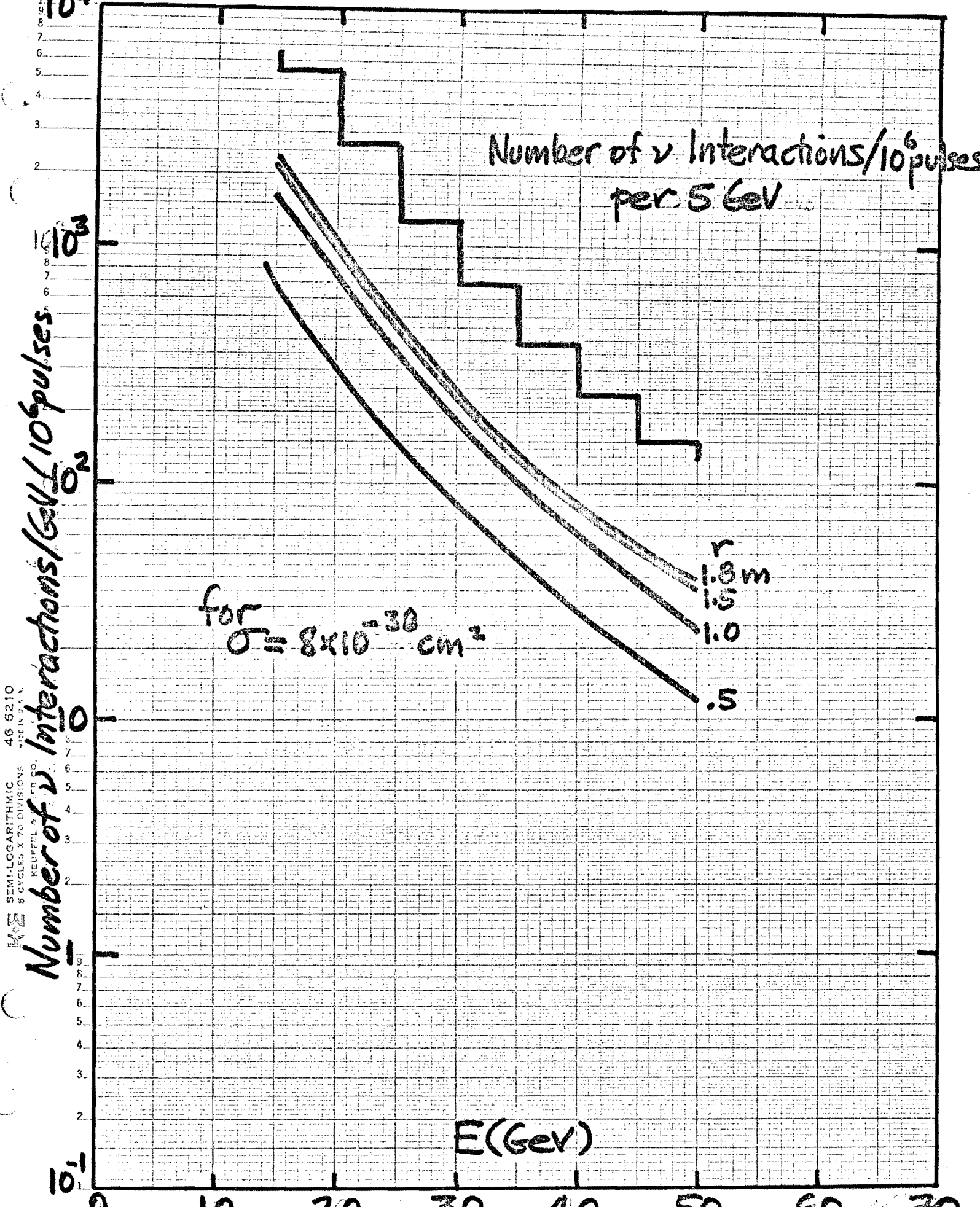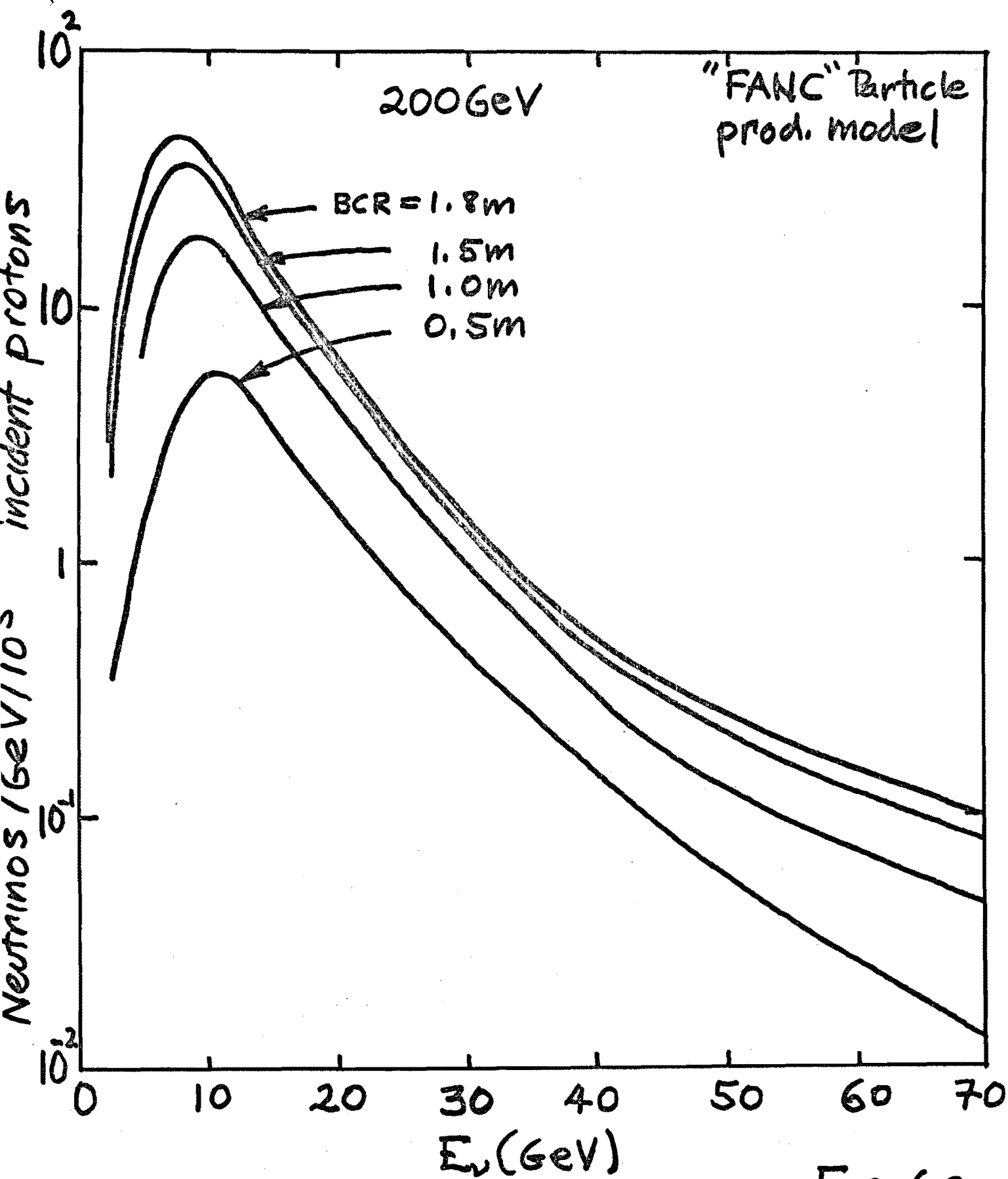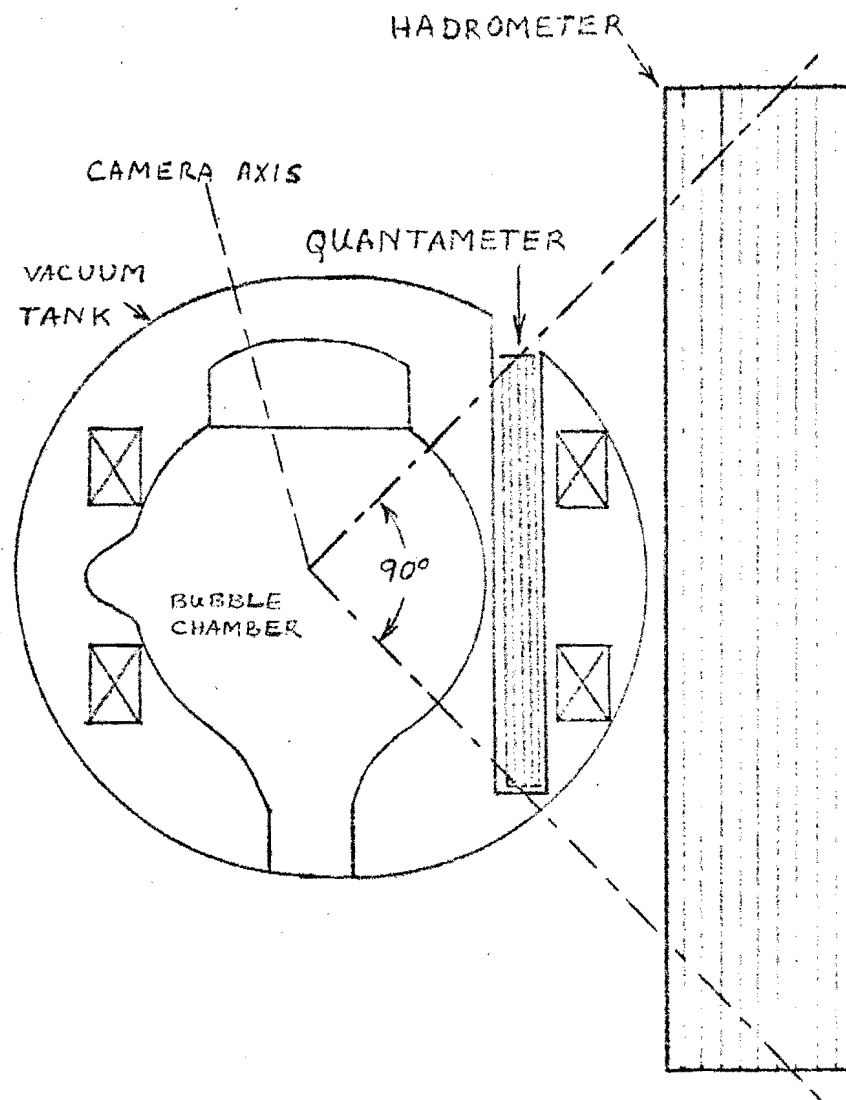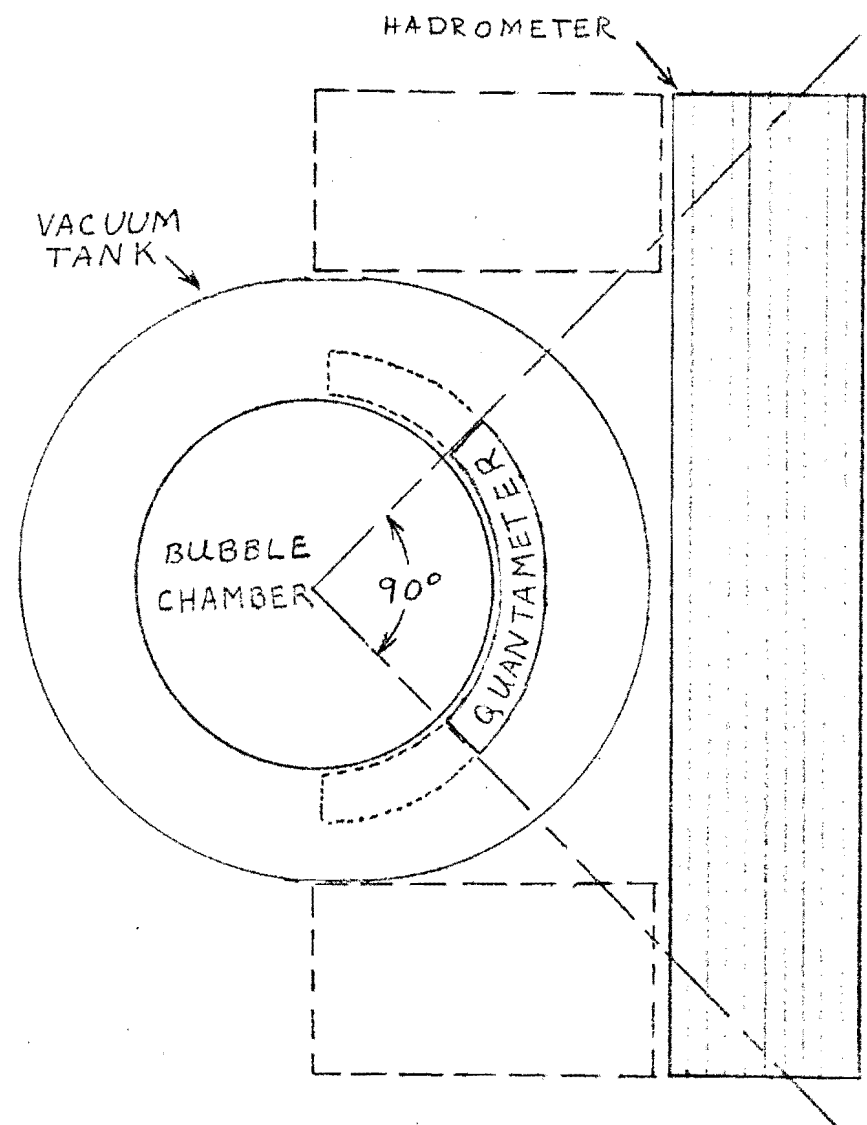
r
1.8 m
1.5
1.0
.5

E(GeV)

Fig 6b

FIG 6C

~0 m³ Hybrid Bubble C for NAL

π Quantam

12' φ Bubble Chamber

Superconducting Coils (30 kilogauss)

Fig 87

HADROMETER

CAMERA AXIS

QUANTAMETER

VACUUM
TANK

BUBBLE
CHAMBER

90°

SIDE VIEW

HADROMETER

VACUUM
TANK

BUBBLE
CHAMBER

90°

QUANTAMETER

TOP VIEW

FIG. 8

T_Z

η p

Y Σ^- Σ^0 Λ Σ^+ I

Ξ^- Ξ^0 O

$Q_p = -1$

$J = \frac{1}{2}^+$ octet

(a)

K^0 K^+

π^- π^+

K^- $\bar{K}^0$

$J^P = 0^-$ octet

(b)

Δ^- Δ^{++}

1237

Σ^- Σ^0 Σ^+

1385

Ξ^- Ξ^0

1530

Ω^-

$J^P = \frac{3}{2}^+$ decimet

(c)

ρ^- ρ^+

$J^P = 1^-$ octet

(d)
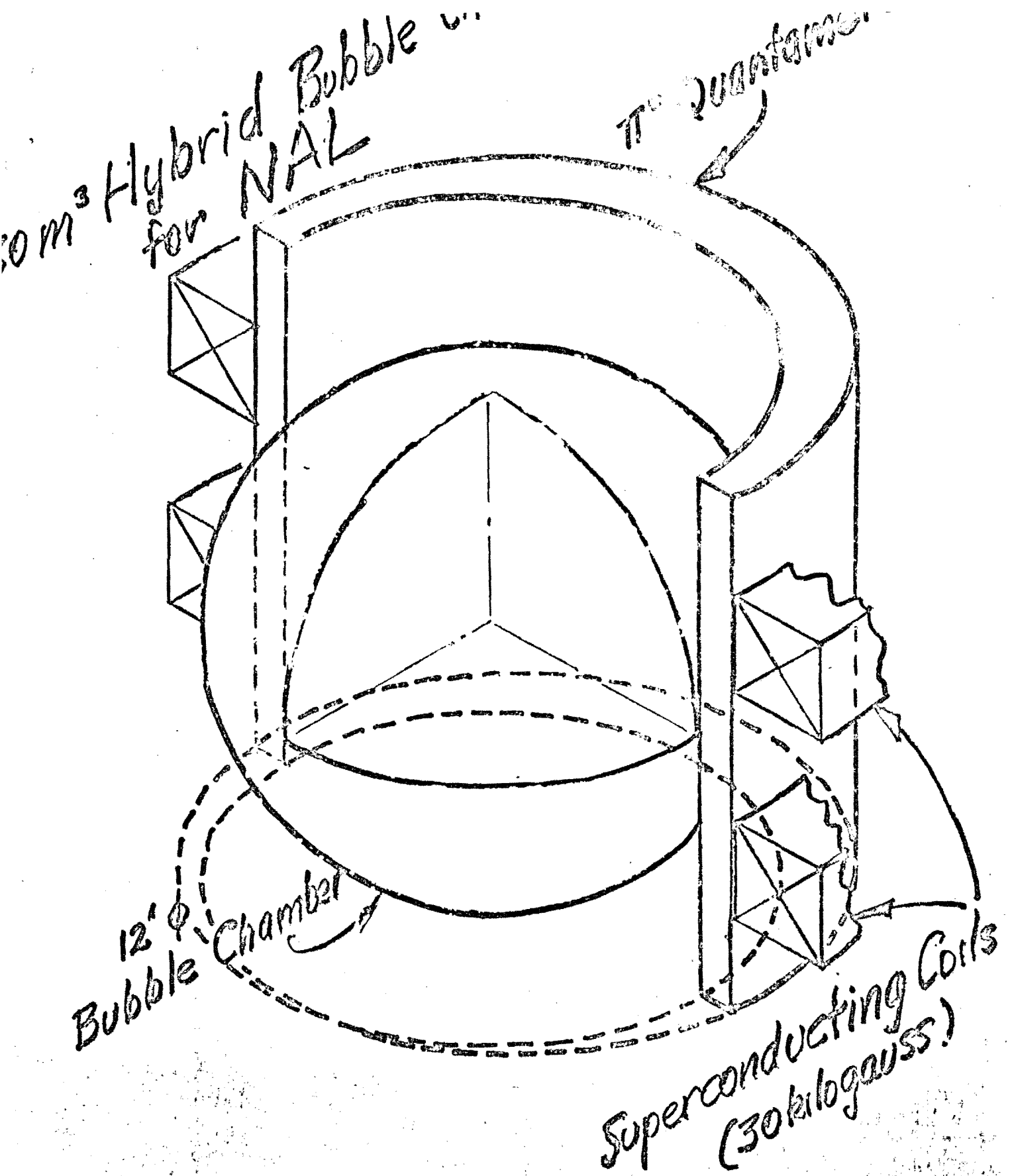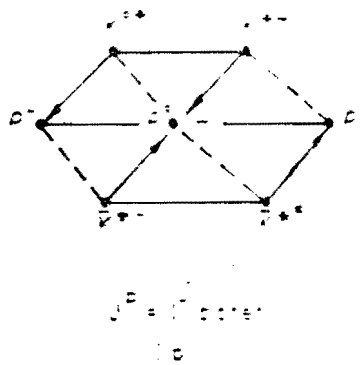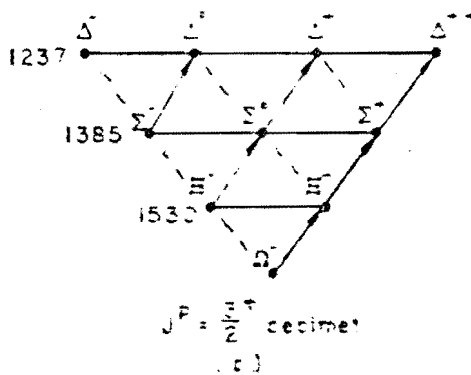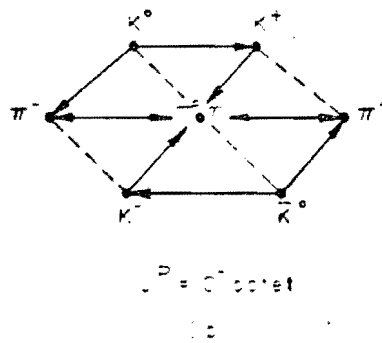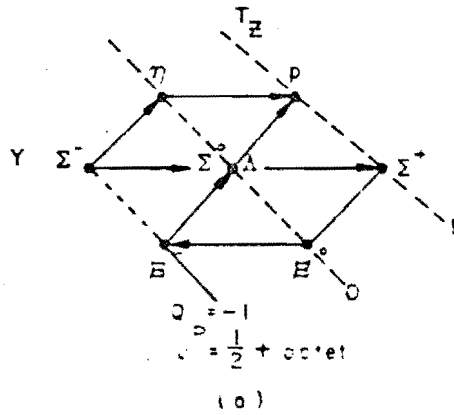
Fig. 9. Hadronic currents allowed in the Cabibbo theory are indicated by arrows. (a) Allowed currents in the baryon octet. (b) Currents in the $\frac{3}{2}^+$ decimet. (c) Currents in the vector octet.

9

FIG 10

$$\lambda = \lambda_\pi$$

$$\frac{n(>\varepsilon)}{n_0 \varepsilon_b^{-b} e^{-\varepsilon}} = \left(e^{\frac{\beta \varepsilon}{\rho}} - 1\right)$$

$$q = \frac{\text{mean}}{\text{Rbosh}} / T_0$$

$T_0 (200 \text{GeV}) = 16.2 \text{ GeV}$

$T_0 (400) = 27.3 \text{ GeV}$

$q_{max} (200) = 12.3$

$q_{max} (400) = 14.7$

$$g = (q - K)^{1/2}$$

K = nucleon inelasticity $\approx \frac{2}{3}$

$q = 0$

$q = 1$

$q = 2$

$q = 4$

6

10

ℓ/λ
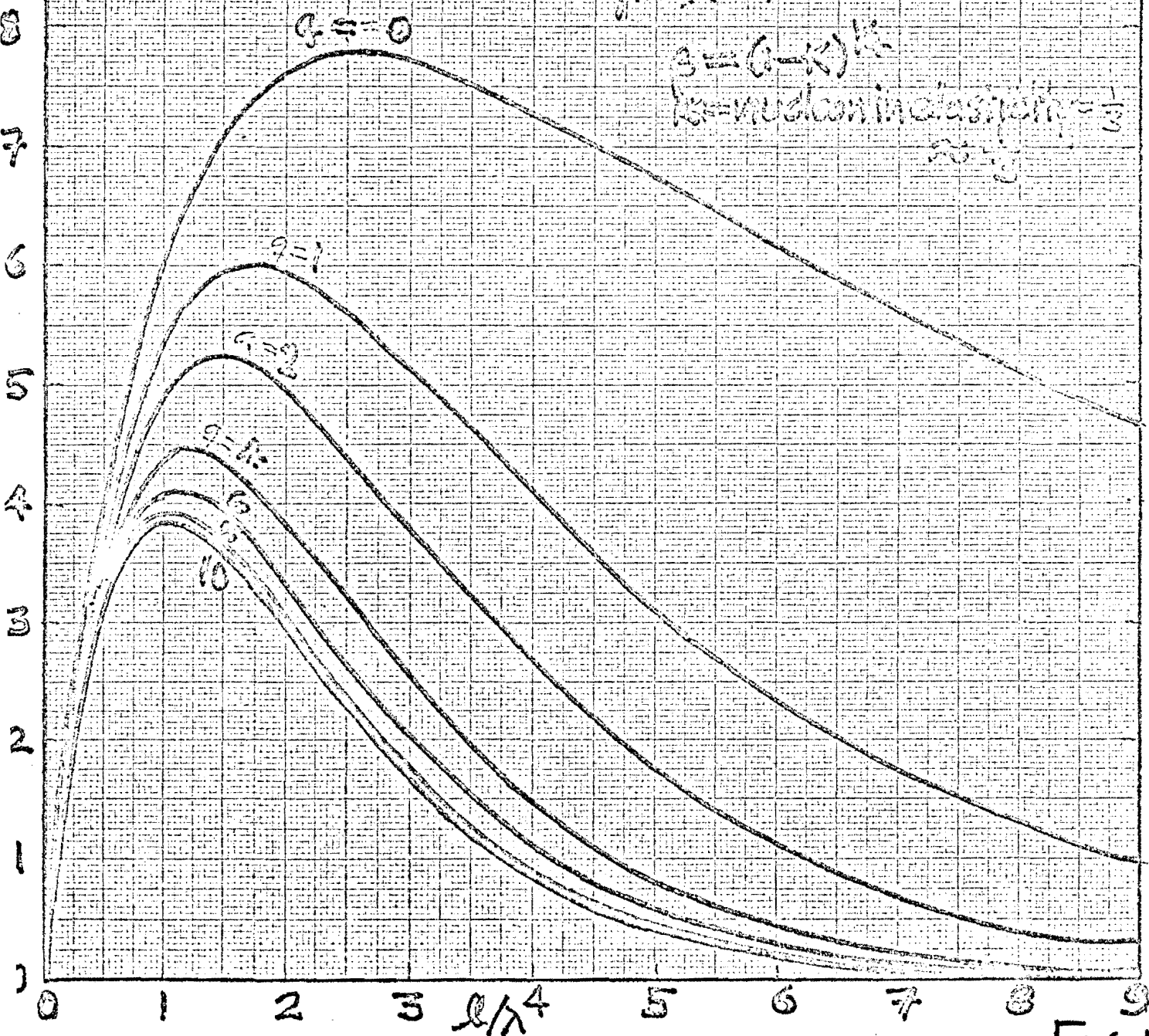
FIG 10

Correspondent: M. L. Stevenson
                Experimental Physics
                Lawrence Radiation Lab
                Berkeley, Calif. 94720

FTS/Commercial 415-843-6301

Proposal for a High-Energy Neutrino Experiment

In The NAL 30 m^3 H$_2$, D$_2$ Bubble Chamber

R. Cence, F. Harris, M. Peters, V. Peterson, D. Yount
University of Hawaii

S. Meyer
Northwestern University

M. Alston-Garnjost, R. Birge, G. Goldhaber
J. Kadyk, S. Parker, M. L. Stevenson, G. Trilling
Lawrence Radiation Laboratory

June, 1970

PROPOSAL FOR A HIGH-ENERGY NEUTRINO EXPERIMENT

IN THE NAL 30 m^3 H$_2$, D$_2$ BUBBLE CHAMBER

University of Hawaii (R. Cence, F. Harris, M. Peters, V. Peterson,
D. Yount)

Northwestern University (S. Meyer)

University of California, Lawrence Radiation Laboratory (M. Alston-Garnjost, R. Birge, G. Goldhaber, J. Kadyk, S. Parker, M.L. Stevenson[*], G. Trilling)   June 1970

ABSTRACT

We propose to study high-energy neutrino interactions in the NAL 30 m^3 bubble chamber. A slight alteration of the chamber design will allow a large-solid-angle quantameter to be placed just outside the thin (1/2 inch steel) wall of the bubble chamber. A detector designed to identify the muon of the interaction is placed outside the vacuum tank. With this hybrid system we can reconstruct the neutrino's energy, the lepton momentum transfer squared, Q^2, the lepton energy transfer (ν = E–E'), and measure many features of the final hadron state. This sytem detects with high efficiency over the entire range of variables and is well suited to making a detailed general survey of neutrino interactions in the neutrino energy range 15 to 80 GeV. A million-picture exposure would yield tens of thousands of neutrino interactions with circulating protons at 200 GeV. A similar number of events should be obtained with protons at 500 GeV. Table I summarizes the preliminary cost estimates.

[*]correspondent

PROPOSAL FOR A HIGH-ENERGY NEUTRINO EXPERIMENT
IN THE NAL 30 m^3 H_2, D_2 BUBBLE CHAMBER

University of Hawaii, Northwestern University,

Lawrence Radiation Laboratory

I. INTRODUCTION

We propose an experimental program for studying the interactions of neutrinos on hydrogen and deuterium for neutrino energies above 15 GeV. This program includes measurements of:

a. the total cross section to see if it saturates or remains linear in neutrino energy,

b. distributions in the deep-inelastic region to test scale invariance and various models such as Pomeron exchange and the parton hypothesis,

c. the elastic differential cross section to learn more about nucleon form factors,

d. interactions involving W mesons, if they exist.

A detector similar to the 14-foot BNL bubble chamber, suitably altered to detect π^0's, neutrons, and muons electronically, seems ideal for neutrino energies up to 80 GeV.

The proposal parallels experiments on elastic and "deep-inelastic" electron scattering: the neutrino provides an independent probe of nuclear structure with, we believe, comparable sensitivity to the electron, while the bubble-chamber technique makes possible a detailed analysis of the final-state hadrons.

In the case of neutrinos, only the direction of the incident lepton is known, and it is necessary to determine its energy E. This can be done by measuring the energies of all final π^0's, charged hadrons, neutrons, and leptons (muons). Provided we identify which of the final particles is the outgoing lepton (energy E'), we can make the same analysis as in deep-inelastic electron scattering. The total and the "elastic scattering" cross sections will also be measured.

Bubble-chamber detection of neutrino events provides precise information on the location of the interaction vertex as well as the momenta of all charged outgoing particles. Photons from π^O's are detected with essentially 100 $^O/_o$ efficiency by a proportional quantameter (lead plates with wire coordinate planes in the gas gaps), and spatial information as well as the total electromagnetic energy is obtained. A "hadrometer" (optical spark chamber buried in a massive concrete absorber 10-15 collision lengths thick) stops all hadrons and makes nuclear cascades visible. Neutrons are detected in the hadrometer by their nuclear cascades, whose energy can be determined by spark counting. Muons are identified when they penetrate this hadron absorber. Backgrounds are suppressed by the time resolution of the trigger logic, by the energy discrimination of the quantameter and hadrometer, and by detailed track analysis in the bubble chamber, quantameter, and hadrometer.

There are several major advantages of the hybrid system consisting of the bubble chamber and electronic detectors. First, the bubble chamber permits an accurate (to ± 3 $^O/_o$) determination of the charged-hadron and lepton energies through track curvature, while the quantameter determines the total electromagnetic energy to about the same precision. The energy appearing in the form of neutrons is detected with the hadrometer to somewhat less accuracy, but this component is normally a small fraction of the total. Detailed vertex information is a second advantage, as already mentioned. Third, the angular acceptance is large, and a wide range of lepton-momentum and lepton-energy transfers is sampled with good efficiency. Finally, since the muon energy is determined in the bubble chamber, the thickness of the muon detector

is much less than the muon range.

In Section II we discuss some of the measurements that might be made in the neutrino energy range from 15 to 80 GeV. We use these considerations as the basis for designing detectors. Section II also contains specifications required for the neutrino beam and a summary of the components of the neutrino facility that participants in this proposal could help to develop. Technical design considerations are discussed in Section III. Finally, in Section IV we suggest a possible schedule for obtaining one million events during both 200-GeV and 500-GeV phases of the accelerator operation.

II. HIGH-ENERGY NEUTRINO INTERACTIONS

A. Kinematics of ν + N → lepton + hadrons

We adopt the notation of Bjorken and Paschos.[1] Fig. 1 then summarizes much of the kinematics where Q^2 is the square of the momentum transfer to the leptons, and ν is the difference in initial and final lepton energies. The solid parallel lines are the loci of equal invariant hadron mass W, given in terms of the nucleon mass M by the following equations:

$$Q^2 = 2M\nu + M^2 - W^2, \tag{1}$$

$$\nu = E - E', \tag{2}$$

$$\gamma_W = (E_H = M + \nu)/W, \tag{3}$$

$$\sin^2 \frac{\theta}{2} = \frac{Q^2}{4EE'}, \tag{4}$$

$$\sin^2 \theta_H = \left[\frac{E'}{E} \frac{\cos^2 \frac{\theta}{2}}{1 + \frac{\nu}{Q^2}} 2 \right]^{\frac{1}{2}}, \tag{5}$$

where θ and θ_H are the laboratory angles of the final lepton and hadron systems, E is the neutrino energy and E' the final lepton energy.

The loci of equal values of γ_W, the Lorentz-contraction factor, are indicated by the dashed parabolic curves in Fig. 1. The straight lines radiating from the point $(Q^2=0, \nu = 50$ GeV$)$ are loci of equal lepton angles for E=50 GeV. Fig. 2 is the corresponding graph for E=20 GeV.

If all the final hadrons are in thermal equilibrium, we can estimate the pion multiplicity $<n\pi >$, which depends only on W. The opening angle for the hadron jet is of order γ_W^{-1}. The rising parallel lines in Figs. 1 and 2 correspond to different values of $<n\pi >$. We believe this model provides an upper limit to the multiplicity and serves to emphasize the scope of the experimental task in detecting neutral pions.

B. Dynamics

    1. Differential Cross Section

The differential cross section for the interaction of neutrinos on hadrons can be written in terms of the quantities just defined as

$$\frac{d^2\sigma}{dQ^2 d\nu} = \frac{G^2}{2\pi} \frac{E'}{E} \beta \left\{ 1 - \frac{Q^2}{4EE'} + \frac{\nu^2 + Q^2}{2\,EE'} \left[(R)+(L) \right] + \frac{E+E'}{2\,EE'} \sqrt{\nu^2 + Q^2} \left[(L)-(R) \right] \right\}$$

(6)

where

$$\beta = W_2 = \frac{1}{2\pi} \frac{Q^2}{\nu} \frac{1}{(1 + \frac{Q^2}{\nu^2})} (1 - \frac{Q^2}{2M\nu})(2\,\sigma_S + \sigma_R + \sigma_L)$$

(7)

$$(R) \equiv \frac{\sigma_R}{2\sigma_S + \sigma_R + \sigma_L} \quad , \quad (L) \equiv \frac{\sigma_L}{2\sigma_S + \sigma_R + \sigma_L}$$

(8)

where σ_R, σ_L and σ_S are cross sections for the appropriate helicity states.

For $Q^2 << \nu^2$, Eq. (6) becomes

$$\frac{d^2\sigma}{dQ^2\,d\nu} = \frac{G^2}{2\pi}\,\frac{E'}{E}\cdot\beta\left[1 + \frac{\nu}{E'}(L) - \frac{\nu}{E}(R)\right] \qquad (9)$$

or

$$\frac{d^2\sigma}{dx\,dy} = \frac{G^2\,M\,E}{\pi}\nu\beta\left[(1-y) + \frac{y^2}{2}((R)+(L)) + y\left(1-\frac{y}{2}\right)\{(L)-(R)\}\right](10)$$

where

$$\nu\beta = \frac{Q^2}{2\pi}(1-x)(2\sigma_S + \sigma_R + \sigma_L) \qquad (11)$$

and

$$x \equiv \frac{Q^2}{2M\nu} \quad , \quad y \equiv \frac{\nu}{E} \, , \qquad (12)$$

$$0 \leq x \leq 1, \; 0 \leq y \leq 1 .$$

Some motivation for the use of the variable x can be seen if one supposes that the neutrino might scatter off only a fraction, x, of the nucleon. The kinematics of quasi-elastic scattering is obtained by replacing M by xM. It would be represented in Fig. 1 by a radial line from the origin with a slope x times that of the one for $Q^2=2M\nu$. Bjorken has shown that at high incident energies if the parts are point-like the σ_R, σ_L, and σ_S are functions of x only (scale invariance). Consequently, when one integrates equation (10) over x and y one obtains $\sigma = (\text{constant})\cdot E$, a relation that we can test experimentally provided we detect all final states.

2. "Spin-$\frac{1}{2}$-Parton" Model

To obtain a feeling for where events would lie in the $Q^2 - vs - \nu$ plane for the "spin-$\frac{1}{2}$-parton" model, we have set $\nu\beta = (\text{constant})\cdot (1-x)$ and $\sigma_R = \sigma_S = 0$. Fig. 3 shows how 1000 50-GeV neutrino interactions would be distributed under these assumptions. The important point is that all sectors contain statistically significant populations.

3. Pomeranchukon-Exchange Model

Predictions for the Pomeranchukon-exchange model can be obtained by setting $\mathbf{v}/\beta$ = (constant) $(1-X)$ and $\sigma_L = \sigma_R$, $\sigma_S = 0$. The distribution of 1000 events at 50 GeV for these assumptions are shown in Fig. 4.

We propose to make our detection efficiency high in all sectors of the Q^2 -vs-$\mathbf{v}$ plot and consequently, to be able to measure the total cross section.

4. Fireball Model

We introduce the notion of the hadron system being in thermal equilibrium to obtain a crude idea as to what the pion multiplicity might be and how this fireball will emit its products in the lab system. It can be shown that half of the products will be emitted into a cone of half angle,

$$\Theta_{cone} \approx \gamma_W^{-1} \approx \sqrt{\left(\frac{2\,M}{E}\right)\frac{(1-X)}{y}} \quad . \tag{13}$$

The laboratory angle for the final lepton is

$$\Theta_\mu \approx \sqrt{\left(\frac{2\,M}{E}\right)\frac{X\,y}{(1-y)}} \quad . \tag{14}$$

and for the laboratory direction of the hadron system is,

$$\Theta_H \approx \sqrt{\left(\frac{2\,M}{E}\right)\frac{X}{y}(1-y)} \quad . \tag{15}$$

In order to summarize the production and decay processes, we distort the triangular sectors of Fig. 3, 4 into rectangular ones. Within the rectangular sectors we draw pictures of how the events might look. The kinematics of the outgoing hadron system and final lepton are shown for some of the sectors/ Most hadrons will be obtained within
in Fig. 5a.
the shaded cones; the vector is the outgoing lepton momentum. Fig. 5b summarizes the corresponding information at E=20 GeV. The hadron

‹c ones are constructed with pessimistic (it predicts too many π^0's with cone angles too large) assumptions, namely, those of a fireball model for the hadron system. The Pomeranchukon-exchange model would predict cones with smaller opening angles and smaller meson multiplicity.

Bjorken and Paschos[1] point out that the difference, $\sigma_\nu - \sigma_{\bar{\nu}}$, is very model dependent. We wish to expose the chamber to both ν and $\bar{\nu}$.

C. Event Rate

In estimating the event rate, we assume the radial distribution for the neutrino beam at the detector obtained from the spectra of D. Carey, et al.[2], (reproduced here as Fig. 6c). We then integrate Eq. (10) over x and y, assuming σ_R, σ_L, and σ_S are functions only of x. The resulting total cross section is proportional to the neutrino energy E. The event rates are calculated for two assumptions: a.) the linear relation, $\sigma = 0.8$ E GeV x 10^{-38} cm^2, holds for all energies; and b.) the cross section saturates at E = 10 GeV and remains constant at 8×10^{-38} cm^2, for higher energies.

The lower set of curves in Fig. 6a indicates the number of neutrino interactions per GeV per 10^6 beam pulses (at 2×10^{13} protons/pulse) per 10^{-38} cm^2. The upper set of curves in Fig. 6a is for assumption a, $\sigma = 0.8$ E (GeV) x 10^{-38} cm^2, while curves for assumption b with a saturated cross section at 8×10^{-38} cm^2 are shown in Fig. 6b. Also shown in Figs. 6a, b are histograms for the number of interactions per 10^6 pulses that lie within 1 meter of the beam axis. Because there is so much uncertainty about K^- yields and hence $\bar{\nu}$

flux, we show no corresponding curves for antineutrinos.

D. Measurement of $\dfrac{d\ N\nu,\bar{\nu}}{d\ E\nu,\bar{\nu}}$

    1. Neutrino Energy Spectrum

In determining cross sections, one must first find the energy
spectrum of the incident neutrinos. This spectrum, normalized with
the data obtained from the neutrino flux monitor, gives the number
of neutrinos incident in each energy interval during the course of
the experiment. Neutrino events occurring in the bubble chamber can
then be assigned to the appropriate intervals once the total energy
of the final-state particles has been measured.

    2. Measurement of Meson Production by Protons

As part of an initial beam survey, measurements should be made
of meson production by protons of 200 GeV from targets of H_2, D_2, Li,
Be, and Al. Data are needed for pion momenta above 20 GeV/c and
laboratory angles between zero and 20 milliradians. Similar studies
should be carried out at 500 GeV as soon as protons of this energy
become available.

We feel that our understanding of the production mechanism would
be significantly enhanced if a bubble chamber of modest size were ex-
posed to primary protons at 200 and 500 GeV. Attention would be
focused on low-energy charged kaons and pions corresponding to the
backward jet in the center-of-mass system. We therefore endorse,
and some of us would like to participate in, the bubble-chamber survey.
proposed by G. Snow.[3] We suggest that NAL investigate the possibility
of making the bending magnets of area 2 capable of bending 500 GeV
protons. Exposure of only 10 to 20 protons per pulse are needed.

The quadrupoles could remain at their 200 GeV values.

3. Meson-Focusing System

The meson-focusing device should maximize the neutrino flux at 35 GeV with incident protons of 200 GeV. To reduce systematic errors in the cross sections resulting from uncertainties in the neutrino energy and thus the neutrino flux, the meson-focusing device should simultaneously minimize the logarithmic derivative,

$\left| d \ln \frac{d N_\nu}{d E_\nu} / d \ln E_\nu \right|$. This can be accomplished by eliminating those mesons that produce low-energy neutrinos ($E < 15$ GeV) and by focusing those mesons that produce neutrinos near 35 GeV. The low-power, high-band-pass devices proposed by Frisch and Kang[4] and by Palmer[5] appear to be well suited to the neutrino energy selection required. For our hybrid system a one-millisecond beam spill would be ideal, that is, short enough for the bubble chamber and long enough for the electronic devices. (We anticipate of order 1 neutrino interaction per pulse in the quantameter and of order 100 per pulse in the hadrometer. The "deadtime" of these instruments is less than 1 μ sec.)

4. Neutrino Flux Monitor

Wachsmuth[6] has described a monitoring system for the neutrino flux which measures essentially the longitudinal and radial distributions of muons within the muon shield in front of the bubble chamber. We believe such a system is necessary for reliable operation of the neutrino beam, as well as for the flux determinations required in obtaining cross sections.

E. Measurement of the Neutrino Energy

1. Curvature and Total Energy of Charged Hadrons

The neutrino energy, E or E_ν, $\bar{\nu}$, is determined for each event

by measuring the energies of all outgoing particles. The energy of the charged-hadron component is given most precisely by track curvature in the 30-KG field of the bubble chamber, while a less-precise check is obtained from the hadron calorimeter associated with muon identification. The hadrometer is limited primarily by the statistics of hadron cascades in which, unlike electromagnetic cascades, a significant and variable fraction of the energy is lost to secondary neutrinos, slow neutrons, and nuclear binding energy.[7] Fluctuations in these losses are characteristic of all hadron calorimeters, and they point up one of the major advantages of the bubble chamber as a tool for doing neutrino physics. Curvature should give the charged-hadron energy to $\pm 3 \, ^o/_o$, while the hadrometer resolution and precision for single events may be about $\pm 10 \, ^o/_o$ at 35 GeV.[7]

2. Total Energy of π^o's via Proportional Calorimeter

Considerable thought has been given to ways in which neutrals could be detected in the large H_2, D_2 bubble chambers.[8] For chambers of volume exceeding 100 m^3, it is possible to place track-sensitive inserts of H_2 or D_2 into mixtures of H_2-N_e and obtain effective volumes* of order 30 m^3 for neutrino physics. NAL has proposed a chamber smaller than 100 m^3, namely 30 m^3, similar to the proposed BNL 14-foot chamber. The effective volume of inserts into this 12-foot-diameter sphere are less than 3 m^3, a volume that would yield too few events in the high-energy region.

---

*"Effective volume" is the volume of the insert multiplied by the efficiency for detecting all of the photons from neutral pions in the H_2-N_e mixture.

To permit the necessary determination of the neutral pion energy, we propose to take advantage of a special feature of the NAL 15-foot (30 m^3) bubble chamber design -- namely the thin exit wall of 1/2" steel, less than one radiation length. The thin wall implies that photons from π^o decay can be detected efficiently and the total shower energy measured precisely by a cylindrical π^o quantameter[9] at the downstream end of the chamber. A possible arrangement is shown schematically in Figs. 7 and 8. The quantameter itself is described in more detail in Section III. The total-energy resolution should be better than ± 3 $^o/_o$ for events in which the total energy into neutral pions is above a few GeV. Precise calibration would then permit an absolute determination of the π^o component in a single event to about the resolution limit.

We propose to install the quantameter in a special reentrant well constructed in the vacuum tank downstream of the hydrogen volume. This location, shown in Fig. 8 requires that the coil diameter be extended about 1/2 meter. These modifications, in addition to permitting a quantameter of 15 to 20 radiation lengths thickness, would preserve the entire useful volume of the bubble chamber. The volume assumed in calculating the yield histograms of Figs. 6a, b is a cylinder of 1-m radius, intercepting a sphere 3.6 m in diameter, and yielding a fiducial volume of 10 m^3. The volume outside this cylinder could be used as a blanket of H-N$_e$ mixture to detect wide-angle photons.

3. Total Energy of Hadrons via Proportional Calorimeter

charged

The total energy of the /hadrons (charged pions, protons and

antiprotons) would be obtained most accurately from track curvature in the bubble chamber; the nuclear cascades in the hadrometer furnish another, less accurate, measure of charged hadron energy. However, the hadrometer will catch neutrons, which escape bubble chamber detection, and will measure their energy. All hadrons will be absorbed within 15 interaction lengths. Optical spark chamber planes at various depths would sample particle trajectories and indirectly measure ionization. Muons above 2 GeV would penetrate the hadrometer. Thus the hadrometer serves three purposes: it stops hadrons permitting muon identification, it measures hadron energy, including the energy of any neutrons emitted from the neutrino vertex, and it follows tracks spatially.

The hadrometer would be located just outside the bubble-chamber magnet as close to the magnet as practical. It's configuration might approximate a vertical half-cylinder, similar to the quantameter, although rectangular modules, such as those shown in Fig. 8, appear to be more practical.

4. Lepton Total Energy

The momentum of the final lepton is measured by curvature. Like the curvature measurements of the charged-hadron energy, this possibility is a major advantage of the bubble-chamber approach: peripheral equipment is required only to <u>identify</u> escaping muons, not to stop them or otherwise determine their energy. Final electrons are identified in the quantameter. Thus the hadrometer or absorber used with the bubble chamber is much thinner than the full muon range. This, in turn, permits much larger solid-angle detection for muons at an acceptable cost -- a feature well matched to intrinsically large solid angle of the bubble chamber.

Any particle penetrating 10-15 collision lengths of hadrometer is almost certainly a muon. Proportional (Charpak) chambers[10] or wire chambers can be used to locate the muon path with high spatial resolution. ·The muon may be identified by projecting each track · from the vertex through the quantameter and hadrometer and testing whether its location at the final muon detector is consistent with location at the observed track. We propose to build into the quantameter and hadrometer a number of coordinate-sensitive planes to follow each track in detail, tracing each detected muon backwards into the bubble chamber.

F. Measurement of Structure of Hadronic State

The bubble chamber is ideally suited to studies of the final hadronic system. Hadrons, like muons, trapped in the magnetic field can usually be identified by their interactions in the hydrogen of the chamber. A much larger class of events can be studied in detail by tracing individual tracks through the quantameter and into the hadrometer where energetic nucleons in the final state may possibly be identified.[11]

Similarly, detailed information on individual π^o's and η^o's can be obtained from a knowledge of the vertex location and the origins of correlated γ showers. In many cases, for example, the π^o energy can be determined from the photon opening angle, and in some cases a separation of π^o and η^o decays should be possible.

·A· procedure of the type just discussed requires extensive use of coordinate-sensitive planes. The proportional-calorimeter design described in Section III permits several planes per gap or per

plate without interfering in any way with the determinations of neutral pion or hadron energy. This option is a major advantage of the proportional (Charpak) chamber.[10]

G. Possible Hadronic Decay Modes of the Intermediate Vector Boson (IVB)

If the mass of the IVB is large many decay modes are possible.[8] Again the high measurement accuracy of the bubble chamber makes it an ideal instrument for detecting these modes. Provided the mass of the IVB is not too large, its width is likely to be much smaller than the experimental resolution function of the bubble chamber. Thus the signal/noise will be improved with increased measurement accuracy.

We list below in diagramatic form some examples of the possible hadronic decay modes of the IVB.

Baryon-Antibaryon

$$W^{\pm} \rightarrow \overline{H}_8 (\tfrac{1}{2}^+) + H_8 (\tfrac{1}{2}^+)$$
$$\rightarrow \overline{H}_8 (\tfrac{1}{2}^+) + H_{10} (\tfrac{3}{2}^+)$$

Boson-Antiboson

$$W^{\pm} \rightarrow \overline{H}_8 (0^-) + H_8 (1^-)$$

The symbol $\overline{H}_8 (\tfrac{1}{2}^+)$ represents an antibaryon of the $\tfrac{1}{2}^+$ octet, etc.

Only those pairs of final particle-antiparticle states that are nearest neighbors in the Y —vs— T plot of Fig. 9 are allowed under the $\Delta S=0$ and $\Delta S=\Delta Q$ rules. For neutral IVB's (if neutral lepton currents exist) the nearest neighbors joined by the dashed lines would be possible decay products.

For low-momentum-transfer production the IVB would receive most of the energy of the incident neutrino. Consequently, the decay fragments would be thrown into a forward cone of half angle $M_W/2E$.

The quantameter would easily detect the π^o's that might be among the decay products.

III. EXPERIMENTAL EQUIPMENT

A. Neutrino Beam

1. Targets

The enhancement of the high-energy portion of the neutrino spectrum requires thin targets consisting of light nuclei. Fig. 10 (Fig. 4a of TM 218)[12] summarizes how the number of neutrinos above a certain energy depends upon the target thickness. Our requirement is for q > 2, thus the optimum target thickness is about 1 mfp. The detrimental effects on the high-energy neutrino spectrum of multiple interactions of the incident nucleon within a complex nucleus provide strong motivation for developing targets of very light nuclei. Experimentation and design studies for the neutrino target should begin as soon as possible.

2. Meson-Focusing System

We wish to participate in the design and testing of a meson-focusing device[4,5] to produce those special qualities in the neutrino beam alluded in Section II D.3.

3. Neutrino Flux Monitor

The CERN neutrino spectrum was measured by placing emulsions and ionization chambers at various depths and radial positrons in the muon shield to determine the muon flux at these points. Wachsmuth[6] asserts that if the pion and kaon spectra are known and the shield measurements taken, $\frac{d\,N_\nu}{d\,E_\nu}$ at the bubble chamber can be determined to about 5 $^o/_o$. The importance of determining $\frac{d\,N_\nu}{d\,E_\nu}$ is

so great for this experiment that some of us would like to participate in these measurements.

While the equipment relating to the neutrino beam would be part of the NAL facility, members of this proposal are prepared to participate in the design and development of this apparatus.

B. Hybrid Detector System

   1. 30 m^3 H_2, D_2 Bubble Chamber

The detector has already been discussed briefly in Section II, dealing with the type of measurements one might make. The hybrid system shown in Fig. 8 is built around the NAL bubble chamber and offers these advantages:

   a. precision on $E_{\nu} = E_{\pi}o + E_H + E_{\mu}$ to $\pm 3 \,^{\circ}/_{\circ}$,

   b. vertex information of the bubble chamber,

   c. absorber (hadrometer) thickness much less, than the muon range

   d. large solid angle,

   e. simplicity.

Of these, the first four follow immediately from the use of the bubble chamber itself, particularly its ability to measure E_H and E_{μ}, once the muon has been identified. Supplementary information on E_H, including identification of baryons, is provided by the hadrometer, while $E_{\pi}o$ is given solely by the quantameter. The advantage of simplicity follows partly from the relatively thin absorber required (since the bubble chamber measures E_{μ}) and partly from the use of porportional calorimeters to be described.

The reentrant cylindrical tank housing the quantameter is an

important change in the preliminary bubble-chamber design and
necessitates an increase in the coil diameter of about 1/2 meter;
this change will greatly increase the effectiveness of the bubble
chamber for both strong and weak interaction physics, particularly
in reactions involving final π^O's.

2. Ionization and Proportional Calorimeters

Parallel-plate ionization calorimeters, such as the quanta-
meters[9] widely used in monitoring photon beams, have several intrin-
sic properties that are essential in determining $E_{\pi}o$ and E_H accurately.
First, the response depends only upon the relative ionization in the
gas gaps as compared to the ionization in the plates; tolerances of
a few percent in these parameters are easily met and insure a uni-
form response to the same level. Second, since the ratio of gap to
plate is independent of track angle in a parallel plate chamber,
such a device is intrinsically isotropic. Third, the output of an
ionization calorimeter is linear in the energy absorbed over a wide
range. Fourth, an ion chamber is operated as a one-parameter device;
there is one high-voltage setting and one output signal proportional
to the total energy deposited in the chamber as sampled periodically
via the ionization in the gas gaps. This last feature greatly simpli-
fies the operation of the calorimeter and results in a highly repro-
ducible instrument.

In the case of electromagnetic showers $(E_{\pi}o)$, virtually all
of the energy appears ultimately in the form of ions, which are
sampled directly in the ionization calorimeter thereby avoiding
such questions as the response of scintillation or Cerenkov counters.

In the case of hadronic cascades, a certain portion of the energy is lost to neutrinos, slow neutrons, and nuclear binding, as mentioned previously.[7] A typical loss might be 20-30 $^{o}/_{o}$ at 35 GeV, although for some events the loss may be catastrophically large. Within the statistical uncertainties of this process, the response is similar for all hadrons, including high-energy neutrons, providing the absorber thickness is sufficient to contain the cascade. The actual gain can be determined by calibration with hadrons of various energy.

The only serious limitation of ionization calorimeters, as far as the present application is concerned, is their relatively low gain, typically[9] 4×10^3 ions per GeV absorbed with 1-atm of A-CO_2. This small signal appears across the relatively large capacity of the parallel plate structure and is not easily detected.

A much higher gain is possible by using the high electric fields surrounding small-diameter (20-100μ) wires to induce proportional avalanche multiplication. Proportional calorimeters[10] retain the uniformity, isotropy, and linearity of ion chambers, and if the signals from the high-voltage plates are added, there is one high-voltage setting and one output signal. The gain of a proportional chamber, unlike an ion chamber, varies exponentially with the high voltage, but good reproducibility can be obtained.

Proportional chambers cease to be linear when the space charge in single avalanches appreciably distorts the electric field near the wires. This occurs typically at 5×10^6 ions, and the high voltage is normally set low enough so that this condition is not

exceeded.

A crucial point in our application is that the primary
ionization of the shower, consisting of some 4000 ions/GeV, in
the gas, is distributed over several hundred tracks in perhaps
10 gaps. As many as 10^3 avalanches may be thus involved so that
an output of 5×10^9 ions or more can be obtained without exceeding
the linear response region. This largely compensates for the greater
capacity of a pair of plates or of an entire chamber, as compared
with the capacity of a single wire, and it yields an output voltage
within one or two orders of magnitude of that normally obtained on
a single wire of a multiwire proportional chamber. Such a net
signal can easily be measured, and if necessary, one can afford
sensitive amplifiers since only a small number of total-energy
outputs are involved. (The situation is quite different when one
must read 10^3 to 10^4 separate wires.)

3. Proportional Quantameter

We presently envision the proportional quantameter to consist
of 15 lead plates and a similar number of gas gaps totaling 15
radiation lengths of lead, about 9 cm. A sector $90^\circ \times 90^\circ$ measured
from the center of the bubble chamber would be about 4 meters high
with a 3-m arc and would weigh about 12 tons. Each double gap would
consist of a single wire plane centered between two lead plates and
defining a total gap of 2x.5 cm = 1.0cm. Fifteen of these gaps would
add an additional 15 cm to the quantameter thickness. Allowing an
additional 5 cm for flanges and windows, we obtain a total quanta-
meter thickness of about 30 cm. A 35-cm-wide reentrant tank would

· allow, in addition, the installation of a couple of scintillation counters or possibly a two-gap spark chamber. Note that the steel walls of the bubble chamber and the reentrant wall will amount to 1-2 radiation lengths and may be considered as the first plate of the quantameter, while the quantameter at 1 collision length may be considered the first plate of the hadrometer. The quantameter itself might then begin with a sensitive gap followed by the first lead plate.

The wires of the proportional quantameter will be read out to provide spatial resolution. A wire diameter of 50μ and a spacing of 2mm is probably convenient[10] although 1mm seems feasible if one is willing to try hard enough. Vertical wires are straight forward in the cylindrical configurations, but horizontal wires may force a modular quantameter design with flat parallel plates.

4. Hadrometer

The hadrometer would consist of about 20 walls of heavy concrete (density = $3.5 \frac{gm}{cm^2}$) 25 cm. thick, separated by 2-gap optical spark chambers. This thickness of concrete provides 14 collision lengths (and 67 radiation lengths) of absorber. The 12-cm lead of the quantameter is equivalent to about 1 collision length for hadrons. The copper coils of the bubble chamber magnet amount to several collision lengths but do not seriously limit the accuracy of the hadron-energy determination for most event types.

We presently envision a hadrometer subtending vertical and horizontal angles of about 90° by 90° as measured at the center of the bubble chamber. The volume of concrete would then be 8mx8mx5m and the weight about 1200 tons. The full 180° azimuth in the bending plane

could be covered (thinner at wide angles) with 2000 tons.

Optical spark chambers with 90° stereo viewing would be used to record muon tracks and nucleonic cascades within the hadrometer. We presently plan 20 planes distributed in an optimum manner to record the maximum number of sparks per cascade. Neutron-initiated cascades will be distinguished from charged pion/proton cascades by lack of incident track. Calibration of total sparks/GeV can be done using protons. Since the typical neutron energies is expected to be a small fraction of the total only, crude energy resolution ($\pm 30 \,^{\circ}/_{\circ}$) is required to retain overall $\pm 5 \,^{\circ}/_{\circ}$ precision in hadron energy.

Muons tracks should be quite distinctive due to lack of inter-action in the hadrometer.

"Accidental" neutrino-induced background within the hadrometer should be distinct from neutron-induced cascades, due to muon second-aries. Assuming that the beam is spilled over 1 millisecond, these accidentals (occurring within spark-chamber sensitive time) should be rare.

5. Range Detector for Muons Leaving the Bubble Chamber

Highly non/peripheral events produce muons at large angles and at sufficiently low momenta that the muons can be trapped in the bubble-chamber magnetic field. Muons of a few GeV and more pass through the 14 collision lengths of photon and hadron absorber and can be identi-fied in that way. A single plane of scintillators downstream of the hadrometer might suffice, while the last several gaps of the hadrometer could provide the spatial resolution necessary to permit muon tracks to be traced back to the bubble chamber. Events with muons in an inter-

mediate energy range, for example the range from 1 to 3 GeV, may frequently remain ambiguous, as far as muon identification is concerned unless the hadrometer subtends a very large solid angle and unless individual tracks are followed through each plane of the hadrometer until they stop.

6. Triggering Options

Signals should be available from the quantameter and hadrometer

within 100 ns of the occurence of an event and with a time jitter
of less than 50 ns.[10]. These signals, in coincidence with scintil-
lator planes, could be used to develop a trigger requiring an inter-
action having total energy above, for example, 10 GeV. Four
scintillator planes might suffice: an anticounter in front of the
bubble chamber, a yes-counter in front of the quantameter and another
in front of the hadrometer, and finally the muon counter plane
already mentioned. The trigger could be used to flash the bubble
chamber illumination or fire peripheral spark chambers, or it
could simply be recorded for use in analyzing the bubble-chamber
film. We presently favor the last option, at least during the
early stages of the experiment.

IV. SCHEDULES AND PARTICIPATION

A. Design and Development of Equipment

We shall explore ways in which the participating groups, and
particularly LRL as a service to other users, can participate in
the design and development of the neutrino beam, quantameter, hadro-
meter, counters and modifications of the bubble chamber. Arrange-
ments for sharing the cost should be negotiated between our groups
NAL, and AEC.

B. LRL Development

Work should begin immediately on some of the special items
just mentioned. Among these is the design of the reentrant tank
for the quantameter, which could be carried out by LRL mechanical
engineers skilled in cryogenic equipment. The design could proceed
at Berkeley in close collaboration with W. Fowler and his group at

NAL. In addition, the shop and experimental facilities of LRL could be made available to the University of Hawaii group and others involved in developing the quantameter and hadrometer.

C. Participation of Our Personnel at NAL.

The development of the neutrino beam equipment would best be done at NAL. We would hope to make the experience of graduate students stationed at NAL as broad as possible. Thus, while a major fraction of their time would be devoted to development of the neutrino facility and bubble chamber, their direct participation in construction and other activities of the accelerator should be encouraged.

D. Beam Survey Experiment

The meson production measurements should start as soon as the survey beam (10^{10} proton/pulse) is available in Area 2. Here, we could provide experienced personnel and some equipment to aid groups that have made specific survey proposals involving major hardware commitments.

A survey bubble chamber of the type suggested by Snow[3] should be available at the turn-on date of Area 2. The present film and data-analysis equipment at our participating institutions is adequate to handle exposure of several hundred thousand pictures on both hydrogen and deuterium. The information from the yield measurements could be used to up-date the operating parameters of the meson-focusing device. Early exposures to 500-GeV protons would be very useful in designing the focusing for the 500-GeV phase. Since only ten or twenty protons per pulse are required, one might consider

designing the bending magnets of Area 2 (super conducting?) to bend
500-GeV protons, allowing the quadrupoles to remain set at their
200-GeV design values. At the low intensities required, no radiation damage would result to the beam transport equipment, and no
additional shielding would be required. Reliable, fail-safe intensity-control equipment would, however, be necessary.

E. Million-Picture Exposure at 200 GeV

The experimental program of preparing the neutrino beam for
this application could easily occupy the first year or more after
beam turn-on. The accelerator operation in its second and third
years is likely to be more reliable, and the bubble chamber will
be better understood. We therefore propose that a one-million picture exposure to hydrogen of both neutrinos and anti-neutrinos of
high energy be made in the second or third year of operation at
NAL. Similar exposures to deuterium would come later.

F. Million-Picture Exposure at 500 GeV

Our reason for requesting an exposure at higher accelerator
energy is to allow the energy at which we have a low value of
$\left| d \ln \frac{d N_\nu}{d E_\nu} \middle/ d \ln E_\nu \right|$ to be increased significantly. This,
in turn, would raise the central neutrino energy from 35 GeV to
70 GeV for an acceptable uncertainty in the number of neutrinos
incident. The 500-GeV exposure would occur at a much later date.

V. PRELIMINARY COST ESTIMATE

A preliminary cost estimate is given in Table I. The principal
assumptions are:

A.   Geometry shown in Fig. 8

B. $.50/pound for lead plates (container 18K),

C.   all wires readout, 2-mm wire spacing, 15 planes/chamber,

   $5/wire to readout, $1.50/wire to fabricate the quantameter,

   $ _ _ _ _ _ _ _ _ _ _ _ _ _ _ _ _ _ _

D. $250/per cubic yard for heavy concrete.

TABLE I

Preliminary Cost Estimates (All Wires Read Out)

			Cost K$	Cost K$
1.	Modifications of Bubble Chamber Coils and Vacuum Tank		300	300
2.	Quantameter:	Lead Plates and Container	40	
		15 Wire Planes	30	
		15x4m/2mm=30,000 Readouts x $5/wire	150	220
3.	Hadrometer:	Concrete (1200 tons at $250/ yds.^{3})	100	
		Optical Spark Chambers	100	
		Camera and Mirrors	100	300
4.	Counter Planes:	4mx4m Anti (8 scintillators 16 PMS)	20	
		4mx4m Yes at Quantameter In	20	
		8mx8m Yes at Hadrometer In (16 scintillators, 32 PMS)	40	
		8mx8m Yes at Hadrometer Out	40	120
5.	Computer Interfacing		50	50
6.	Fast Logic, Slow Logic, etc.		50	50

TOTAL = $1040K   (90°x90° Hadrometer)

REFERENCES

1. J.D. Bjorken and E.A. Paschos, SLAC-PUB-678, December, 1969 (Lectures by Bjorken at 1969 Summer Study).

2. D. Carey, Y.W. Kang, F.A. Nezrick, and R. Stefanski, TM-222 "A Note on the 200-GeV Neutrino Design."

3. G.A. Snow (correspondent) "Preliminary Proposal to Study Multiparticle p-p and π-p Interactions from 75 to 200 GeV/c (and higher momenta as soon as they become available), April 23, 1970. University of Maryland High Energy Physics Group.

4. D. Frisch and Y.W. Kang, "D.C. Horn for Very-High-Energy Spark-Chamber Neutrino Experiments," 1969 NAL Summer Study 1, 389.

5. R.B. Palmer, "The Design of Long-Pulse Monopole Focusing Elements," 1969 NAL Summer Study 1, 383.

6. H. Wachsmuth, "Neutrino Spectrum Determination from Muon Flux Measurements," 1969 NAL Summer Study 1, 367.

7. V.S. Murzin, Progress in Elementary-Particle and Cosmic-Ray and Cosmic-Ray Physics, (North-Holland Publishing Company, Amsterdam, The Netherlands, 1967), Vol. IX, p. 245.

8. See for example M.L. Stevenson, "High-Energy Neutrino Physics $< E_\nu > 20$ GeV and the Constraints Placed on Detectors," 1969, NAL Summer Study 2, 121.

9. R.R. Wilson, Nucl. Instr. 1, 101 (1957). A high-energy (multi-GeV) quantameter is described by D. Yount, Nucl. Instr. Methods 52, 1 (1957).

10. G. Charpak, D. Rahm, and H. Steiner, "Some Developments in the Operation of Multiwire Proportional Chambers," CERN Preprint.

11. A. Pais, "Weak Interactions at High Energies," Presented at the Conference on "Expectations for Particle Reactions at the New Accelerators," University of Wisconsin, 1970; S.D. Drell and Tung-Mow Yan, "Final Particle Correlations in Deep Inelastic Lepton Processes," Phys. Rev. Letters 24, 855 (1970).

12. M.L. Stevenson, "Targets for the Neutrino Beam: Concepts," NAL Report TM 216.

13. D.D. Jovanovic, R. Palmer, and B. Roe, "Muon Detectors after the 25-foot Chamber" NAL 1969 Summer Study, 2, 207.
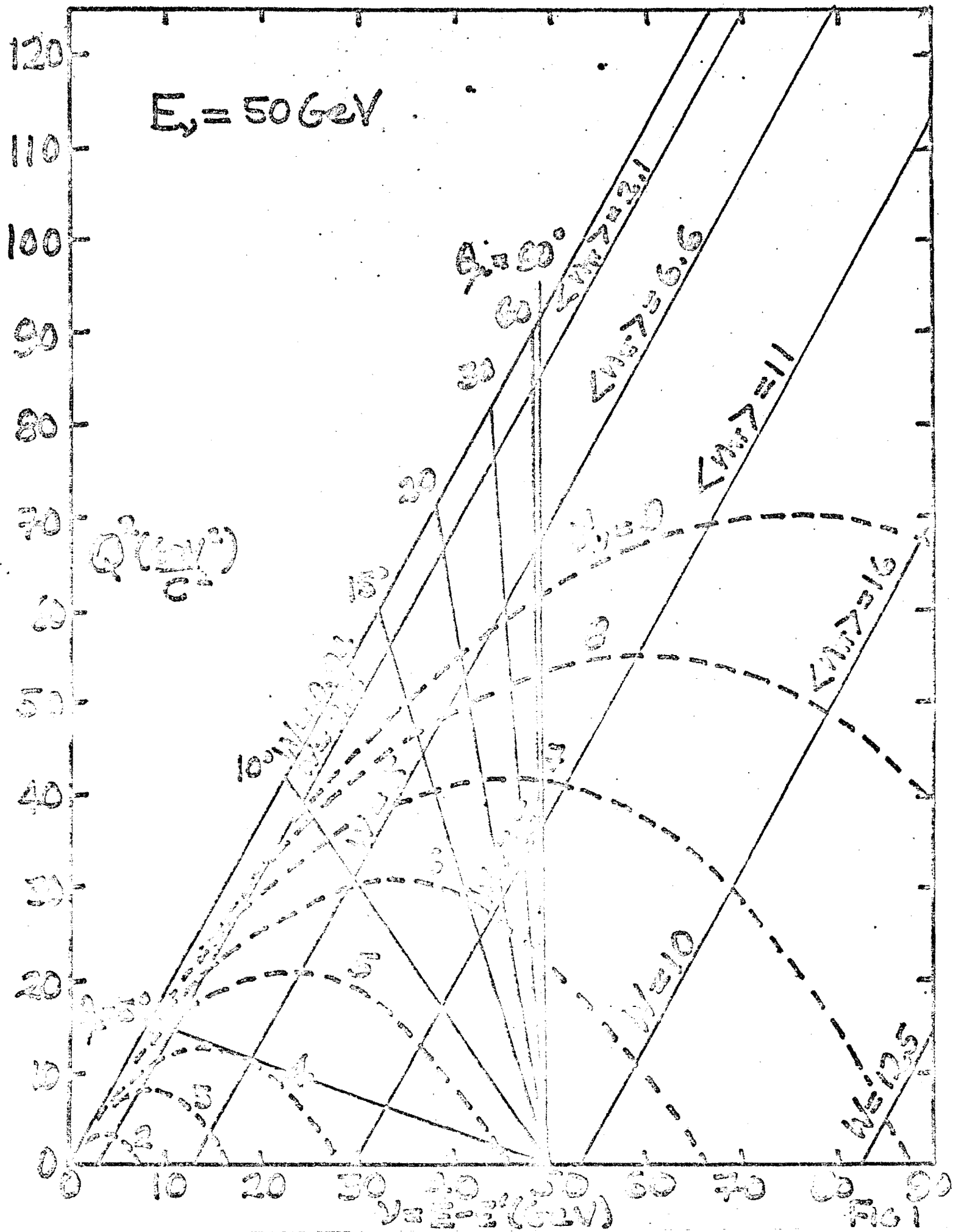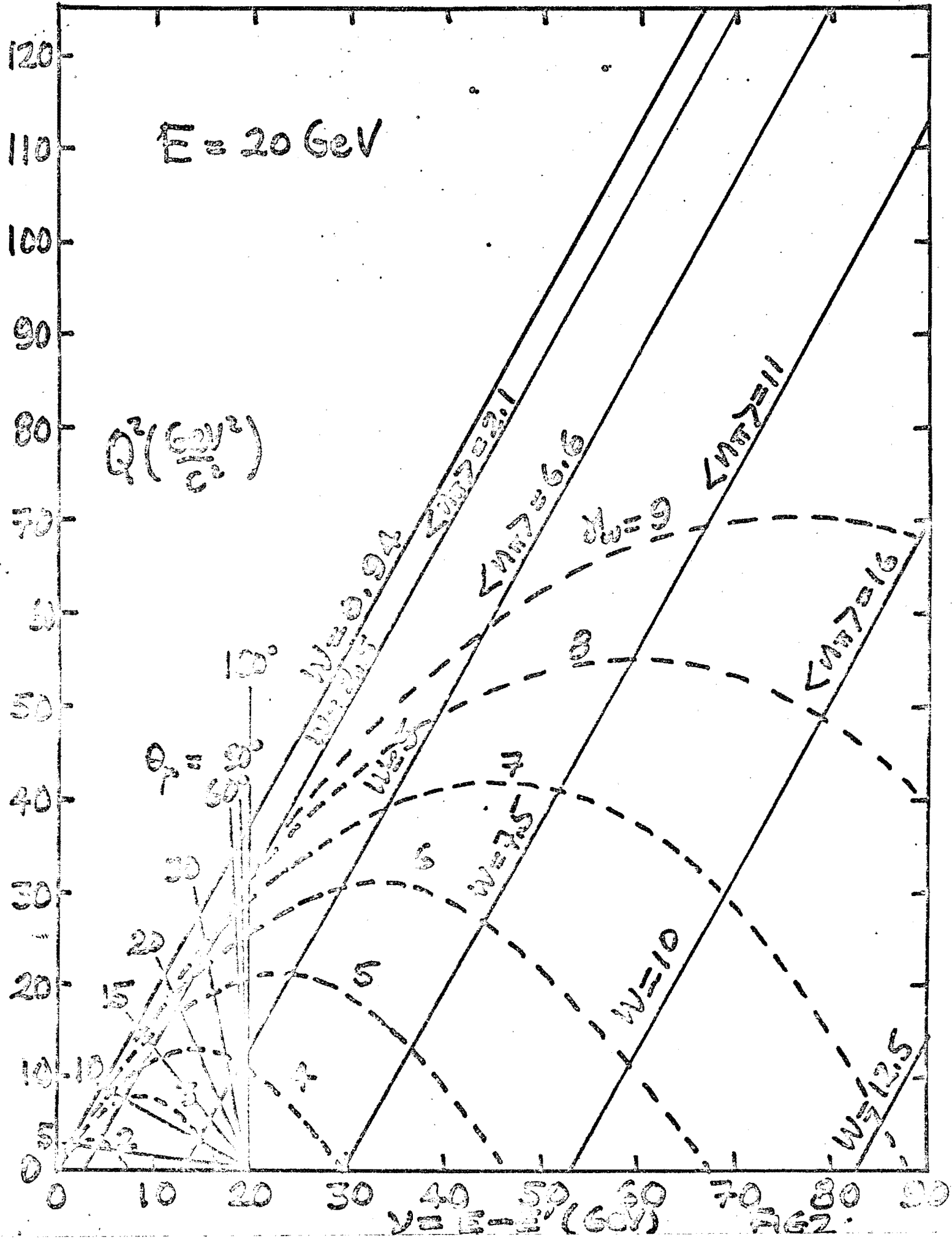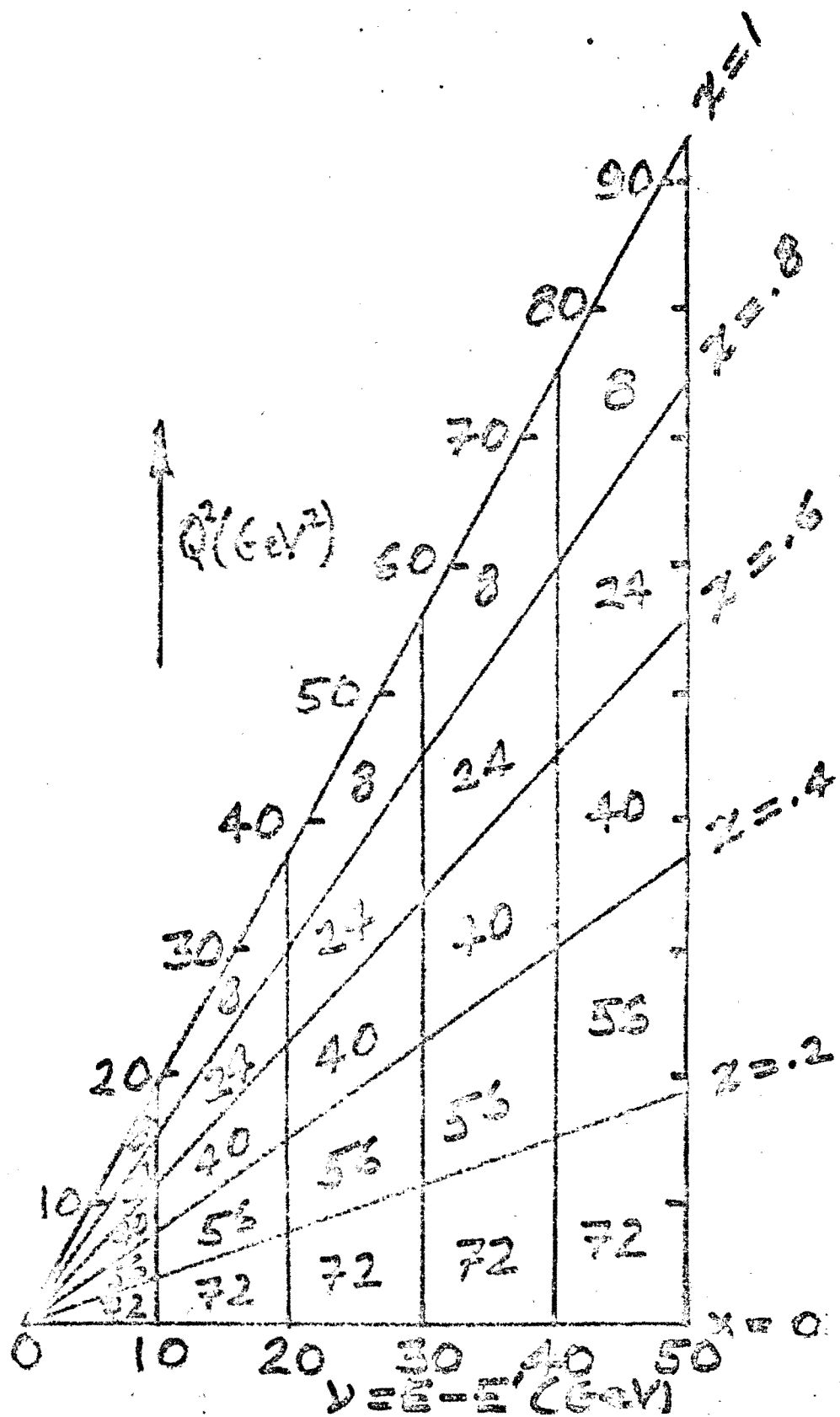
Fig. 1

$E = 20 \, GeV$

$Q^2 \left(\frac{GeV^2}{c^2} \right)$

Distribution of 1000 Events

$Q^2 (GeV^2)$

$y=1$

$z=.8$

$z=.6$

$z=.4$

$z=.2$

$x=0$

$E_\nu = 50\,GeV$

for $xy = K(1-x)$

$\sigma_R = \sigma_S = 0$

SPIN $\frac{1}{2}$ PARTONS

$M_W = \infty$

90

80

70

60

50

40

30

20

10

8 8 24

24 24 40

40 40 55

5³ 5³ 72

72 72 72

$\nu = E - E' \, (GeV)$

0   10   20   30   40   50

FIG 3.

Distribution of 1000 Events

$Q^2 (GeV^2)$

N
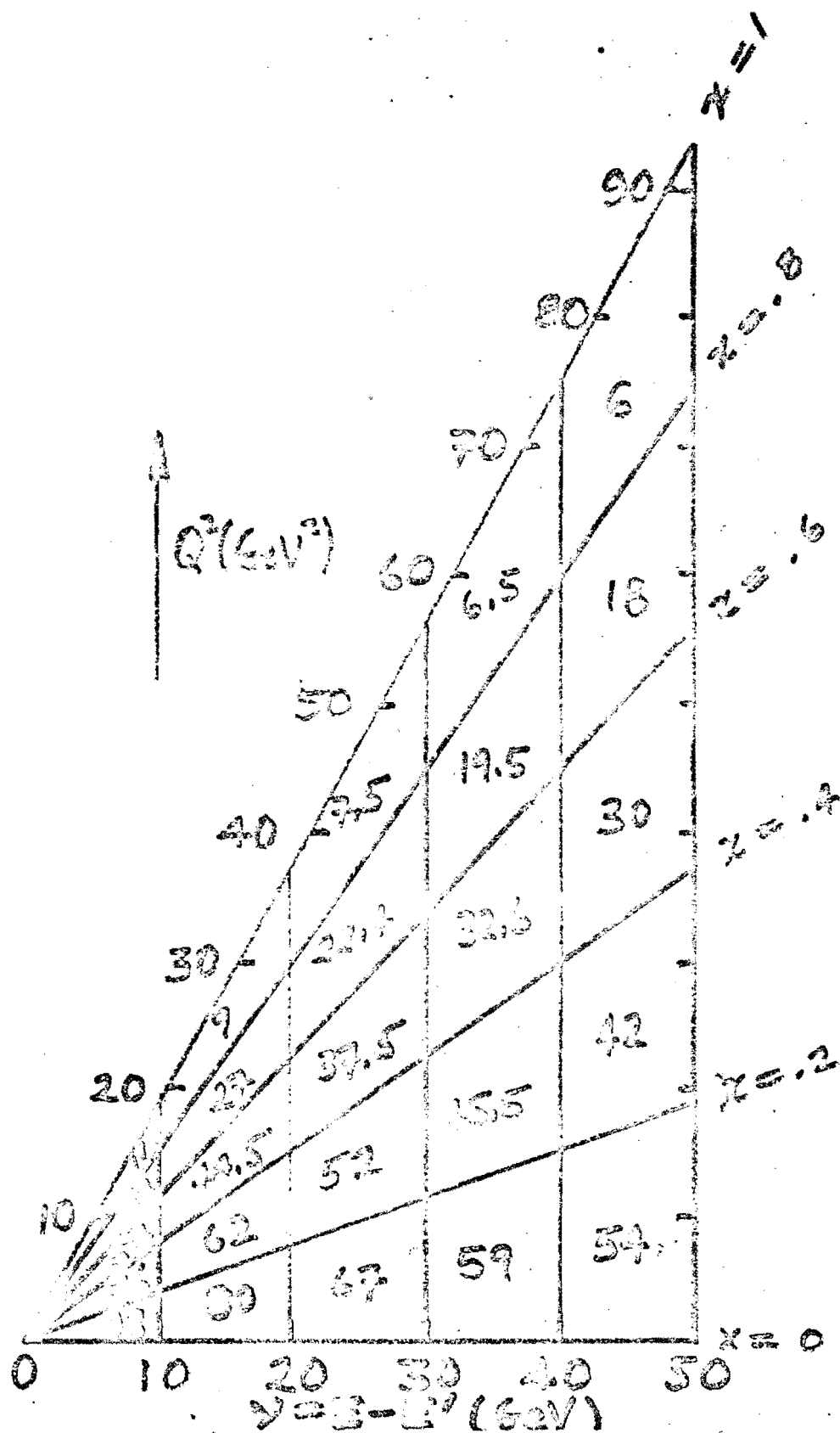
$E_\nu = 50\,GeV$

for $y \doteq k(1-x)$

and $\sigma_L = \sigma_R$

(POM. EXCH)

$M_W = \infty$
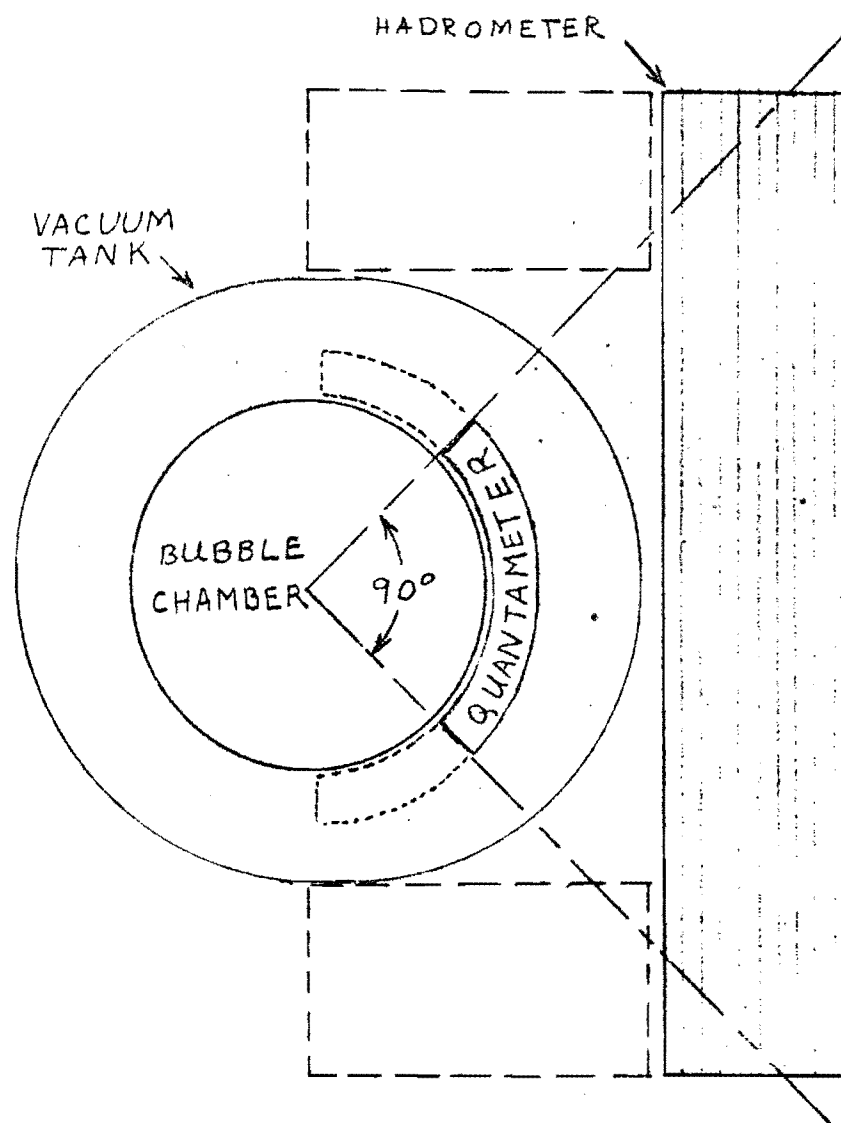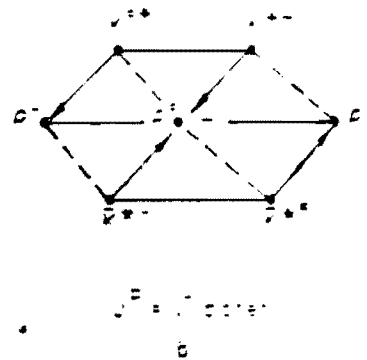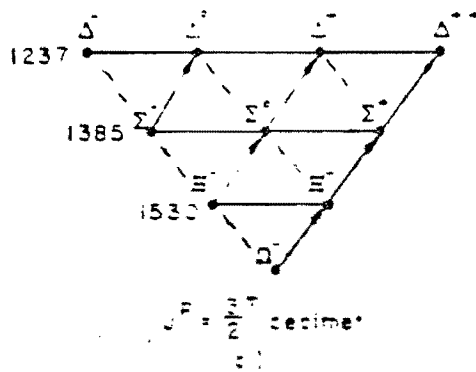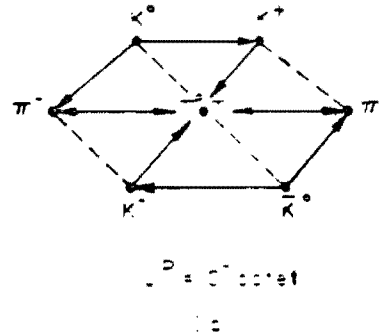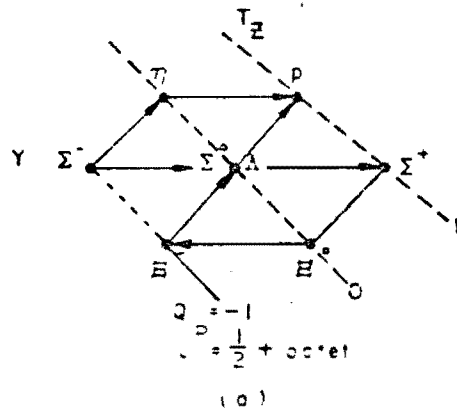
$x = .8$

$x = .6$

$x = .4$

$x = .2$

$x = 0$

90

80

6

70

60   6.5   18

50

40   19.5   30

30

20   42

10

62   67   59   54.7

$y = 3 - E'' (GeV)$

FIG 4

Fig 5a

E = 20 GeV

z

$\langle n_{\pi} \rangle = 0$ 0   0   0.5   1.0

$\langle n_{\pi} \rangle = 1.0$ 3.4   5.1   6.5   7.6

$y = \nu/E$

FIG. 5b

Number of ν Interactions/10^6 pulses per 5 GeV, r=1m.

$\sigma = .3 \, E(GeV) \, 10^{-38} \, cm^2$

r
1.0 m
.75
.10
.5
$\}$ $\sigma = 3.83 \times 10^{-38}$ all E.

r
1.0 m
.75
.10
.5
$\}$ $\sigma = 10^{-38} cm^2$

Yields in NAL 12' Spherical H_2 Bubble Chamber using neutrino flux calc of Cocconi et al. TM1222 (Fireball model at 200 GeV)

E(GeV)

Number of ν Interactions/10^6 pulse
per 5 GeV

for $\sigma = 8 \times 10^{-39} \text{ cm}^2$

r
1.3 m
1.5
1.0
.5

E(GeV)

Fig 6C

30 m³ Hybrid Bubble Chamber for NAL

π° Quantameter

12' ∅ Bubble Chamber

Superconducting Coils (30 kilogauss)

Fig 37

HADROMETER

CAMERA AXIS

QUANTAMETER

VACUUM TANK

BUBBLE CHAMBER

90°

SIDE VIEW

VACUUM TANK

HADROMETER

BUBBLE CHAMBER

90°

QUANTAMETER

TOP VIEW

FIG. 8

Fig. 9

$$\lambda = \lambda_\pi$$

$$\frac{n(>Q)}{n_0 E_0^{1.4} e^{-q}} = \left(\frac{e^{\beta e^{-\ell/\lambda}} - 1}{\beta}\right)$$

$$q = P_{thresh}^{meson}/T_0$$

$$T_0(200\,GeV) = 16.2\,GeV$$
$$T_0(400) = 27.3\,GeV$$

$$q_{max}(200) = 12.3$$
$$q_{max}(400) = 14.7$$

$$\beta = (1-K)^K$$
K = nucleon inelasticity $\approx \frac{1}{3}$

q = 0
q = 1
q = 2
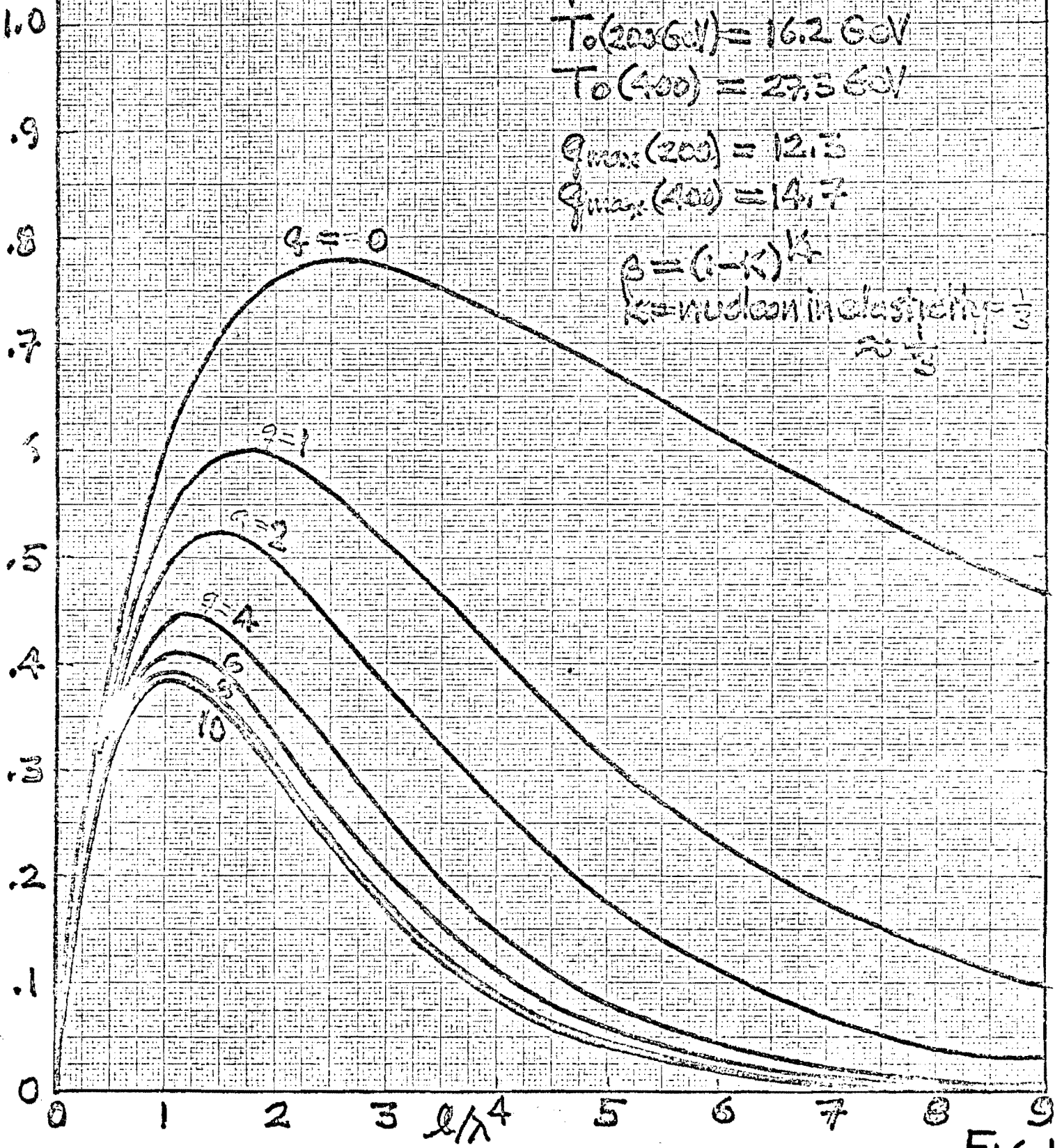q = 4
6
8
10

ℓ/λ

FIG 10

SUPPLEMENT TO NAL PROPOSAL (#9) FOR A HIGH ENERGY

NEUTRINO EXPERIMENT IN THE NAL $30m^3$ H_2, D_2 BUBBLE CHAMBER

University of Hawaii (R. Cence, F. Harris, M. Peters, V. Peterson, D. Yount)

Northwestern University (S. Meyer)

University of California, Lawrence Radiation Laboratory (M. Alston Garnjost,

R. Birge, G. Goldhaber, J. Kadyk, S. Parker, M.L. Stevenson[*], G. Trilling)

July 1970

We wish to respond here to some of the misunderstandings and criticisms of

our proposal to make the NAL $30m^3$ bubble chamber a hybrid system consisting of

a fifteen radiation length quantameter and a fourteen collision length

hadrometer.

I. Why Hydrogen and Deuterium?

We admit that our preference for using these targets is subjective. It is

formed from years of observing strange and unexpected phenomena while scanning

hydrogen and deuterium bubble chamber film. One is much more likely to struggle

for an explanation to a peculiar event if it occurred on hydrogen. When the

target nucleus is more complex one can usually invent many superfluous explan-

ations for the event. Therefore, we believe it is essential to study high

energy ν and $\bar{\nu}$ interactions on H_2 and D_2 in a bubble chamber where the

interaction vertex is seen and the momentum of all charged tracks measured. The

understanding of the unexpected H_2 events will aid in untangling peculiar events

in D_2. Observations must be made over all possible kinematic variables. Two

important questions must then be answered; 1) Which charged track is the

lepton, and 2) What is the momentum of the neutral system? The hybrid system

provides the answers.

[*]correspondent

II. Why Build the Hybrid System When Track Sensitive Targets (TST) are Planned for the NAL 30m^3 Chamber?

The motivation that led us to develope the hybrid system was our awareness of how marginal the usefulness of TST's for high energy neutrino plysics became when the size of the NAL chamber was reduced from 100m^3 to 30m^3. The reason for the marginality is that at least two conversion lengths of Ne-H$_2$ mixture must blanket the TST. When the chamber volume is reduced, the TST volume reduces at a much greater rate. The solid curves of Fig. 1 summarize the effective TST volumes* for 0, 1, 2, and 3π^o physics as a function of bubble chamber diameter (in feet). The transverse distribution of neutrinos is assumed to be uniform. Pure Ne is used as the blanket. The design using a 12 foot diameter chamber described by Roe et al in NAL proposal number 44 is used as normalization.

Our original proposal (June 1970) for the development of a hybrid system called for an enlargement of the coils to allow the Quantameter to be inserted. We now believe a much better solution both for TST's and for Quantameter accuracy is to enlarge the chamber to fill the space and to slice two feet off the rear portion of the chamber as shown in Fig. 2. The reasons are discussed on pages 8-10 of Appendix 1. The solid curves of Fig. 3 show the fiducial volume of the hybrid system as a function of the bubble chamber diameter for two possible neutrino transverse distributions. The fiducial volume of the hybrid system is defined to be that space in which a neutrino event can occur and all π^os be detected. The dashed curves of Fig. 3 show the TST effective volumes that could be placed in a truncated sphere of that diameter. The broken curve of Fig. 3 is the estimated bubble chamber cost. This number is based upon $0.2 million/ft $\emptyset$ incremental coil cost. Chambers within the range of 10' $\emptyset$ to 14' $\emptyset$ will fit in the 22' $\emptyset$ vacuum tank, use the same expansion system, and the same optics.

* "Effective volume" is defined to be the product of TST volume and the probability of converting all γ's of all π^os.

We add \$0.1 million/ft $\emptyset$ to take account of added bubble chamber body cost. This brings the total cost differential to \$0.3 million/ft $\emptyset$. The percentage bubble chamber-cost-increase per foot $\emptyset$ is $\overset{\sim}{\sim}$ 4.3%/ft $\emptyset$. The percentage increase in fiducial volume is 65%/ft $\emptyset$ for TST's in the truncated spheres and is 30%/ft $\emptyset$ for the hybrid system. The large percentage increase in TST effective volume per foot $\emptyset$ is the reason for our belief that the present 12' $\emptyset$ design is very marginal for TST's.

The hybrid system with a 12' $\emptyset$ truncated sphere has (12/4.1 = 3) times the effective volume for one π° physics with TST's in a complete 12' $\emptyset$ sphere and (12/2.3 = 5.2) for three π° physics. These factors become (12/3.3 = 3.6) and 12/1.6 = 7.5), respectively, for TST's in a truncated 12' $\emptyset$ sphere.* The cost of the Quantameter is approximately \$0.35 million. In summary, for modest incremental chamber costs (4.3%/ft $\emptyset$) great gain in usefulness both for TST's (65%/ft $\emptyset$) and the hybrid system (30%/ft $\emptyset$) can be obtained. We urge NAL to expand the chamber size to correspond to a truncated sphere of 14 foot diameter (total volume $\overset{\sim}{\sim}$ 30m^3).

III. Determination of the Momentum of the Neutral System

The Quantameter

A. How can we determine the γ's energy when we have no information about the showers in the first two radiation lengths? This is a natural question for heavy liquid bubble chamber physicists to ask. The quantameter operates on a much different principle. It is well established that for photons of energy

---

*The hybrid system has an advantage for doing "no π°" physics over the bubble chamber without TST's. With "no π°" events there is an ambiguity where the event can have a π° moving directly downstream or directly upstream. The quantameter can rule out the downstream π°. The upstream π° ambiguity usually involves low energy π°'s.

greater than 1 GeV more than 96% of its energy appears in the form of ionization beyond the first two radiation lengths. Details are given in Appendix I.

B. <u>Is the preliminary cost estimate for the electronic readout realistic?</u>
The proposed multi-wire proportional chamber (MWPC, or "Charpak chamber") measures the position (and ionization) of each charged particle in the Quantameter. An area of 25 meters^2 corresponds to $180^\circ \times 90^\circ$ coverage. We assume an average of 10 gaps (5 to 15 gaps, depending on position) of cm each. Thus $250m^2$ of area is to be digitized. Position accuracy to ± 1 mm in two coordinates is desired; in addition, pulse height to $\pm 3\%$ is required.

Standard techniques (one amplifier/wire) are very expensive. However, recent developments in higher gain in proportional multiplication (Charpak et al, 1970) and delay-line readout (Perez-Mendez et al., 1970)[1] make possible simplifications. The delay-line can readout 500 wires with one amplifier. Using the positive induced pulses on steps in the negative planes (oriented, say at ± 45 deg to the positive wires) one can readout both x- and y-coordinates in a single gap.

A module of 100 cm width and 300 cm height will require about 2000 center wires (at 45°) and two Mylar planes with 2 mm wide aluminized strips to readout x- and y- into orthogonal delay lines. The estimated cost of delay line readout is $5000/module,[2] including pulse-height; 70 molules would cost about $350K.

IV. Identification of the Lepton

The primary purpose of the hadrometer is to absorb all hadrons, permitting the muons to pass through and be identified. Further details are given by Mukhin and Yount.[3]

<u>How can the hybrid system deal with mesons that decay into muons?</u> Fast pions of momentum P can decay into muons whose momenta range from 1/2P to P. Thus accurate momentum measurements ($\pm 3\%$) within the H_2-D_2 bubble-chamber should be able to detect more than 90% of $\pi \rightarrow \mu$ decays within the chamber. Decays outside

the chamber (in Q, or in H, or between) are more difficult to detect, except that for low momenta (<2 GeV/c) π-μ decays will usually give anomalously short ranges in the hadrometer for the measured momentum.

Thus despite the long average pion decay distance from production vertex to the hadrometer center ($\sim$ 5 meters), corresponding to 9% (at 1 GeV/c) to 1% (9 GeV/c) decay fractions, range and momentum measurements will detect most of these π-μ decays. Full use of the H_2 volume for momentum measurements along a suspected muon track is essential.

The "ambiguous" region includes mainly the quantameter (35 cm) and space between quantameter and hadrometer ($\sim$100 cm).

V. Trigger Rate for Quantameter and Hadrometer

The electronics trigger will require (a) an anti against incident charged particles (or charged particles from the upstream coil), (b) one or more tracks passing through the Quantameter and (c) a muon (penetrating particle) leaving the Hadrometer. This signature rejects muons from the shield, cosmic ray muons, neutrino interactions in the Quantameter or Hadrometer, and neutron interactions. It strongly favors neutrino interactions in the hydrogen.

The Quantameters's proportional chamber is continuously sensitive with fast readout which can be combined with scintillation logic to decide on spark-chamber triggers in <1 μsec. Thus the Hadrometer is fired only when the signature is complete.

If the trigger rate exceeds one per burst, it is possible to refine the Quantameter and/or scintillator logic to define the penetrating muon trajectory more precisely. Multiple electronic "events" per burst can be handled if necessary. This would require more than one vidicon camera (with electronic shutter) for the Hadrometer.

VI. Why Don't the Quantameter and Hadrometer Subtend More Solid Angle?

We have the possibility at a later date to increase the hadrometer to cover 180° thereby detecting muons below 4GeV. The addition of a TST cylinder that runs the full length of the chamber can also be added later.

VII. How Does One Take Account of Hadron Interactions in the Quantameter?

Most of the γ's from a π° are confined in a cone of full angle $2/\gamma$. If a charged pion has a large probability of being emitted into this cone then it will pose some problems for us. However, we wish to give some crude arguments to suggest that this is not the case. Under these circumstances we can track the charged hadron through the quantameter, not being bothered by the γ showers, and get a good measure of the energy it deposits in the quantameter.

The argument is based on a fireball type model [4] where one assumes that a substantial number of pions come into thermal equilibrium at a temperature $kT \stackrel{\sim}{\sim} 0.18$ GeV. Their energy distribution is a Planck-like one. The "overlap" problem is best considered in the rest frame of this fireball. Suppose for the moment that all the pions were neutral, each with its γ ray cone subtending a solid angle of π/γ^{2}. Here γ is the energy of the pion, E, divided by the pion rest energy μc^{2}. The fraction of the total solid angle, 4π, that is "used up" by all the γray cones is,

$$f = \frac{\langle n_{\pi} \rangle \, X_{o}^{2}}{4} \cdot \frac{\displaystyle\int_{X_{o}}^{\infty} \frac{1}{X} \frac{\sqrt{X^{2} - X_{o}^{2}}}{e^{X} - 1} \, dx}{\displaystyle\int_{X_{o}}^{\infty} X \frac{\sqrt{X^{2} - X_{o}^{2}}}{e^{X} - 1} \, dx},$$

where, $X_{o} \equiv \dfrac{\mu c^{2}}{kT}$, $X \equiv \dfrac{E}{kT}$

Evaluation of the integrals yields, $\quad f = \dfrac{\langle n_{\pi} \rangle}{27}$

Usually, one third of the mesons will be neutral, in which case

$$f_o \simeq \frac{\langle n_\pi \rangle}{8\ 1}$$

Let us consider the worst possible case.

From Fig. 1 of our original proposal (#9) one sees that for $E_\nu = 50$ GeV, $\langle n_\pi \rangle < 15$, $f_o < 0.18$ for 50 GeV nutrinos.

The probability that all charged pions miss these cones is $(1-f_o)^{n_{ch}}$. for $\langle n_\pi \rangle = 15$ this probability is $(.82)^{\left(\frac{2}{3} \cdot 15 = 10\right)} \simeq 0.14$

The probability that all but <u>one</u> pion miss

$$\text{is} \ = \ \frac{\langle n_{ch}\rangle !}{(\langle n_{ch}\rangle - 1)!\ 1!}\ (1-f_o)^{\langle n_{ch}\rangle - 1}\ f_o^1 \ = \ \left(\frac{10!}{9!} = 10\right)(.82)^9 (.18)$$

$$= (10)(.168)(.18) = 0.30$$

that all but <u>two</u> pions miss is,

$$\frac{\langle n_{ch}\rangle !}{(\langle n_{ch}\rangle - 2)!\ 2!}\ (1-f_o)^{\langle n_{ch}\rangle - 2}\ f_o^2 \ = \ \left(\frac{10!}{8!\ 2!} = 45\right)(.82)^8 (.18)^2$$

$$= 45(.204)(.0324) = 0.30$$

that all but <u>three</u> pions miss is,

$$\frac{\langle n_{ch}\rangle !}{(\langle n_{ch}\rangle - 3)!\ 3!}\ (1-f_o)^{\langle n_{ch}\rangle - 3}\ f_o^3 \ = \ \frac{10!}{7!\ 3!}(.82)^7 (.18)^3 = 0.174$$

and so on. Each charged pion that strikes a cone has a probability of $e^{-1} = .368$ of <u>not</u> interacting in the quantameter.

In the proposal we assumed that the entire final hadron state comes into thermal equilibrium. In this way we obtain an upper limit on the multiplicity. For Pomeranchuka exchange $\langle n_\pi \rangle$ would be much lower than these.

In Table I we summarize for various multiplicities, $\langle n_\pi \rangle$, a) the probability that no charged pion strike within the "γ-cones", and b) the probability that no charged pion interacts in the Quantameter within the "γ-cones".

At this stage we feel confident of our ability to deal with this problem.

We intend to demonstrate capability of the Quantameter to perform the function we describe in our proposal by doing a modest experiment.

TABLE I

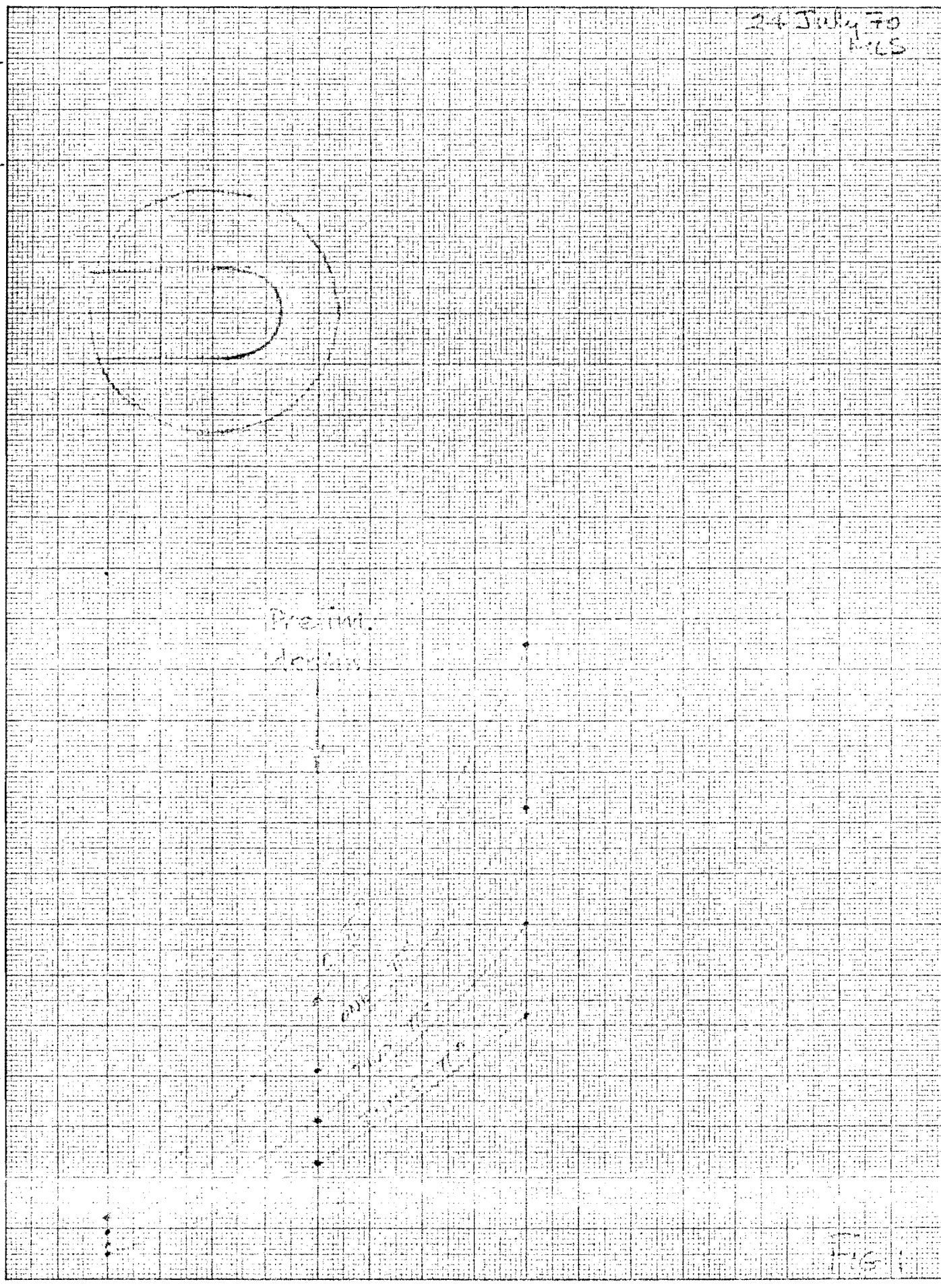| $\langle n_\pi \rangle$	Probability that all charged pions miss cones	Probability that no charged pion interact within γ cones.
3	0.928	0.928 + 0.0262 + ... = 0.954
6	0.735	0.735 + .087 + .004 + ... = 0.83
15	0.140	0.140 + 0.110 + 0.040 + 0.009 = 0.30

REFERENCES

(1) "Electromagnetic Delay Line Readout for Proportional Wire Chambers", by R. Grove, K. Lee, V. Perez-Mendez, and J. Sperinde, UCRL-19858, July 1970. Appended to this note.

(2) See LRL Engineering Note F.ET-1361 (July 1, 1970), "Digitizing System for Proportional Chambers Using Delay Line Readout", by F.A. Kirsten for component costs ($0.47 per wire for 512 wire chamber), including scalers, amplifiers, and delay line.

(3) A. Mukhin and D. Yount, "External versus Internal Muon Identification in the 15-Foot Bubble Chamber" 1970 NAL Summer Study.

(4) M.L. Stevenson "The Role of the Planck Distribution in Understanding the Constancy of the Transverse Momentum in High Energy Nucleon-Nucleon Collisions NAL Internal Report TM-219, and Y.W. Kang and M.L. Stevenson "Properties of the Neutrino Beams at a 400 GeV Accelerator" TM 217, page 6.

24 July 70
H. S.

Effective Volume (m³)

Bubble chamber Diameter (feet)

Prelim.
design

FIG 1

K+E 10 X 10 TO THE CENTIMETER   46 1510
18 X 25 CM.   MADE IN U.S.A.
KEUFFEL & ESSER CO.

TOP VIEW

ID SCALE

Fiducial volume
of hybrid system
reduced by 20%
to ≈ 8m³.
Effective vol of
5.5m³ TST is 4.1m³ for π^0
3.1m³ " $2\pi^0$
2.3m³ " $3\pi^0$
in full 12'φ sphere

3.6 m
.5 m
3.1 m × $\pi \cdot r^2$ = 9.8

Ele[ ]on View

For a shield of m Froom, the fiducial vol is a factor of 1.5 larger.

FIG 2

Fig. 3

Effective Volume (m^3) vs. Bubble chamber diameter (feet)
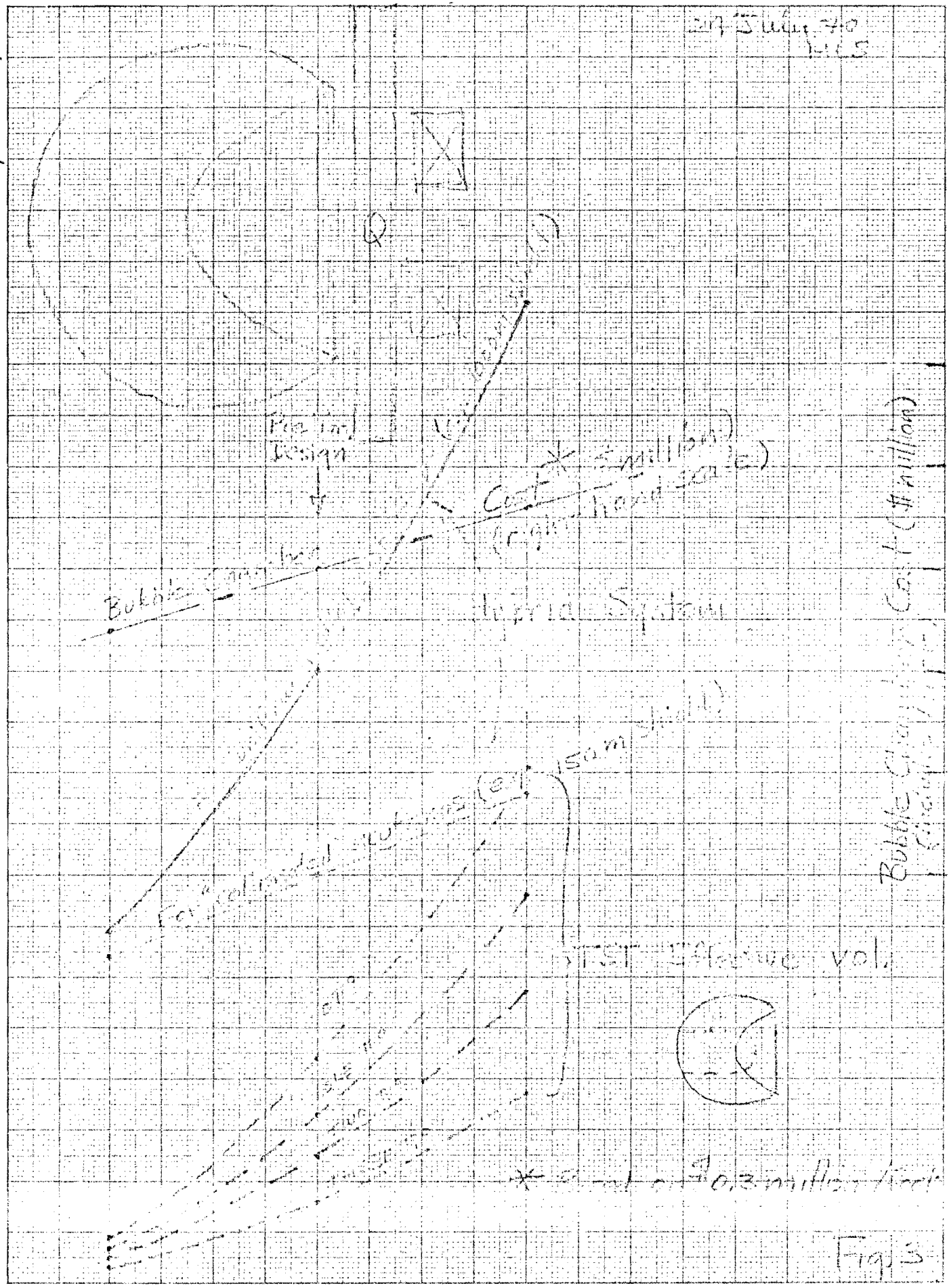
PROPORTIONAL QUANTAMETER FOR THE 15-FOOT BUBBLE CHAMBER

D. Yount

University of Hawaii

ABSTRACT

The performance of a quantameter to detect and measure
the energy of the neutral pions produced by neutrino interactions
in the 15-foot bubble chamber is evaluated.

INTRODUCTION

Since the neutrino energy spectrum is broad, measurement
of the νp and νd total cross sections requires that the full
energy of each interaction be determined. Essentially, there
are four components: charged hadrons, charged leptons, neutrons,
and neutral pions. The charged component can be found with
high precision ($\pm$ 3%) from track curvature in the 15-foot
H_2, D_2 bubble chamber, although additional equipment is required
to identify leptons, particularly muons, with good efficiency.
The neutron component may be small for most interactions and can
probably be determined with an external hadrometer to sufficient
accuracy that the uncertainty in the total energy is not dominated
by this source. The most efficient method for measuring the
photon energy from neutral pion decay appears to be the lead-plate
quantameter: the purpose of this note is to estimate the resolu-
tion and precision of this type of detector, thereby emphasizing

2.

the importance of allowing for such a device in the bubble-chamber design.

Typically half the energy in a neutrino interaction appears in the form of charged leptons. Perhaps 1/3 of the total hadron energy appears in the form of neutral pions, which therefore account for 1/6 of the total neutrino energy. The fraction is large enough so that neutral pions must be detected with good conversion efficiency in any total-cross-section experiment; it is small enough so that even a modest accuracy ($\pm$ 10% of the neutral-pion component) would imply that the dominant error results from track curvature. It may therefore be possible to determine the total neutrino energy to $\pm$ 3% in the hybrid H_2, D_2 bubble chamber, while an estimate of $\pm$ 5% has been given in an NAL proposal.[1] Corresponding estimates for the neon bubble chamber range as high as $\pm$ 20%.[2]

Parallel-plate ionization calorimeters, such as the quantameters[3] widely used in monitoring photon beams, have several intrinsic properties that are essential in determining the neutral-pion energy accurately. First, the response depends only upon the relative ionization in the gas gaps as compared to the ionization in the plates; tolerances of 1% or less in these parameters can be met and insure a uniform response to the same level. Second, since the ratio of gap to plate is independent of track angle in a parallel-plate chamber, such a device is intrinsically isotropic. Third, the output of an ionization calorimeter is linear in the energy absorbed over a wide range.

Fourth, an ion chamber is operated as a one-parameter device; there is one high-voltage setting and one output signal proportional to the total energy deposited in the chamber as sampled periodically via the ionization in the gas gaps. This last feature greatly simplifies the operation of the calorimeter and results in a highly reproducible instrument.

In the case of electromagnetic showers, virtually all of the energy appears ultimately in the form of ions, which are sampled directly in the ionization calorimeter thereby avoiding such questions as the response of scintillation or Cerenkov counters using phototubes. The SLAC quantameter,[4] for example, has been shown to be linear in energy to ± 0.2% from 1 GeV to 14 GeV, the highest energy at which linearity was tested. The response for incident electrons or positrons[5] was found to be the same to about ± 0.3%, and the reproducibility over long periods of time is also on this level. The SLAC quantameter has been calibrated with a Faraday cup so that it can be used as an absolute monitor to a few tenths of one percent. One simply fills the chamber with a standard gas and sets the high voltage.

The precision, linearity, and reproducibility of ionization quantameters under very favorable circumstances are clearly excellent. The performance of a large proportional quantameter in detecting the electromagnetic energy in a single neutrino-induced event from the bubble chamber can be estimated by considering those factors which cause the response to deteriorate, as compared with ordinary quantameters used in beam

monitoring. The analysis below indicates that a statistical
uncertainty of $\pm$ 3% (1000 tracks for 10 GeV neutral-pion energy)
results from shower sampling every 1/2 radiation length, while
sampling every radiation length would give $\pm$ 4%. When systematic
effects are taken into account, the overall accuracy should be
better than $\pm$ 6% for 10 GeV neutral-pion energy or about $\pm$ 1%
of the total neutrino energy in a 60-GeV event. Unlike the neon
bubble chamber, which has a radius of about 3 radiation lengths,
the quantameter improves with energy, the accuracy varying roughly
as $1/\sqrt{E_{\pi^0}}$.

SHOWER STATISTICS

The gain of the SLAC quantameter with 1-atm argon-CO_2
filling is about 4000 ions per GeV incident.[4] The copper plates
are 0.963 cm = 0.72 radiation lengths thick with an average
gas gap of 0.476 cm. An output of about 40 ions/track would
result from a single minimum ionizing particle passing through
such a gap indicating that the number of tracks sampled is of
order 100/GeV. For a total π^0 energy of 10 GeV, 1000 tracks would
be expected yielding a statistical uncertainty of about $\pm$ 3%.
Monte Carlo calculations for electron-photon showers in lead[6]
predict about 600 electrons above 1.5 MeV for a 6-GeV shower
sampled at intervals of 1/2 radiation length. This is equivalent
to 1000 electrons at 10 GeV, consistent with the first estimate.
(The quantameter plates are somewhat thicker than 1/2 radiation

5.

length, but particles of less than 1.5 MeV are detected.)

SHOWER SAMPLING AFTER 2 RADIATION LENGTHS

A recent 15-foot bubble-chamber design specifies a thin exit wall of 1/2 inch steel, equivalent to about 0.7 radiation lengths. The front wall of the reentrant tank would be of comparable thickness. Photons originating at the center of the bubble chamber will pass through about 0.3 radiation lengths of liquid hydrogen, so that the total thickness before entering the quantameter is about 1.7 radiation lengths. This may be considered as the first plate of the quantameter, which would begin with a thin window followed by a sensitive gas gap. Since photon cascades are displaced in the direction of the shower axis by about 1 radiation length with respect to electron cascades,[6] photon-shower sampling beginning after 2 radiation lengths should be excellent.

Quantitatively, only about 0.5% of the total ionization in a photon shower at 6 GeV occurs in the first radiation length, while at 1 GeV the value is the same to 0.2%. Less than 4% of the ionization occurs in the first two radiation lengths, the difference in 1 and 6 GeV being less than 1%. The shower multiplicities versus thickness in lead for these two energies are shown in Figure 1 to illustrate this point.[6] Since the quantameter will be calibrated, only the linearity is in question: this appears to be of order 1% for photons above 1 GeV, even

if sampling begins after 2 radiation lengths. Clearly, it makes negligible difference if 10 GeV reaches the quantameter as two photons or a dozen. In fact, the thickness after which sampling begins can be varied from 0 to 2 radiation lengths without affecting the quantameter output by more than 4%.

SHOWER PENETRATION

The shower penetration in percent depends on the incident photon energy and could affect the energy linearity if the quantameter is too thin. About 7% of the ionization in a 6-GeV photon shower occurs after 15 radiation lengths, while less than 2% appears after 20 radiation lengths.[6] In ionization quantameters,[3] the spacing of the last gas gap is usually made large enough to "compensate" for shower penetration, reducing this loss by perhaps one order of magnitude. Compensation is also possible in the proportional quantameter: for example, the gain of the last gap can be increased so that the signal from this gap is proportional to the penetrating ionization rather than simply the ionization of one gap at the particular thickness in radiation lengths. In any case, it is straight forward to design a quantameter for which shower penetration alters the energy linearity by less than 1%. The back-scattered energy from a 6-GeV photon cascade in lead is about 0.12% of the total.[6]

7.

SHOWER DATA

Before considering other systematic effects peculiar to
the hybrid application, it is useful to compare the estimates
of intrinsic quantameter performance with existing data. An
energy resolution of ± 19% (HWHM) has been obtained at 200 MeV
by counting sparks in a lead plate chamber with plates 0.15
radiation length thick.[7] Scaling to 1 radiation length and 10
GeV would give

$$19\% / [\frac{10 \text{ GeV}}{50 \text{ MeV}} \times \frac{0.15 \text{ r.l.}}{1.0 \text{ r.l.}}]^{\frac{1}{2}} = \pm \ 7.4\%$$

as compared with the statistical limit of ± 4%. The scaling is
pessimistic for two reasons: 1. tracks observed in a photon
shower at intervals of 0.15 radiation lengths are not independent
in a statistical sense, and 2. spark counting is less efficient·
than a direct ionization measurement.

Backenstoss et al.[8] have measured the resolution of a
lead-scintillator shower counter consisting of 20 lead plates
each 0.8 radiation lengths thick. Their result at 10 GeV is
± 4.9%, which scales to ± 5.4% at 1 radiation length. This
value is more applicable to the quantameter configuration than
that obtained by scaling track-counting results, but it is
still somewhat pessimistic since it involves phototube resolution,
light attenuation in plastic scintillator, etc. .

8.

Hofstadter and Hughes have studied the resolution in a Pb-NaI array as a function of the thickness of lead.[9] Their results for incident electrons at 8 GeV are shown in Figure 2. The resolution is observed to vary from ± 1% (HWHM) with no lead to ± 6% with 0.75 inches, about 3 radiation lengths, in front of each successive crystal. Since the NaI crystals are 7 inches = 7 radiation lengths thick, the results are not directly applicable to the thin gas gaps of a proportional quantameter. They do, however, illustrate that even very crude sampling of an electromagnetic shower at high energy can yield excellent resolution.

MAGNETIC FIELD

Electrons and positrons from photon conversion in the 0.7-radiation-length exit wall of the bubble chamber must pass through a magnetic field of 30 kG before reaching the quantameter. Since the H_2, D_2 container is spherical and the reentrant quantameter tank cylindrical, as presently envisioned, the distance traveled in the magnetic field depends upon where conversion occurs. A reasonable approximation is

$$s = 5 \text{ cm} + 200(1 - \cos\theta) \text{ cm}$$

where s is the separation, 5 cm is assumed to be the separation in the median plane, 200 cm is the approximate radius of the bubble chamber, and θ is the angle between the median plane and a line from the center of the bubble chamber to the place on the 1/2-inch-steel wall where photon conversion occurs. A track with radius equal to the separation will just miss the quantameter. The momentum cutoff for detection is then given by

$$p(\text{GeV}/c) = 3\ B(\text{kG})\rho(\text{cm})$$
$$= 100s.$$

Values of s and p are plotted versus the height above the median plane of the bubble chamber in Figure 3a.

Assuming the distribution function for the fraction of the total energy given to an electron or positron is constant, energy losses occur in $2(p/p_0)$ of the conversions where p_0 is the incident photon energy. The mean energy carried away when a particle is lost is $(p/p_0)/2$ so that the average for all photon conversions is $(p/p_0)^2$. The average energy loss in percent, computed in this way, is plotted versus the height above the median plane in Figure 3b for several photon energies. This model, while exceedingly crude, suggests that measurements of the total π^0 energy can be made with accuracy of a few percent or better over most of the quantameter area when the total energy is above a few GeV. The losses in the median plane

are small even at quite low photon energies, and this property

could be extended to the entire quantameter by matching bubble-

chamber and quantameter geometries, either making the back of

the bubble chamber cylindrical or making the quantameter locally

spherical. Nine modules 1 m square in a 3 m x 3 m array would

approximate a spherical surface nicely if a reentrant tank of

suitable shape were made to contain them.

INCIDENT CHARGED LEPTONS

Muons penetrating the quantameter would contribute to the

total ionization about one track per gap. For 20 radiation

lengths and 40 gaps, this amounts to about 40 tracks/1000 tracks

= 4% of the signal from a 10-GeV neutral-pion shower. A correction

of this magnitude is straight forward once the penetrating muon

has been identified, for example, by a hadrometer in the hybrid

system.

Electrons or positrons entering the quantameter will be

detected with exactly the same response as incident photons.

If the electrons arise from conversion of π^0 photons in the bubble

chamber or steel vacuum tank, the resulting signal should be

combined directly with that due to π^0 photons, a case already

discussed. Electrons from an electron-neutrino ν_e vertex can

be identified by associating a shower in the quantameter with

with a charged track in the bubble chamber: spatial resolution in the quantameter is required. The energy of the identified electron can be determined from track curvature in the bubble chamber and can be subtracted from the total quantameter signal, leaving the neutral pion component intact. Dalitz decays are rare and yield pairs of electrons which can be identified in the quantameter and retained in the neutral pion signal.

NEUTRONS AND INCIDENT CHARGED HADRONS

Corrections of order 4% per hadron can be made to the quantameter signal for charged hadrons that penetrate without interacting. No correction is necessary for neutrons that do not interact. For interacting hadrons the correction may be comparable with the neutral pion signal, and it can only be made by analyzing each event in detail, taking into account the incident hadron energy, the penetrating hadron energy (determined, for example, by a hadrometer), and the spatial information provided by the wire readout of the proportional quantameter.

A thickness of 15 - 20 radiation lengths of lead is equivalent to about 1 collision length for strongly interacting particles. Perhaps a third of the energy in each collision goes into neutral pions[10] which shower and are detected with good efficiency by the quantameter unless the interaction occurs in the last few radiation lengths. Depending upon the

event configuration, it may be necessary to determine the neutral

pion component from the neutrino vertex by track counting

rather than by measuring the total quantameter signal. Since

the sum of the π^0 and interacting-hadron energies is measured

absolutely by the quantameter, only the relative numbers of

tracks in various showers is required. An accuracy approaching

the statistical limit might still be possible in this case,

but the analysis would become more complex. A modular quantameter

design would substantially reduce the probability for more than

one shower signal to occur in a single readout.

SHOWER POINTING ERROR

Experimental data on the accuracy with which the direction

of a photon shower can be determined are shown in Figure 4.[11]

The results suggest that the pointing error improves slowly

after 1 GeV, while the variation with plate thickness may

be $t^{1/2}$. The result, scaled to a plate thickness of 1 radiation

length, is a pointing error of about $\pm 10^0$. This should be

sufficient to associate individual showers detected in the quantameter

with particular events seen in the bubble chamber when more than

one event occurs during an expansion. It would also exclude

photons from interactions in the coils upstream of the bubble

chamber in most cases and would permit pairs or single electrons

and positrons to be associated with photons converting in the

1/2-steel wall of the bubble chamber.

PROPORTIONAL READOUT

The primary ionization from a single electromagnetic shower at 10 GeV is not sufficient to produce a practical signal across the high capacitance of a large parallel-plate quantameter. In the proportional chamber[12] several orders of magnitude additional amplification can be obtained through avalanche formation in the high electric field surrounding wires 20 - 50 u in diameter and spaced 1 - 3 mm apart. In the proportional quantameter[1] shower formation and avalanche multiplication combine to yield a signal across the full capacity of one gap or of one chamber that is comparable with the single-avalanche signal across the capacity of one wire. Furthermore, since a small number of signals are involved in a total-energy measurement, high quality amplifiers can be used to preserve the output linearity and stability. The performance of a proportional quantameter, as compared with an ionization quantameter, appears, therefore, to be limited mainly by such considerations as the wire uniformity, the characteristics of avalance formation, and the time distribution and time interval sampled. Each of these effects should be greatly reduced in the statistical average over 1000 tracks. A rough guess is that collection times of several tens of nanoseconds would be sufficient to permit reproducibility, uniformity, and

14.

energy linearity approaching the statistical limit (± 4% for
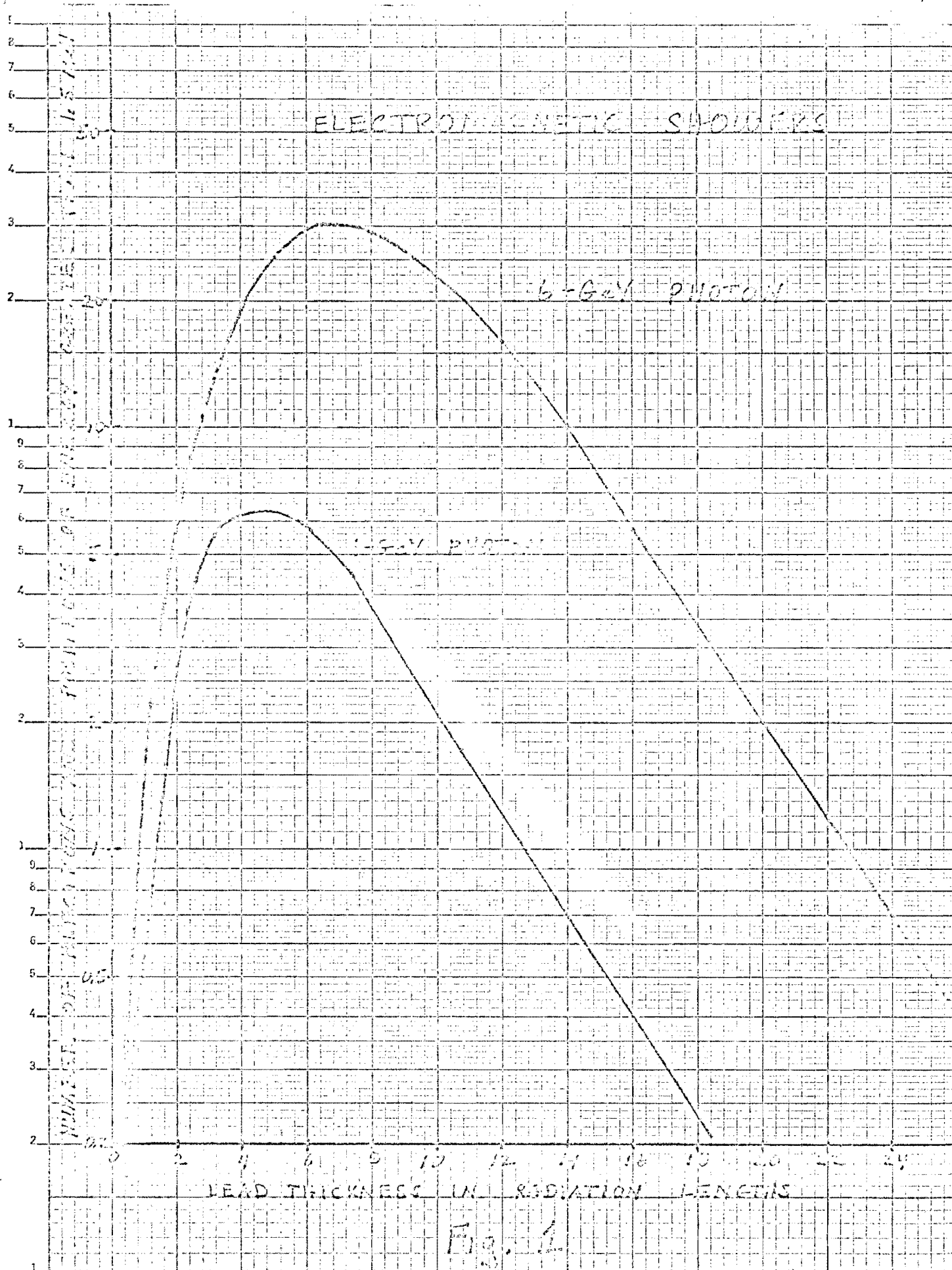1-radiation-length plates at 10 GeV).

DISCUSSION

It appears that a lead-plate proportional quantameter of
15 - 20 radiation lengths thickness and a similar number of gaps
could be used to determine the neutral-pion energy from individual
neutrino interactions in the 15-foot bubble chamber with an
accuracy well under ± 10%. Certain classes of events, par-
ticularly those in which hadrons interact in the quantameter,
would require detailed analysis, including shower-track counting,
before this level could be reached. Since on the average only
1/6 of the energy in a neutrino interaction is expected to go
into neutral pions, an uncertainty as large as ± 10% in this
component would contribute a smaller error to the measurement
of total neutrino energy than results from track curvature in
the H_2, D_2 bubble chamber, ± 3%. In this sense, it seems clear
that a lead-plate proportional quantameter would be highly useful,
even if its resolution is several times worse than presently
seems feasible.

REFERENCES

1. M. L. Stevenson et al., "Proposal for a High-Energy Neutrino Experiment in the NAL 30 m^3 H_2,D_2 Bubble Chamber," NAL Proposal Number 9.

2. C. Baltay, R. B. Palmer, and N. P. Samios, "Search for the Intermediate Boson, Lepton Pair Production, and a Study of Deeply Inelastic Reactions Utilizing High Energy Neutrino Interactions in Liquid Neon," NAL Proposal Number 53.

3. R. R. Wilson, Nucl. Instr. 1, 101 (1957).

4. D. Yount, Nucl. Instr. Methods 52, 1 (1967).

5. D. Yount, Symposium on Beam Intensity Measurement (Daresbury, England, 22-26 April 1968, V. W. Hatton (Ed.)) pp. 75-96. (See DNPL/R-1.)

6. H. Nagel, Zeitschrift fur Physik, 186, 319 (1965); U. Völkel, DESY Report 65/6, July 1965.

7. R. Cence (Private Communication) July, 1970.

8. G. Backenstoss, B. D. Hyams, G. Knop, and U. Stierlin, Nucl. Instr. Methods 21, 155 (1963).

9. E. B. Hughes, "Observations on the Total Absorption of Electrons and Pions in Matter at GeV Energies," HEPL 603, June, 1969.

10. V. S. Murzin, Progress in Elementary Particle and Cosmic Ray Physics (North-Holland Publishing Company, Amsterdam, The Netherlands, 1967), Vol. IX, p. 245.

11. V. Peterson (Private Communication) July, 1970.

12. G. Charpak, D. Rahm, and H. Steiner, Nucl. Instr. Methods 80, 13 (1970).

ELECTROMAGNETIC SHOWERS

6-GeV PHOTON

1-GeV PHOTON

LEAD THICKNESS IN RADIATION LENGTHS

Fig. 1

ENERGY DEPOSITED IN NaI(Tℓ) vs Pb THICKNESS

ELECTRON RESOLUTION vs Pb THICKNESS

Fig. 2.

CUTOFF MOMENTUM VERSUS HEIGHT ABOVE THE MEDIAN PLANE

FIG. 3a

AVERAGE ENERGY LOSS VERSUS HEIGHT ABOVE THE MEDIAN PLANE

FIG. 3b

SHOWER POINTING ERROR

o——o LRL-UH 10-300 MeV PHOTONS
         0.16 r.l. LEAD PLATES

x——x RHEL-CERN 100-2000 MeV PHOTONS
         0.06 r.l. ALUMINUM PLATES

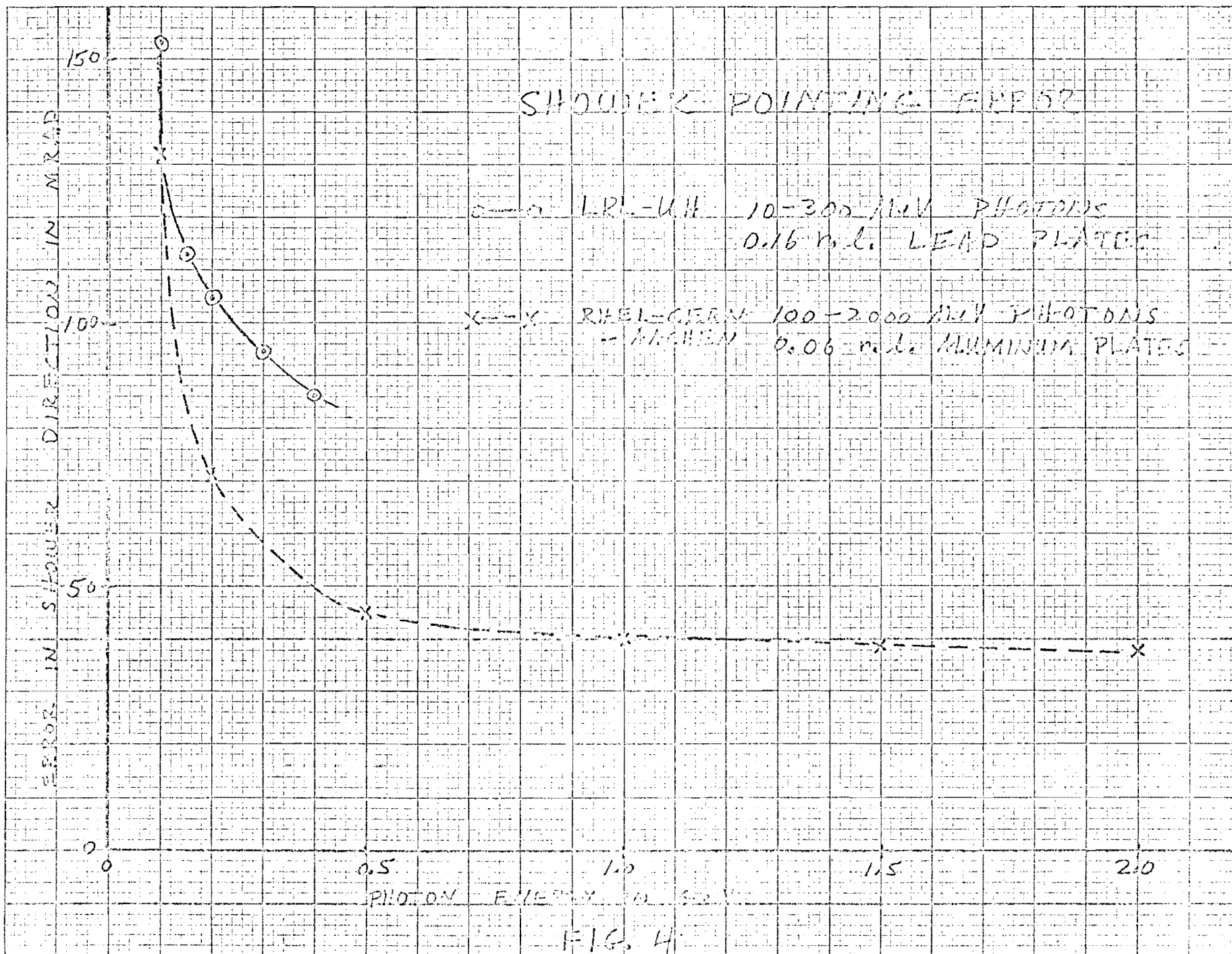ERROR IN SHOWER DIRECTION, IN MRAD

PHOTON ENERGY, IN GeV

FIG. 4

UCRL 19858
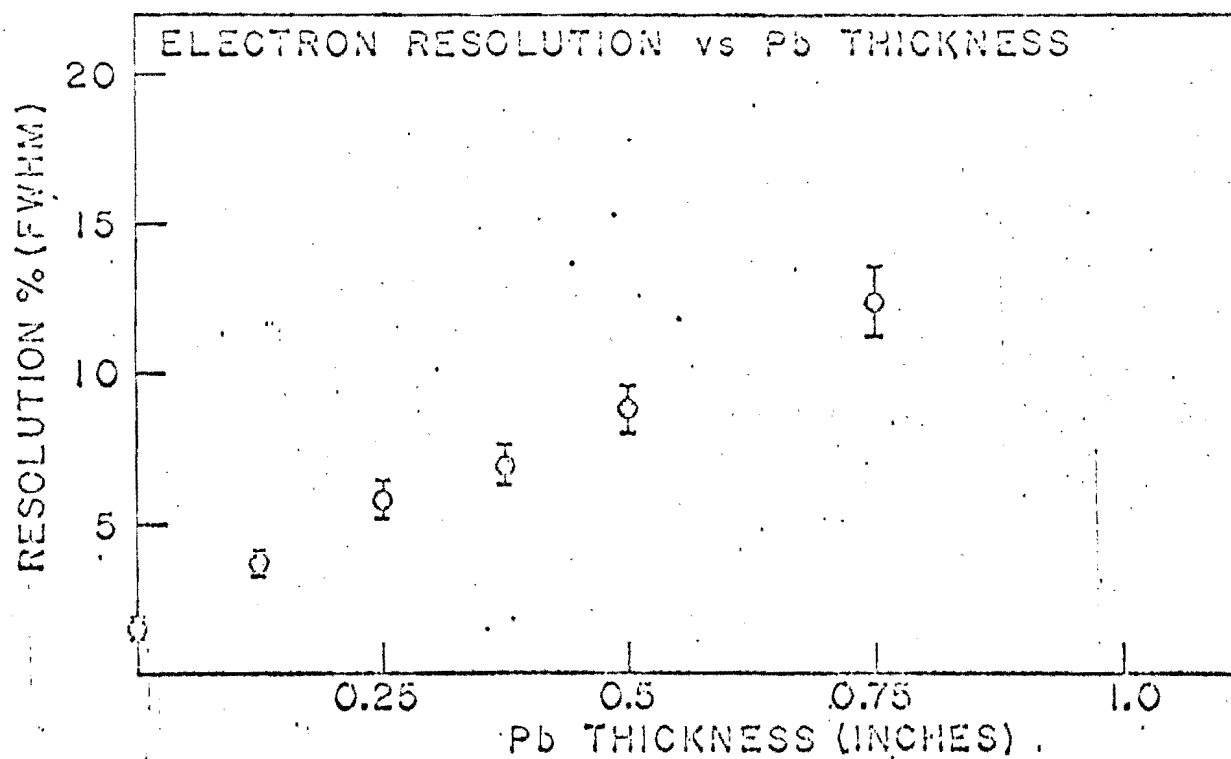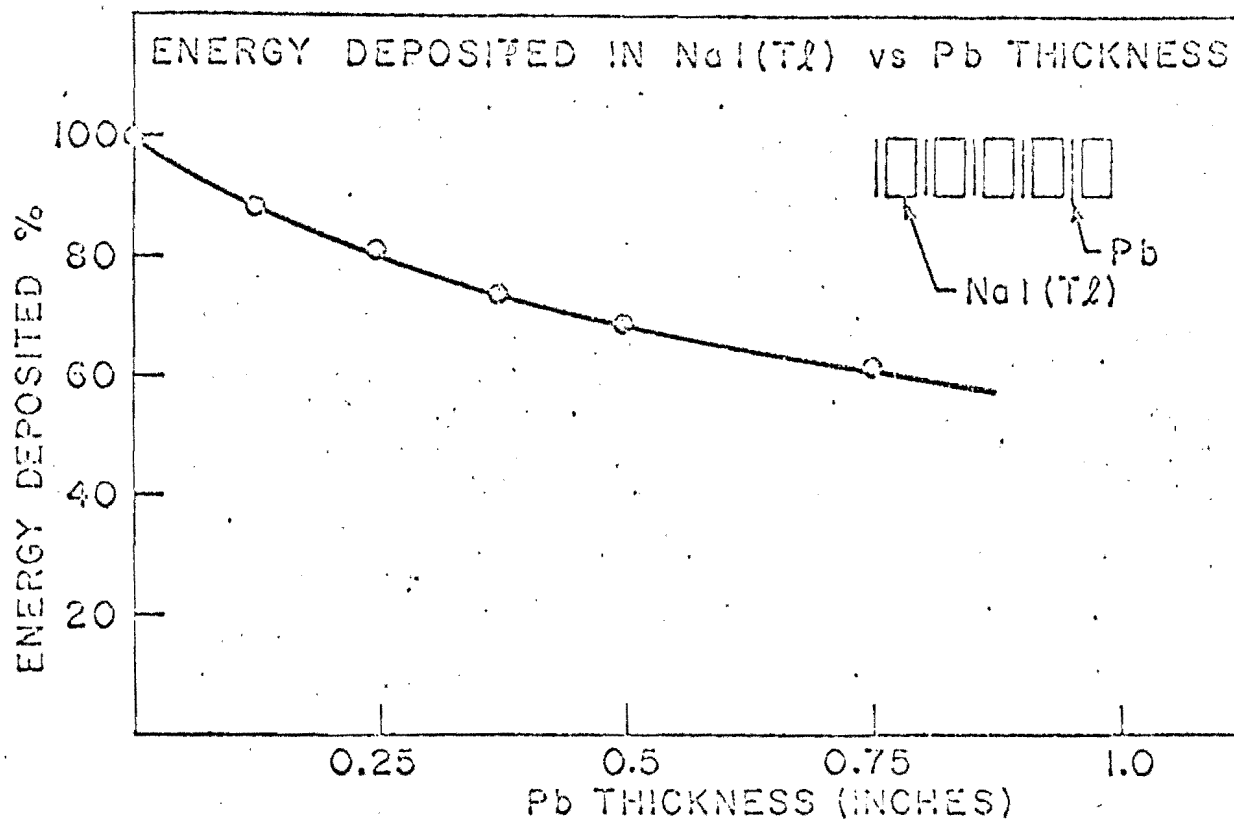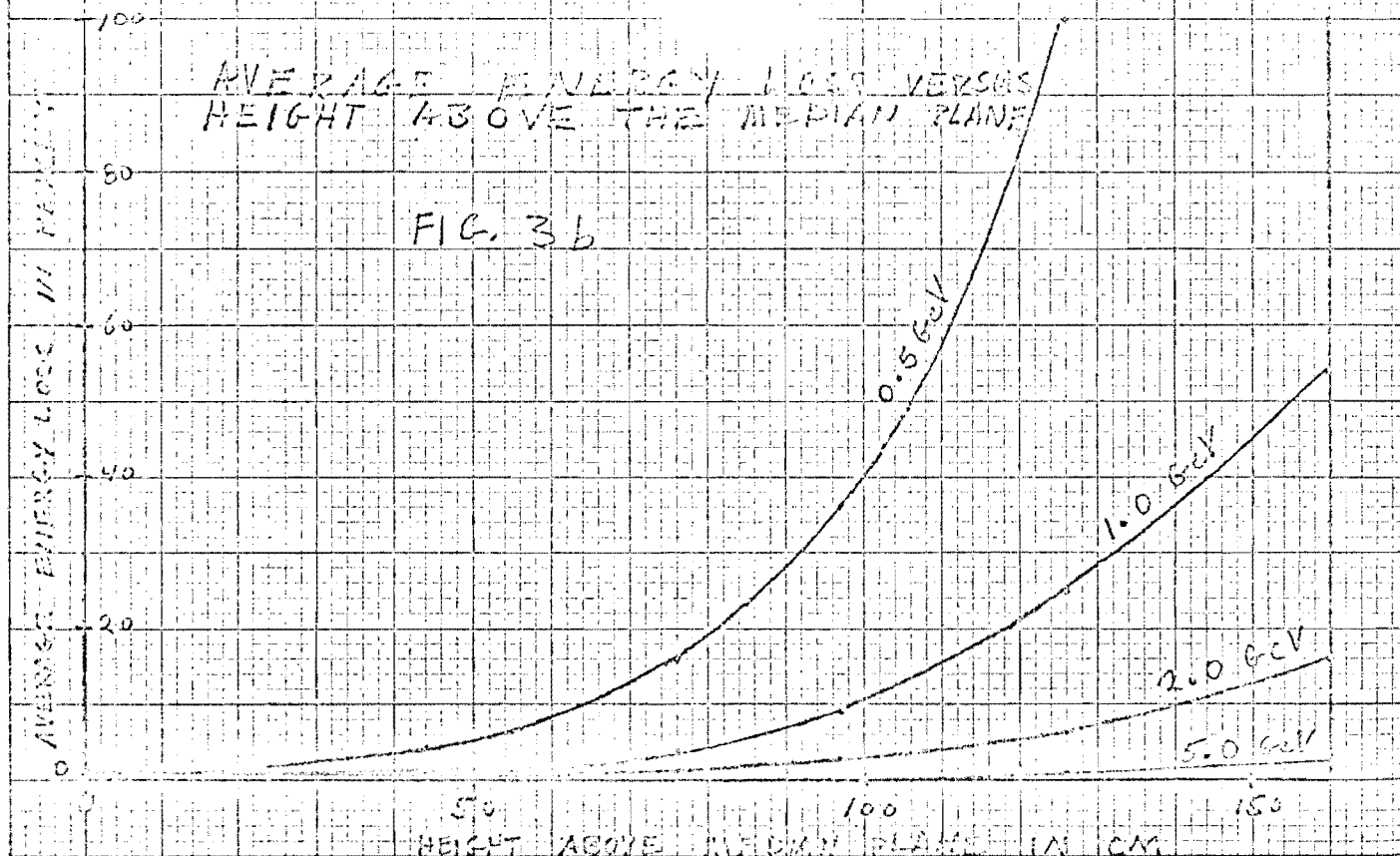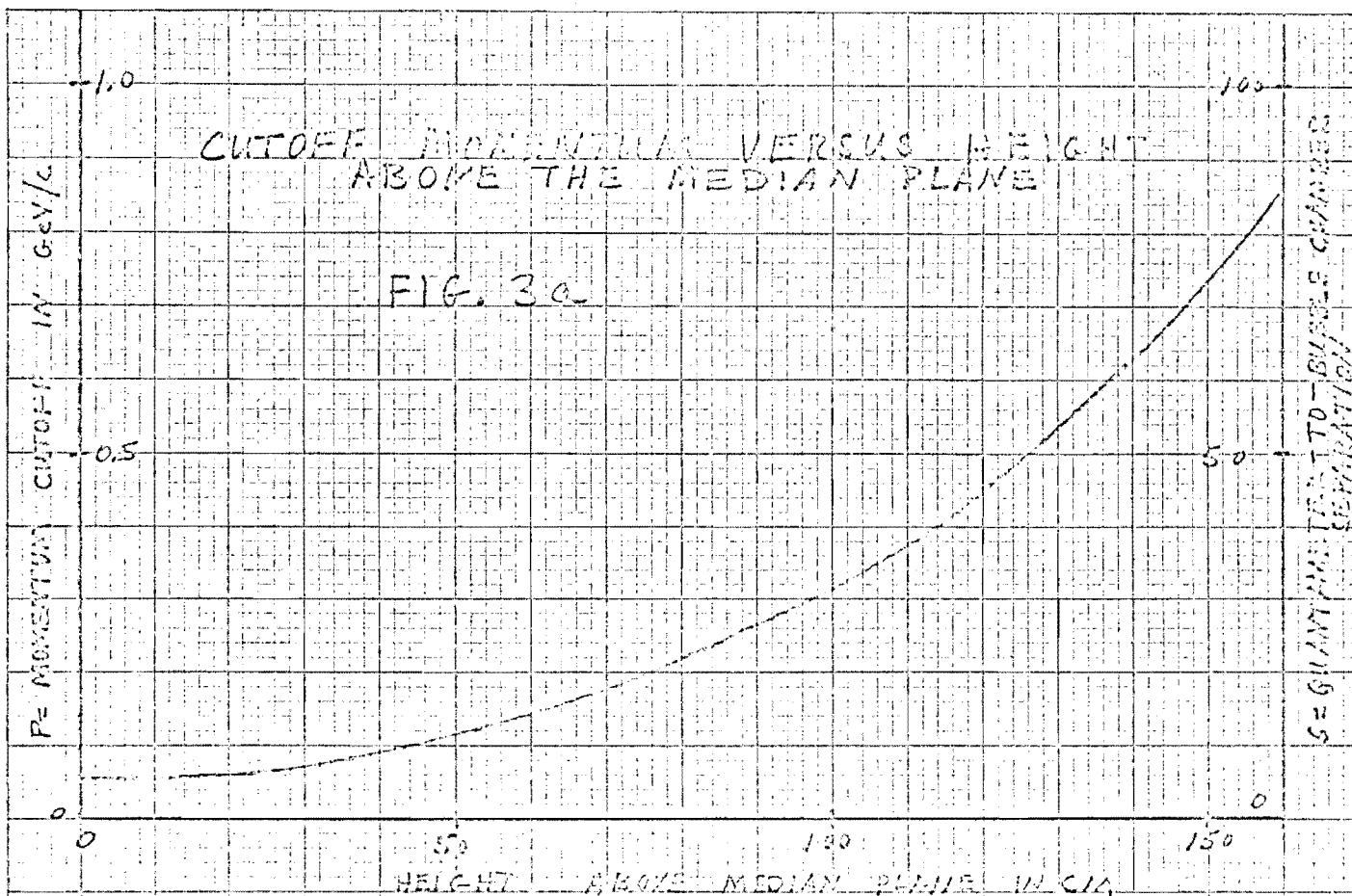
UNIVERSITY OF CALIFORNIA

Lawrence Radiation Laboratory

Berkeley, California

ELECTROMAGNETIC DELAY LINE READOUT FOR PROPORTIONAL WIRE CHAMBERS

R. Grove, K. Lee, V. Perez-Mendez and J. Sperinde

ELECTROMAGNETIC DELAY LINE READOUT FOR PROPORTIONAL WIRE CHAMBERS[*]

R. Grove, K. Lee, V. Perez-Mendez and J. Sperinde
Lawrence Radiation Laboratory
University of California
Berkeley, California

June 25, 1970

ABSTRACT

We describe the use of electromagnetic delay lines to read out

the position of ionizing events in multi-wire proportional chambers. The

delay line used is a ceramic core (non-magnetic) type with a delay of

80 nanosec/cm. The readout accuracy achieved depends on the wire plane which

is read out: for the positive plane which forms the electron avalanche, the

accuracy is ± 1 mm. (half the wire spacing). For the negative plane, which

records the induced signal produced on a number of adjacent wires by the

positive ions, the interpolation property of the delay line permits an accuracy

of ± 0.15 mm.

I. INTRODUCTION

Multi-wire proportional chambers are now coming into extensive use

in nuclear and elementary particle physics. Their main advantage over wire

spark chambers is the ability to record events at high rates whereas the spark

chambers are limited by the recovery time of the chamber. The main difficulty

with wire proportional chambers so far has been the readout--which in the

simplest case is done by using an array of amplifiers and storage logic ele-

ments connected to the individual wires. In a previous paper[1] we showed that

a readout scheme using an electromagnetic delay line could be made which was

considerably cheaper and simpler than the amplifier array method. The delay

line that we used was a ferrite loaded delay line to which the individual wires

of the chamber were coupled by coils: the positioning accuracy that we were

able to achieve was approximately 3 mm. which was the same as the spacing of

the wires. In this paper we discuss a similar readout scheme using a differ-

ent type of electromagnetic delay line without any ferrite or magnetic material

in it. This type of delay line has a number of advantages. The ratio of delay

to rise time of a pulse and the delay per unit length are higher than in the

ferrite line. Furthermore the dispersion of the signal per unit delay is

smaller. The combination of these properties makes it possible to use a readout

scheme which achieves a position accuracy better than ± 0.15 mm. and can be

used in the presence of magnetic fields of any strength.

II. DELAY LINE CHARACTERISTICS

For this project we have been using a commercially available ceramic

core delay line of a type that is well described in the literature.[2] Fig. 1

shows the construction of the delay line.[3] The center conductor consists of

silver painted longitudinal strips on a ceramic core which is non-magnetic.

The outer conductor consists of a copper winding as shown in the figure, made

of insulated copper wire 0.09 mm. in diameter with 100 turns/cm. The line is

wound in 3 mm. sections with each section overlapping the previous one by

1.5 mm (see Fig. 1 insert). All turns of the winding are in the same dir-

ection. This type of delay line has the following characteristics: Delay =

80 nanosec/cm., band pass = 3.6 Mc/sec, attenuation = 1.5 db/microsec delay.

The readout methods described below depend on the high coupling

possible through external coils (current coupling) or through external conducting

straps wrapped around the line (capacitative coupling). Both of these coupling schemes are possible due to the fact that the center conductor of the line is operated as the grounded conductor.

The efficiencies of these coupling methods are shown in Fig. 2. Fig. 2a shows the amplitude of the output signal for different rise times of current pulses and various numbers of turns in the coupling coils: Fig. 2b shows the corresponding curves for the capacitative coupling.

An important point to consider is the effect of the external coupling on the delay line characteristics, since we want to maintain an accuracy of timing of the pulses to within 1-1.5 nanoseconds. This loading effect is shown in Fig. 3 for both couplings; it is seen that the capacitative coupling intro- duces less dispersion and 'ringing' than the coil coupling. Since it is also considerably easier to construct mechanically and electrically, by wrapping plastic with conducting strips etched on it around the delay line, it is the method we prefer to use.

III. PROPORTIONAL CHAMBER MEASUREMENTS

Our measurements were done on chambers with three wire planes: a central plane consisting of wires 25 microns in diameter, spaced by 2 mm. which collected the electrons and whose field gradient produced the avalanches. The positive ion collecting planes were made of wires 100 microns in diameter, spaced by 2 mm. and with the wires oriented at 90° relative to those of the central plane. We collected signals from both the central and the outside planes. The arrangement we used is shown schematically in Fig. 4. For timing purposes we used a zero-cross [4] method.

The positioning accuracy attainable with this delay line depends on the following: (a) the amplitude of the signals above the noise level of the

electronics (b) the polarity and wire spacing of the plane which is being read-out. The zero-cross electronics will locate the pulse with a jitter of less than 1 nanosec for pulse amplitudes at the output of the delay line above 400 micro-volt. This corresponds to an output of 10-20 millivolts from the chamber wire. This amplitude is attainable with an Argon-Isobutane (70% Ar: 30% Isobutane) gas mixture with the total number of electrons pairs in the avalanche equal to $\approx 5 \times 10^6$.

The accuracy of spatial distribution depends on the polarity of the plane which is being readout due to the asymmetry in the signals induced on the electron collecting wires or on those that receive the displacement current due to the positive ions. Since the signal produced on the delay line is a composite of the signals from a number of wires adjacent to the source of ionization, interpolation between wires is possible if the amplitude of these pulses falls off monotonically with distance. Fig. 5 shows the electric lines of force. An ionizing event will produce an avalanche on wires a or b depending on whether it occurs in the region AA or AB. The position of the avalanche along the wire has a displacement error which is due mainly to diffusion of the electron trajectory due to scattering collisions in the gas. The displacement current signal induced on the positive ion collecting planes centers on the point perpendicularly opposite to the center of the avalanche, since due to the shape of lines of force there is no 'quantizing' effect.

Our measurements confirm this effect, as shown in Fig. 6, in which we plot the position of the ionizing event measured by the delay line, as a function of the position of a collimated source of 5.9 KeV γ-rays from Fe^{55}. The width of the error bars is the full width at half maximum of the distribution observed from the output of the P.H.A. This is due to source width distribution,

jitter in electronic timing and diffusion of the electrons in the gas. The difference in position accuracy and interpolation between the two planes is evident. A proportional chamber with this asymmetry is however quite useful in magnetic spectrometer experiments where the position of the particle trajectories in the plane perpendicular to the magnetic field of the deflecting magnet is usually required to the highest accuracy for the momentum determination.

If symmetry in positional accuracy in two coordinates is desired from one chamber the simplest method is to build it with the positive ion collecting planes oriented at $\pm 45^{\circ}$ relative to the central plane and which are then used for the readout.

The width of the signal pulse on the delay line, relative to the velocity of propagation determines the pulse pair resolution for two simultaneously occurring ionizing events. This is shown in Fig. 7. The results are obtained by simultaneously putting two signals on the delay line and then observing the arrival of the signals at one end of the line. The position of A is fixed and B is moved. The two dashed lines indicate the results which would be obtained for a single pulse at position A or B. Interference between the two pulses will cause the measurements to deviate from the straight lines. In the present setup the two pulse resolution is 30 mm., as can be seen from the figure. We are limited here by the simple zero-cross method of finding the pulse center. Measuring the leading edge of the pulse at each end of the delay line and a suitable coding method would improve the two pulse resolution.

IV. CONCLUSIONS

A delay line readout of the type described above has the advantages

over the individual amplifier per line scheme of greater simplicity and less

expense. It is also more accurate due to the ability to interpolate among wires.

The two track resolution as noted above is somewhat poorer, but can be improved.

We should also point out that electromagnetic delay lines of this

type can be used for reading out wire spark chambers in magnetic fields. The

signals from these chambers--current coupled or capacitatively coupled are large

enough so that very little amplification is needed.
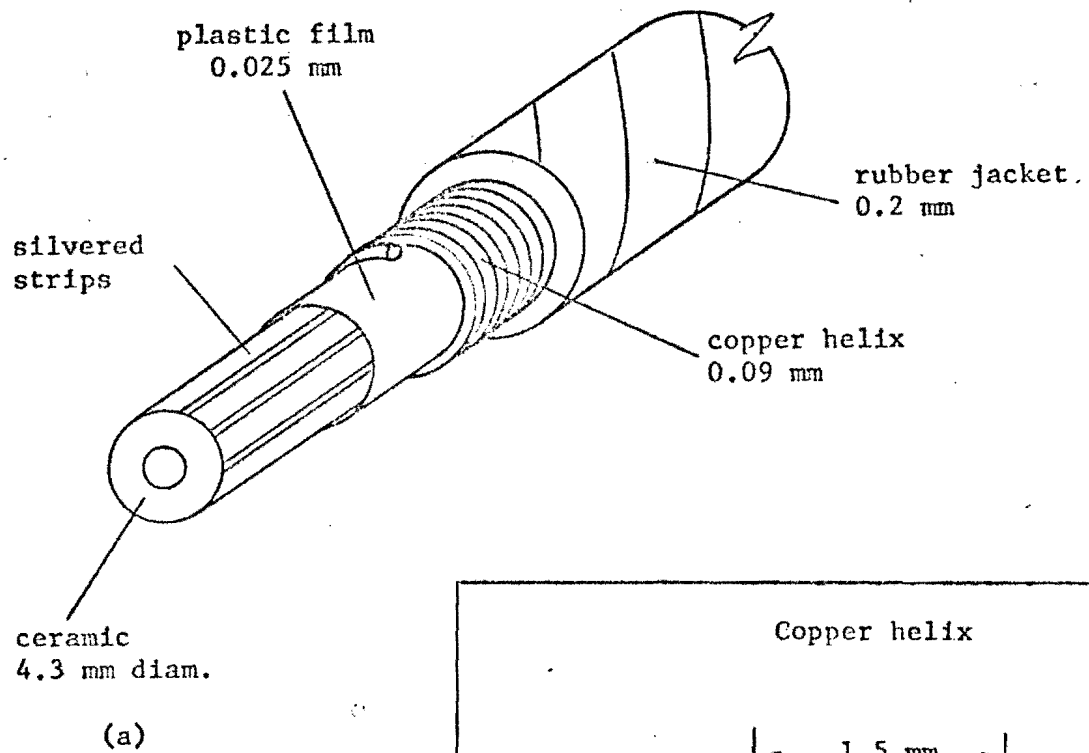
Acknowledgements

We would like to thank Ray Fuzesy and Herb Steiner for their help

and cooperation in constructing and lending us some of the chambers on which

these measurements were made.

FOOTNOTE AND REFERENCES

*   This work was done under the auspices of the U. S. Atomic Energy Commission.

1) A. Rindi, V. Perez-Mendez and R. T. Wallace, Nucl. Inst. and Methods $\underline{77}$ (1970) 325.

2) J. Blewett, Proc. IRE $\underline{35}$ (1947) 1580; W. J. Carley, Tele-Tech. and Electronic Industries $\underline{13}$ (1954) $\overline{74}$.

3) 'Mini Lines' manufactured by Columbia Technical Corp, 24-30 Brooklyn-Queens Express Way, West Woodside 77, New York.

4) We used type T140/N zero-cross discriminators manufactured by Edgerton, Germeshausen & Grier, Inc., 160 Brookline Ave., Boston, Mass., U.S.A.
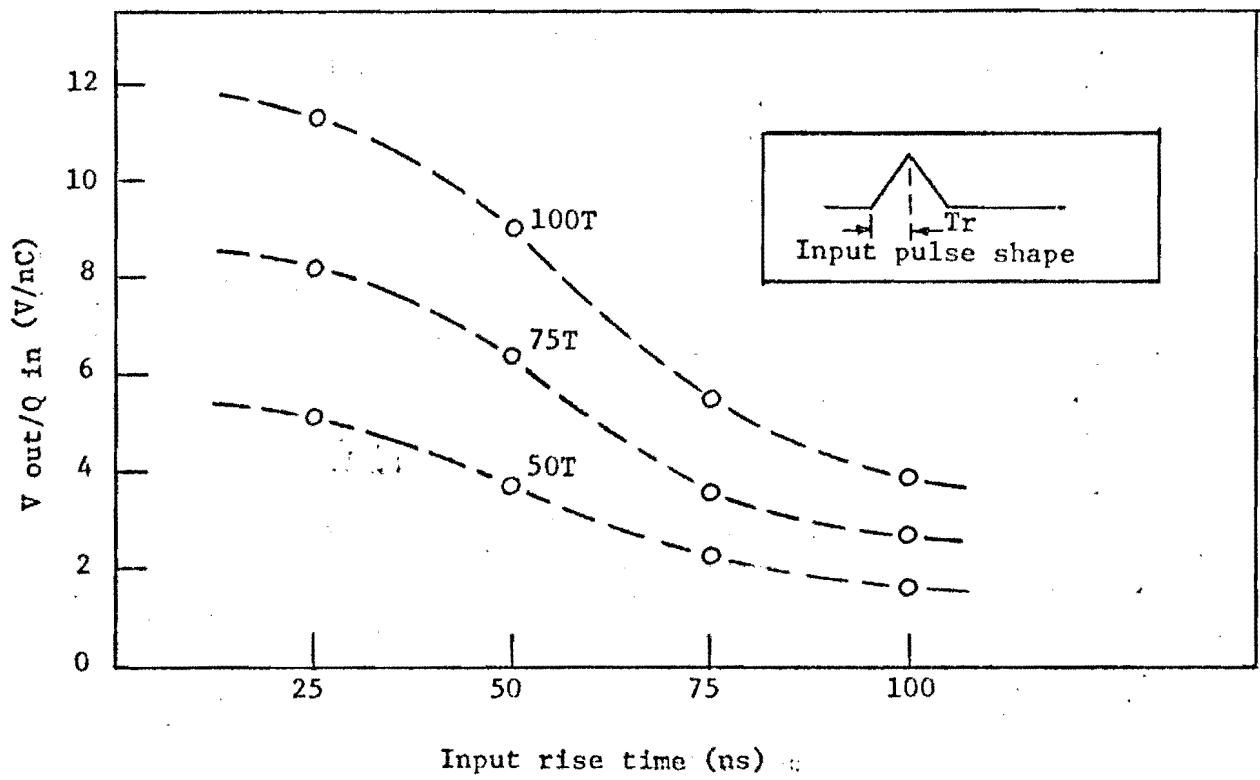
FIGURE LEGENDS

Fig. 1.   Perspective view of ceramic core delay line.

Fig. 2.   Efficiency of coupling from the chamber to the delay line as a
           function of the input pulse rise time for (a) coils of 50, 75 and
           100 turns and (b) copper straps 1 mm. and 2 mm. wide.

Fig. 3:   Loading effect of coupling on a 10 cm. delay line for (a) capacitative
           coupling and (b) coil coupling. The delay lines are loaded with coils
           or straps, one every two millimeters.

Fig. 4:   Block diagram of the electronics used for timing the pulse. The delay
           line is capacitatively coupled to the chamber and zero-cross dis-
           criminators are used to locate the center of the pulse.

Fig. 5:   Electric lines of force in the chamber in (a) the view normal to the
           central wires showing the origin of the quantizing effect and (b)
           the view parallel to the central wires. To make the lines of force
           in (b) as parallel as possible flat strips should be used for the
           negative plane.

Fig. 6:   Measurements of the position accuracy for locating ionizing events
           as read out by the delay line. Figure 6a shows the event location
           as a function of position when the delay line is connected to the
           electron collecting wires. Figure 6b shows a similar measurement
           with the event read out from the positive ion collecting plane.

Fig. 7:   Output pulse separation as a function of the input pulse separation.
           The dashed lines represent the measured position for a single pulse
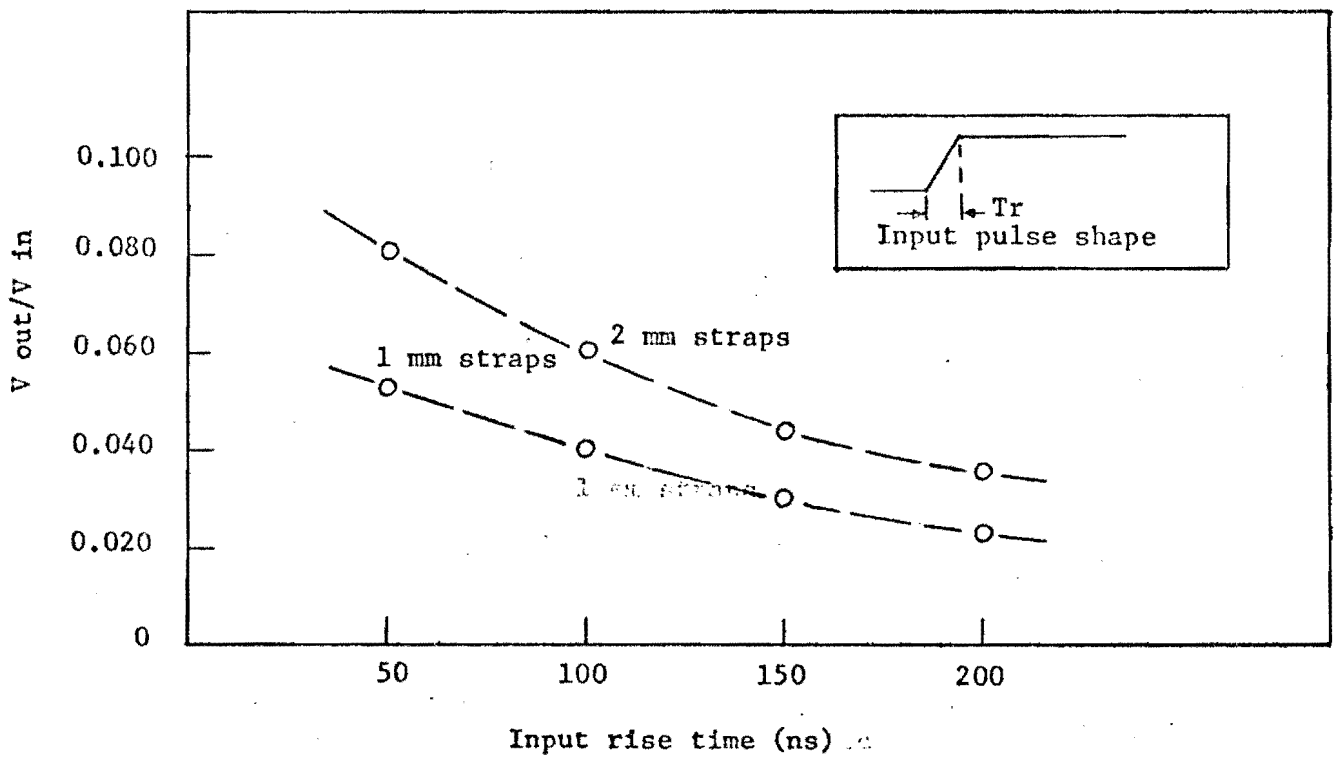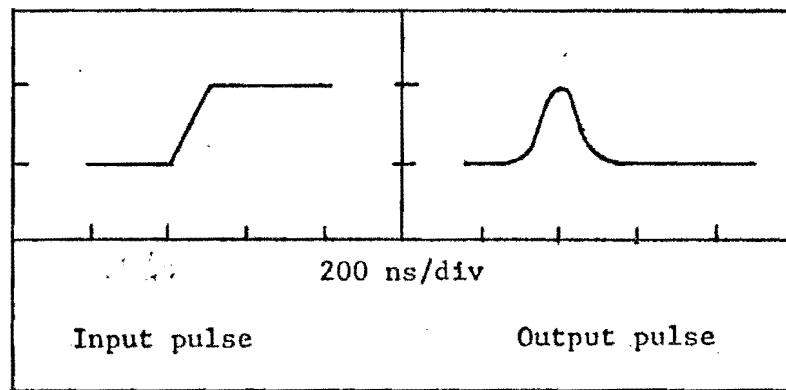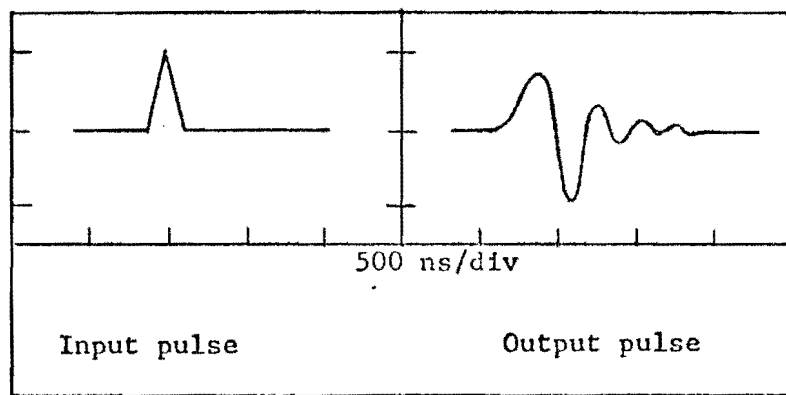   at A or B.

plastic film
0.025 mm

silvered
strips

ceramic
4.3 mm diam.

rubber jacket.
0.2 mm

copper helix
0.09 mm

(a)

Copper helix

1.5 mm

3.0 mm

(b)

Fig. 1

(a)

(b)

Fig. 2

200 ns/div

Input pulse   Output pulse

(a)

500 ns/div

Input pulse   Output pulse

(b)

Fig. 3

Fig. 4

central wires

negative plane

(a)
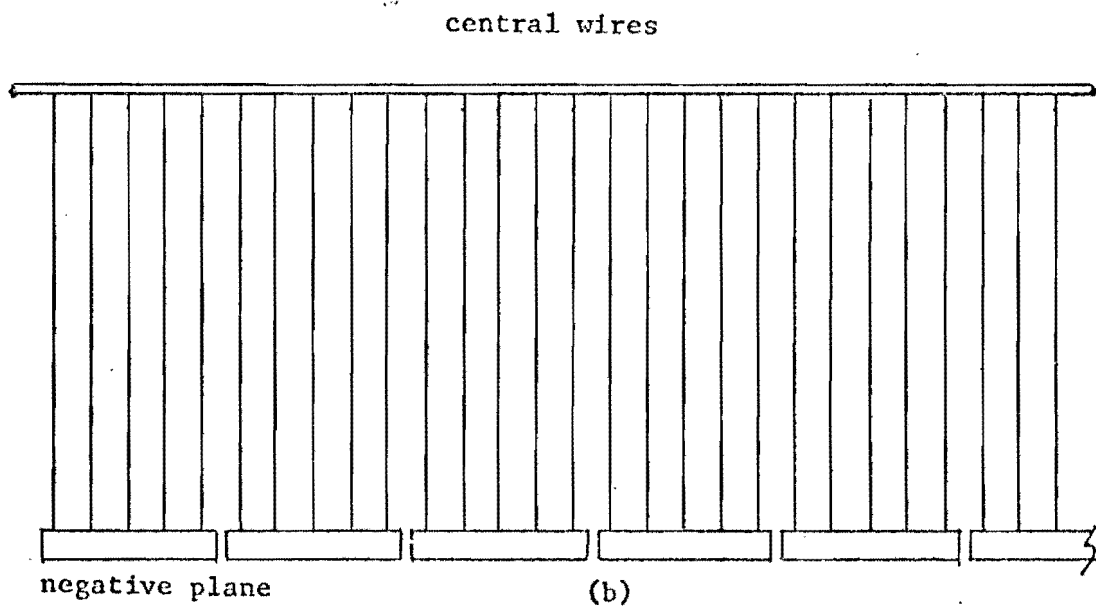
central wires

negative plane   (b)
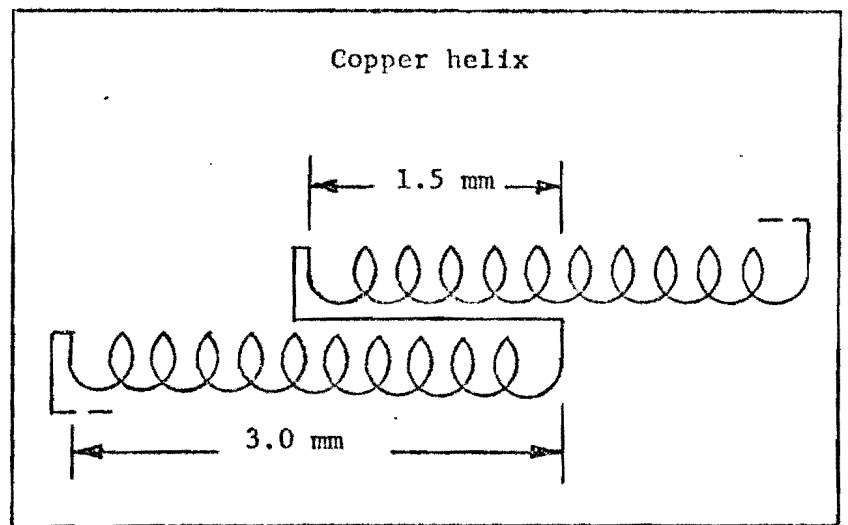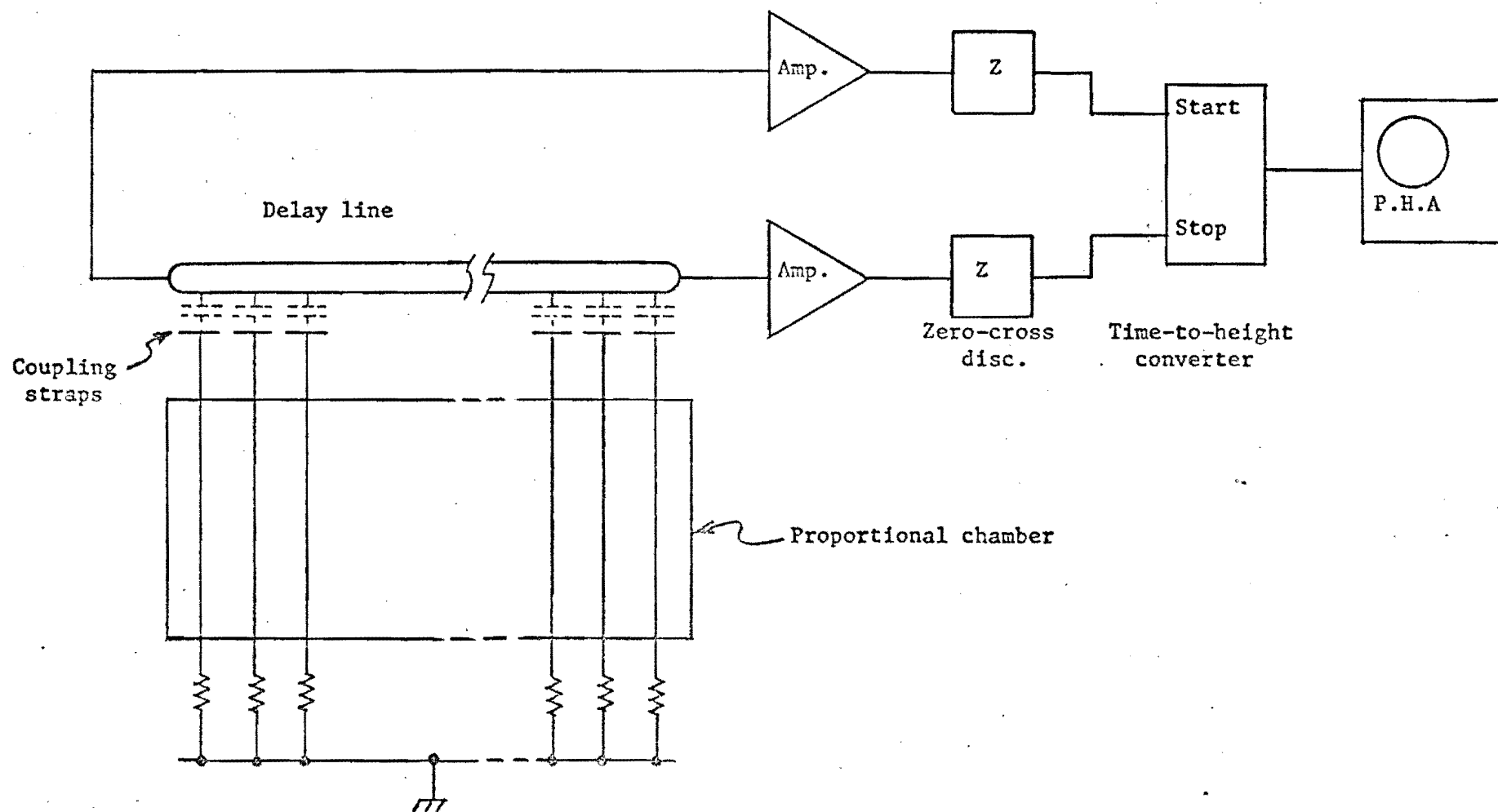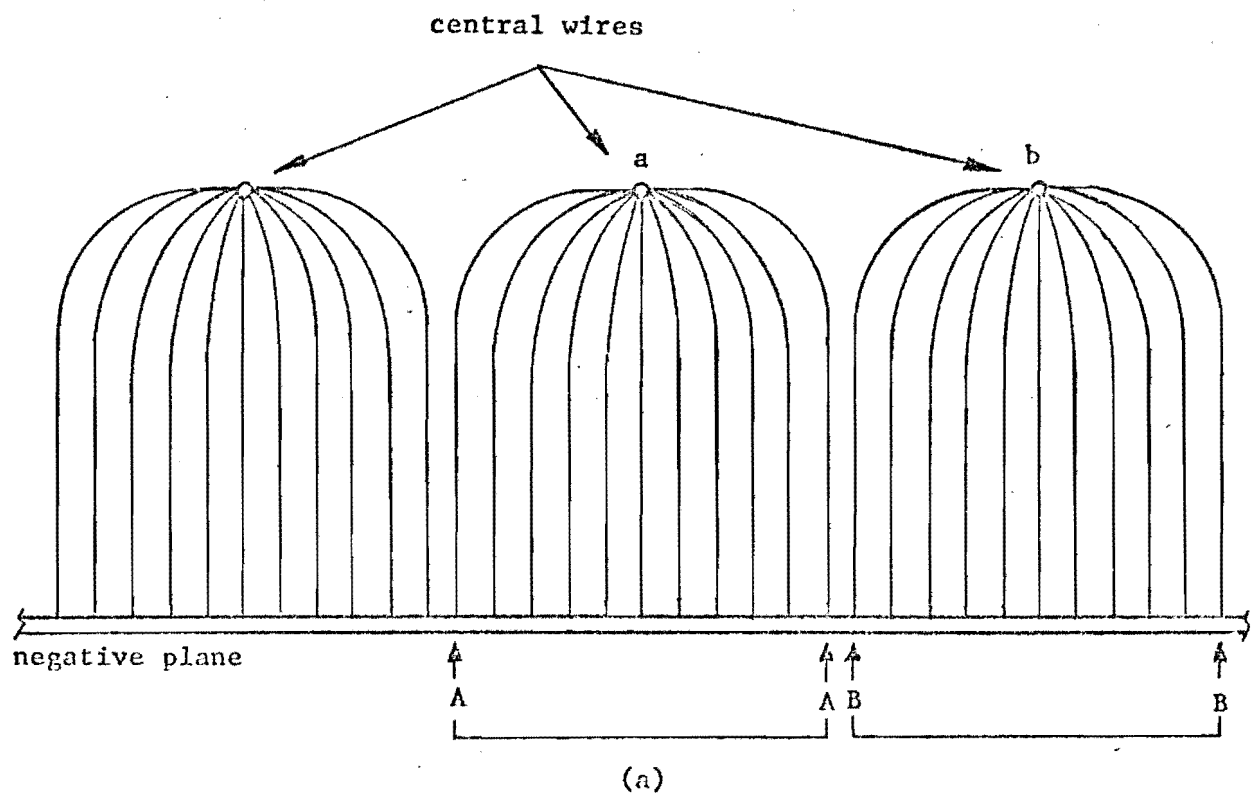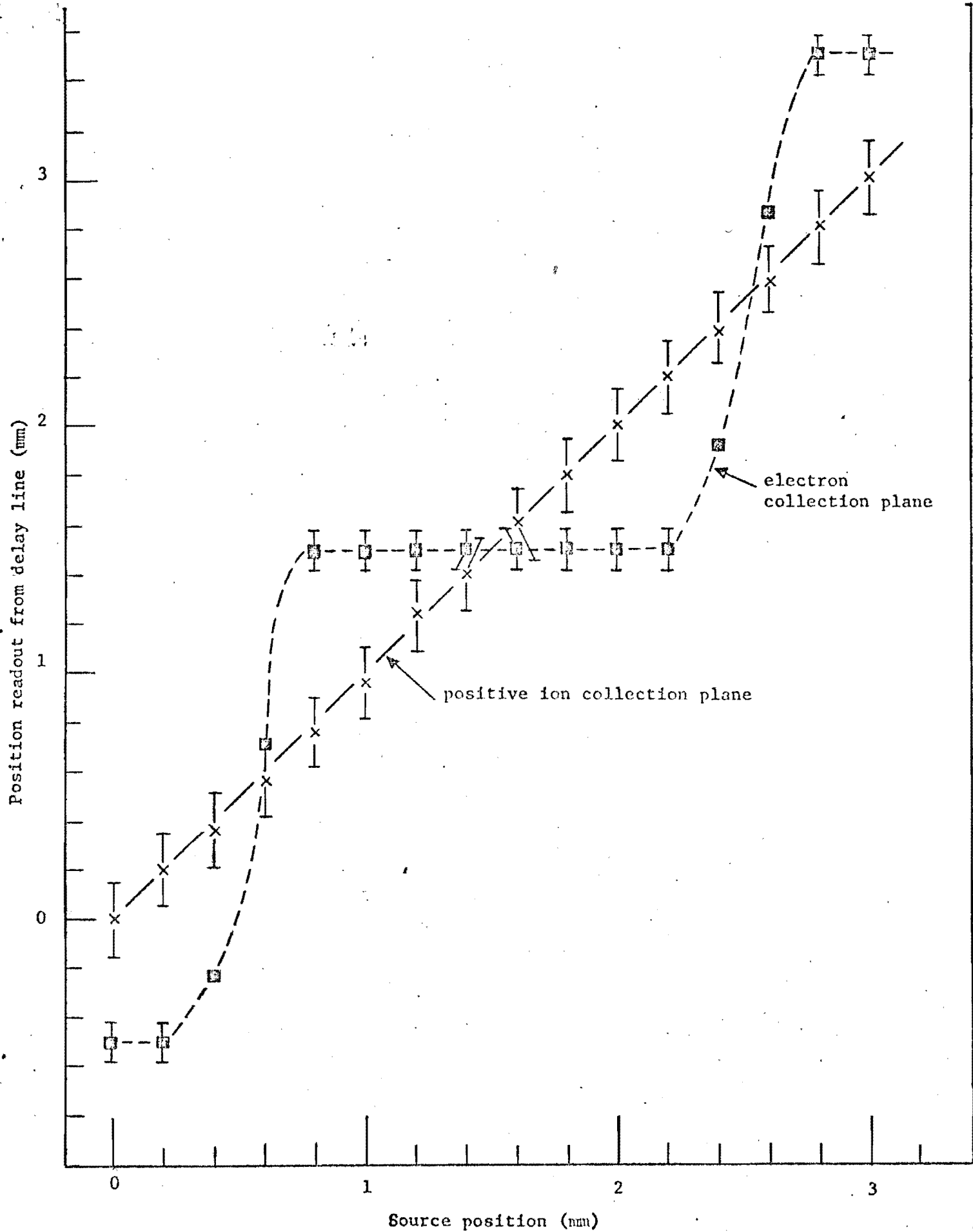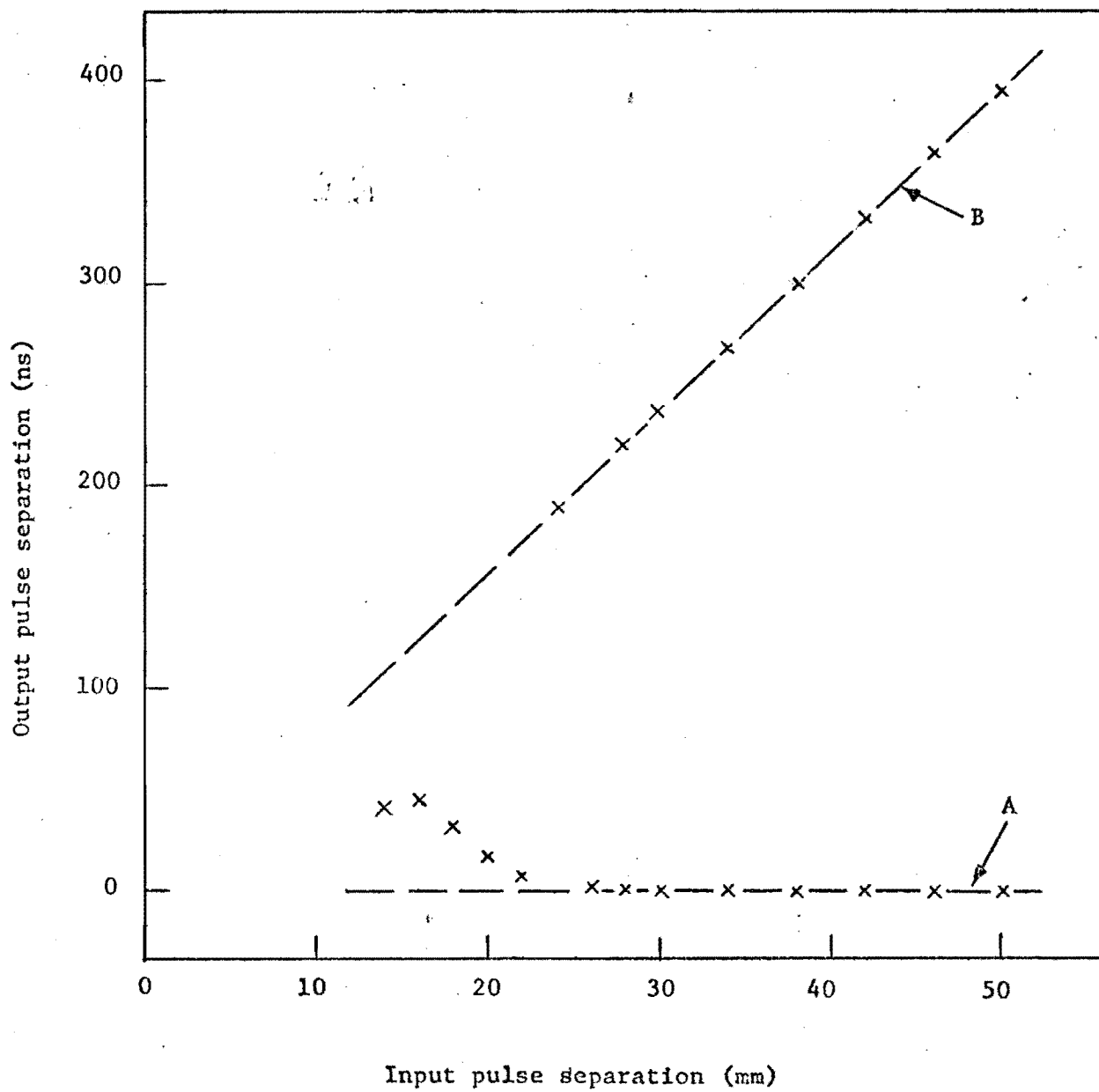
Fig. 5

Fig. 6

Fig. 7

Correspondent: M.L. Stevenson

University of California
Lawrence Berkeley Laboratory
Berkeley, California 94720
Telephone: FTS 18-415-843-2740 Ext. 6301

PROPOSAL TO STUDY <u>ANTI</u> NEUTRINO INTERACTIONS IN THE

30 m^3 NAL BUBBLE CHAMBER WITH THE PHASE I EXTERNAL MUON IDENTIFIER

R.J. Cence, F.A. Harris, S.I. Parker, M.W. Peters
V.Z. Peterson, V.J. Stenger
University of Hawaii

A. Barbarro-Galtieri, G.R. Lynch, J.P. Marriner,
F.T. Solmitz, M.L. Stevenson
University of California
Lawrence Berkeley Laboratory

October 3, 1974

SUMMARY

We will have analyzed approximately 2500 neutrino interactions by the time the 50,000 pictures test of the Phase I External Muon Identifier (EMI) is completed (E-155). We are now requesting 300,000 pictures of the 15 foot-hybrid*-bubble chamber, filled with hydrogen and exposed to a wide band anti neutrino beam, in order to obtain a comparable number of anti neutrino interactions. We request that at least 50,000 of these anti neutrino pictures be taken during the April-May 1975 run sequence. By that time we will have analyzed 200 neutrino interactions from the copied portion of Experiment 45A film   and, hopefully, 500 additional events from the 10,000 picture portion of the above mentioned test sample that we are requesting from the October-November 1974 run sequence. In this way we will make an early comparison of the hadronic final states for neutrinos and anti neutrinos on hydrogen using the wide band beam. This was the original spirit of the deferred portion of our physics proposal 9B (9 July 71) which called for 50,000 wide band events.

Most of the physics arguments and how the kinematics of anti neutrino interactions place constraints on the detectors are contained in that proposal. The first three figures of that proposal are reproduced here. The first summarizes the kinematics, the second shows pictorial momentum vector diagrams to give some idea of what a 20 GeV neutrino interaction might look like. The Landau thermodynamic model[3] was used as a "worst-case" estimate of hadron multiplicity. The third figure summarizes how the muons are bent by the magnetic field and shows why we wanted to place the EMI proportional chambers at 90° azimuth to the neutrino direction.

---

* With External Muon Identifier. (See reference 2)

Physics Justification

The main purpose of the experiment is to supplement the information that has been obtained by the two counter neutrino experiments,[1] namely to provide detailed information about the hadronic state of <u>anti</u> neutrino interactions. Muon identification is crucial to a clear understanding. The geometrical efficiency of the EMI is greater for <u>anti</u> neutrinos because more of their muons go forward. (See Figs 1 & 3.) Furthermore, any neutrino contamination in the <u>anti</u> neutrino beam can be more readily dealt with if one employs the EMI.

A.   Charged lepton current

1.   Although, the neutrino energy is low ($\lesssim 50$ GeV) we will search for jet-like structure of the "dressed up" recoiling parton and observe how the charge-momentum distribution compares with the corresponding neutrino induced state. It is very important in this analysis to know the direction of the momentum transfer vector. Unless the muon is identified and neutral current events removed from the sample, errors will be introduced into the analysis. (See Fig. 2)

2.   The known $(1-y)^2$ dependence of the anti neutrino charged lepton current cross section makes anti neutrinos very useful for searching for the production of rare, massive hadronic states. From Fig. 1, which shows lines of constant hadron invariant mass W, one observes that thresholds for massive hadronic states occur at large y and small x ($\equiv Q^2/2M\nu$) where a paucity of events occurs. Fig. 4 shows, approximately, how the 2500 events will distribute themselves in the x, y space. Here, for simplicity, we have used $\nu W_2 \propto 1-x$. Charmed particles, if they exist, are expected to have leptonic decay modes. Here, again the EMI is useful for detecting its muonic decay mode.

3. Observation of the relative rates of $\Delta S = \Delta Q$ and $\Delta S = 0$ reactions à la Cabibbo, where the final state baryon systems may not be in the same SU(3) multiplet as the proton. For example,

$$\bar{\nu} + p \rightarrow \mu^+ + \left[\Sigma^{0*}_{(1385)} \rightarrow \begin{matrix} \Lambda \pi \\ \Sigma \pi \end{matrix} \right] \,, \; \Delta S = \Delta Q$$

$$\bar{\nu} + p \rightarrow \mu^+ + \left[\Delta^0 (1235) \rightarrow N \pi \right] \,, \; \Delta S = 0$$

Here, there is a greater chance for misidentifying the muon than when the baryons are in the same multiplet as the proton. The EMI will eliminate the ambiguity.

4. Test of Adler's relation,

$$\lim_{E_\nu \rightarrow \infty} \frac{d\sigma (\bar{\nu} p)}{dQ^2} - \frac{d\sigma (\nu p)}{dQ^2} = \frac{G^2}{\pi} \left(\cos^2 \theta_c + 2 \sin^2 \theta_c \right)$$

B. Neutral lepton current.

1. Although the neutral lepton current events can be identified in approximately 20 or 30% of the cases we have little chance of being able to determine x and y for them because of our inability to measure the energy-momentum of the neutral portion of the hadronic state. We will, however, try to extract the maximum amount of information from the charged portion. We are submitting a separate proposal to use the EMI with a light mixture of Ne in the hydrogen bubble chamber so as to be able to measure x and y.

2. Neutron background studies are crucial to an ultimate understanding of neutral current physics. We intend to search for <u>anti</u> neutrino interactions in the surrounding super conducting coils where the associated neutron interacts in the bubble chamber. From this we will be able to estimate the neutron background .

C. <u>Possible Surprising Physics</u>

With a detector system that maximizes particle identification, one is best able to detect unusual processes.

Apparatus Needed

A.   15' -- Hydrogen filled bubble chamber.

B.   External Muon Identifier.

       The twenty-five $1m^2$ - multiwire proportional chambers (MWPC) envelope the downstream portion of the 22' diameter vacuum tank. Fig. 5 summarizes the geometrical coverage of the 22 MWPC's used during the July-Aug 74 run of E45A. It shows the vertical and azimuthal coverage as viewed by an observer at the center of the bubble chamber. The plotted points are the predicted hit positions in the MWPC of incoming regenerated muons (from the berm and earth shield) that traverse the visible volume of the bubble chamber. Fig. 6 shows the deviation of the measured position in the EMI from the predicted one.[2] The RMS deviation is very nearly that expected from multiple scattering in the four inter-action lengths absorber between the bubble chamber body and the MWPC's. More than 80 percent[†] of the observed hits fall within the "96% circle" centered at the predicted point. Less than two percent of these incoming tracks interact;consequently, they are mostly muons. Details of this earlier run (400 GeV triplet load) are given in TM513.[2]

C.   Neutrino Beam Monitoring Equipment.

D.   We would like to assist Experiment 31A   (Derrick) in determining the effectiveness of the plug that is likely to be first installed for the April-May 75 run. We plan to operate the EMI during a reasonable fraction of E-31A's exposure in Oct-Nov 74.

E.   Scan Projector suitable for monitoring the quality of the bubble chamber pictures from the test strips.

[†] Some of the beam spill was known to be out of time with the EMI gate during this early run.

Scope of the Experiment

1. 50,000 of 300,000 <u>anti</u> neutrino pictures to be taken during the April-May 1975 run sequence.

2. The remaining 250,000 pictures to be acquired as the schedule permits.

3. At this early stage of bubble chamber operation we shall assume that 30,000 pictures can be accumulated per <u>week</u>. The first 50,000 pictures will take about two weeks, and the remaining 250,000 another eight weeks.

4. Very little testing of equipment is required. We assume implicitly that all beams that are capable of producing neutron or charged background in the bubble chamber will have their spill times <u>not</u> during the bubble chamber sensitive time.

REFERENCES

1. NAL Experiment 21, California Institute of Technology - NAL Group. NAL Experiment 1A, Harvard-Pennsylvania-Wisconsin Group.

2. "Matching 'Muon' Tracks in The 15' Bubble Chamber To The EMI Proportional Chambers", University of Hawaii-LBL Group; Experiment 155, TM-513 (10 October 1974).

   "Surveying The External Muon Identifier and The 15' Bubble Chamber With 250 GeV Mesons", TM-509 (16 July 1974), University of Hawaii-LBL Group.

   Complete details of the construction and electronics of the MWPC's and an early test of muon identification are found in the following references:

   a) NAL Proposal 155, "Development and Test of an External Muon Identifier for the 30 m^3 Bubble Chamber", R.J.Cence, F.A.Harris, S.I.Parker, M.W.Peters, V.Z.Peterson, V.J.Stenger, D.E.Yount; (UH) A.Barbarro-Galtieri, J.P.Marriner, F.T.Solmitz, M.L.Stevenson; (LBL) V.Z.Peterson, Proceedings of 1973 International Conference on Instrumentation for High Energy Physics at Frascati, Italy; "Hybrid Bubble Chamber Detection of Neutrino Events - The External Muon Identifier".

   b) "Muon Identification Using Multiwire Proportional Chamber", F.A.Harris, S.I.Parker, V.Z.Peterson, D.E.Yount, M.L.Stevenson; Nuclear Instruments and Methods 103, 345 (1972).
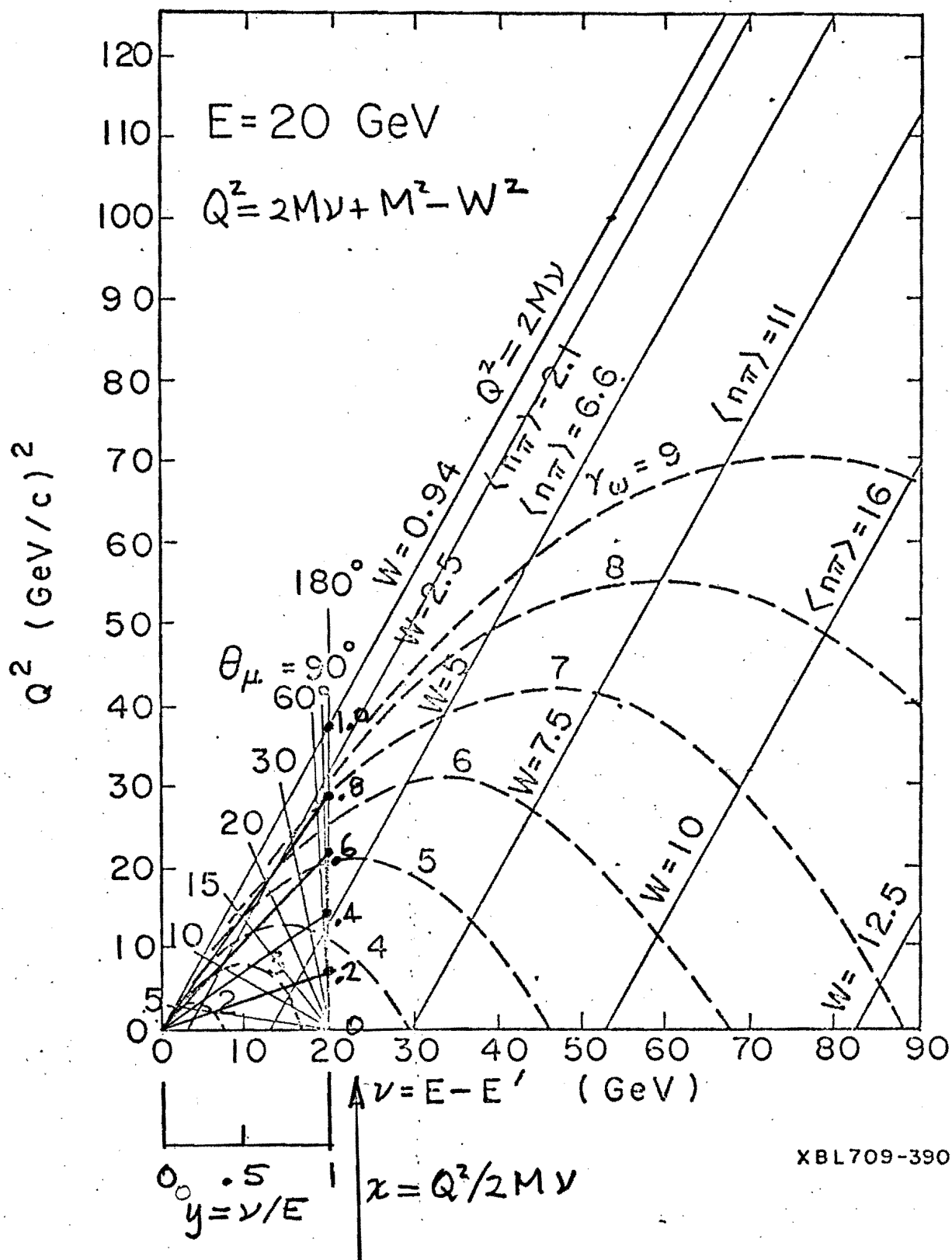
c) "EMI Development - Half Meter Proportional Chamber Test
    Results", S.I.Parker and R.Jones, NAL TM-359, LBL 797,
    UH-511-122-72.

d) "Digitizing Electronics for the EMI Multiwire Propor-
    tional Chambers", E.Binnall, F.Kirsten, K.Lee and
    C.Nunnally, NAL TM-360, LBL 798.

3) For a recent discussion of this model see J.D.Bjorken and
    B.L.Ioffe "Annihilation of e^+e^- into Hadrons" SLAC-PUB-1467
    (T/E) August 1974. (To be published in Izv. Acad. Nauk,
    SSSR, Ser. Fiz.)

FIGURE CAPTIONS

Figure 1. The kinematics of inelastic lepton scattering are
summarized here. The solid lines radiating from
$Q^2=0$, $\nu(=\nu_{max}=E)$ are loci of equal final lepton
scattering angle. The parallel solid lines are loci
of equal invariant final state hadron mass. They
also show "worst case" predictions of hadron multi-
plicity. The radial line originating at $Q^2=0$,
$\nu=0$ are loci of constant $x(=Q^2/2M\nu)$. The dashed
curves are loci of constant Lorentz factors, γ_W
of the hadron system.

Figure 2. Typical momentum vector diagrams for various regions
in the x, y space are shown. The opening angles of
the cones are typical of those expected of the
Landau Thermodynamical model. A jet-like model
would predict opening angles and multiplicities much
smaller than these.

Figure 3. Typical Muon Trajectories in the 30 kG field of the
15' chamber are shown. The two solid curves for each
(x,y) are the extremes for muons produced in the
equatorial plane. The dashed curve is that for a
muon emitted with its extreme dip value.

Figure 4. This figure shows approximately how the 2500 anti
neutrino events will populate the x,y space.

Figure 5. The azimuthal and vertical coverage of the EMI, as
viewed by an observer at the center of the bubble

chamber, is summarized here. It also shows where regenerated muons (from the rear portion of the 1000 meter earth shield) are predicted by the bubble chamber measurements to strike the EMI.
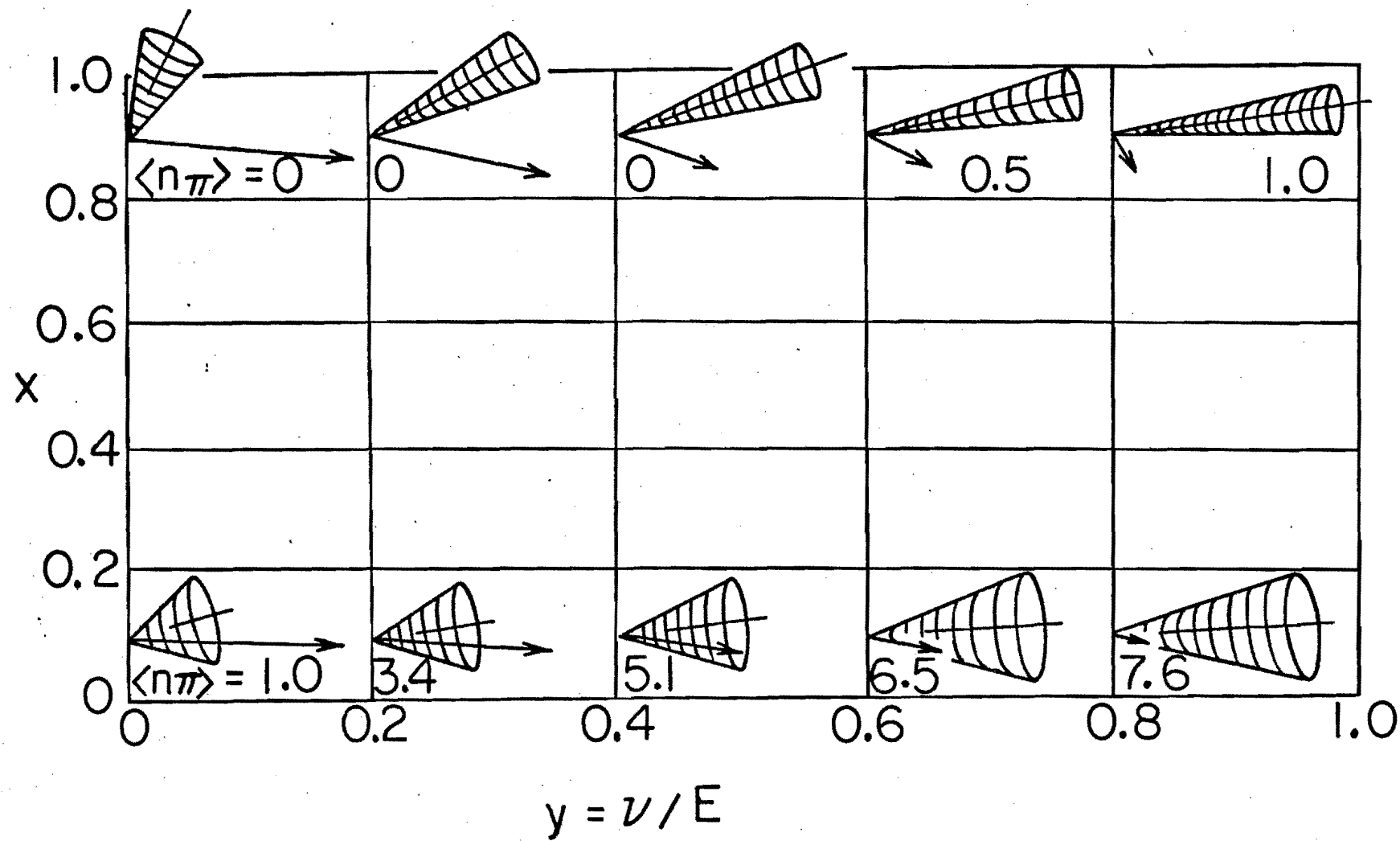
Figure 6. Summary of the deviation of the measured position of muons in the EMI from the predicted position using the bubble chamber picture. x is horizontal and y is vertical.

FIG. 1

E = 20 GeV

FIG. 2

XBL709 - 3896
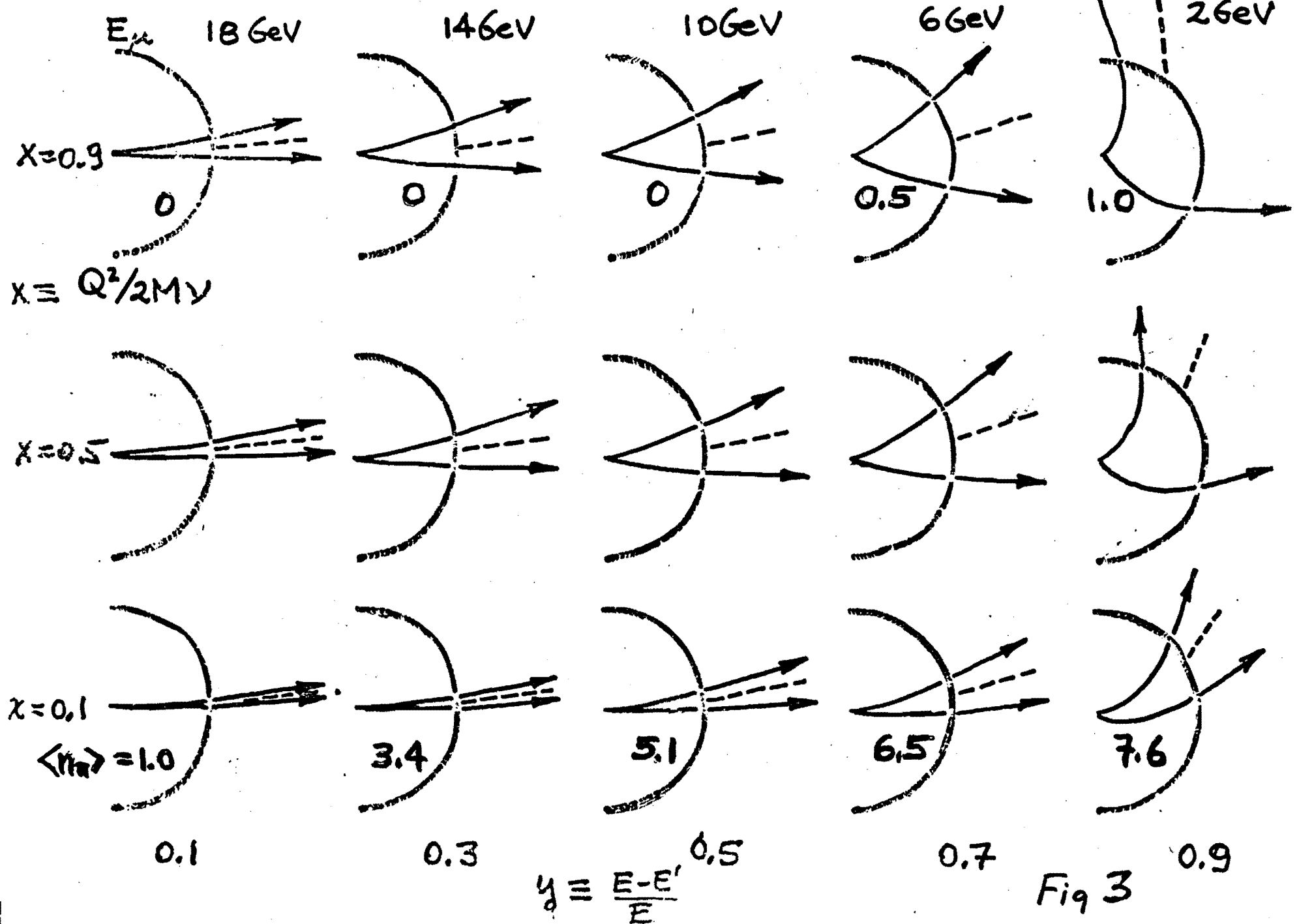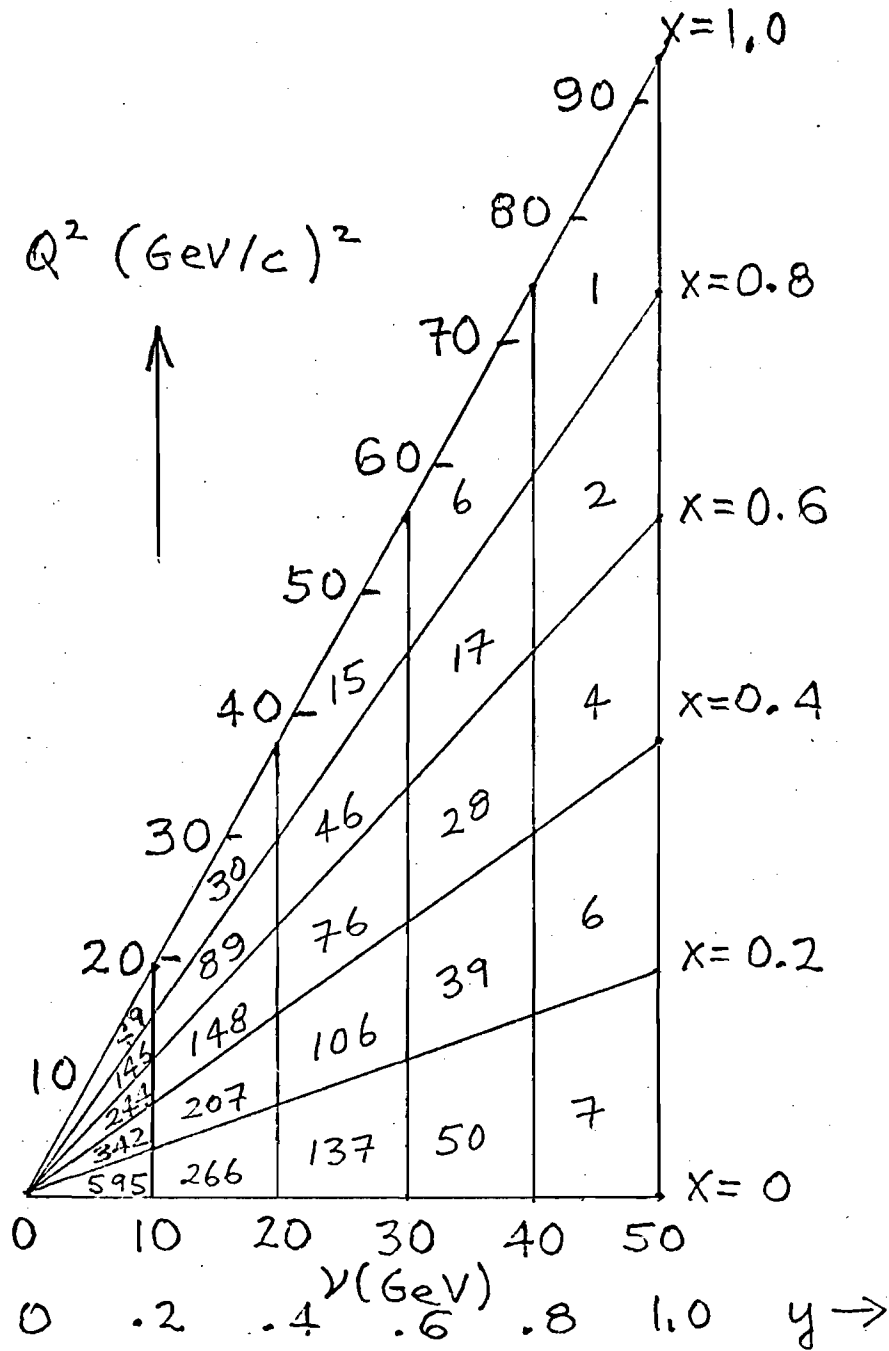
Muon Trajectories

Fig 3

$E' = 20$ GeV

E_μ 18 GeV   14 GeV   10 GeV   6 GeV   2 GeV

$x = 0.9$ 0   0   0   0.5   1.0

$x \equiv Q^2/2M\nu$

$x = 0.5$

$x = 0.1$

$\langle n_{ch} \rangle = 1.0$ 3.4   5.1   6.5   7.6

0.1   0.3   0.5   0.7   0.9
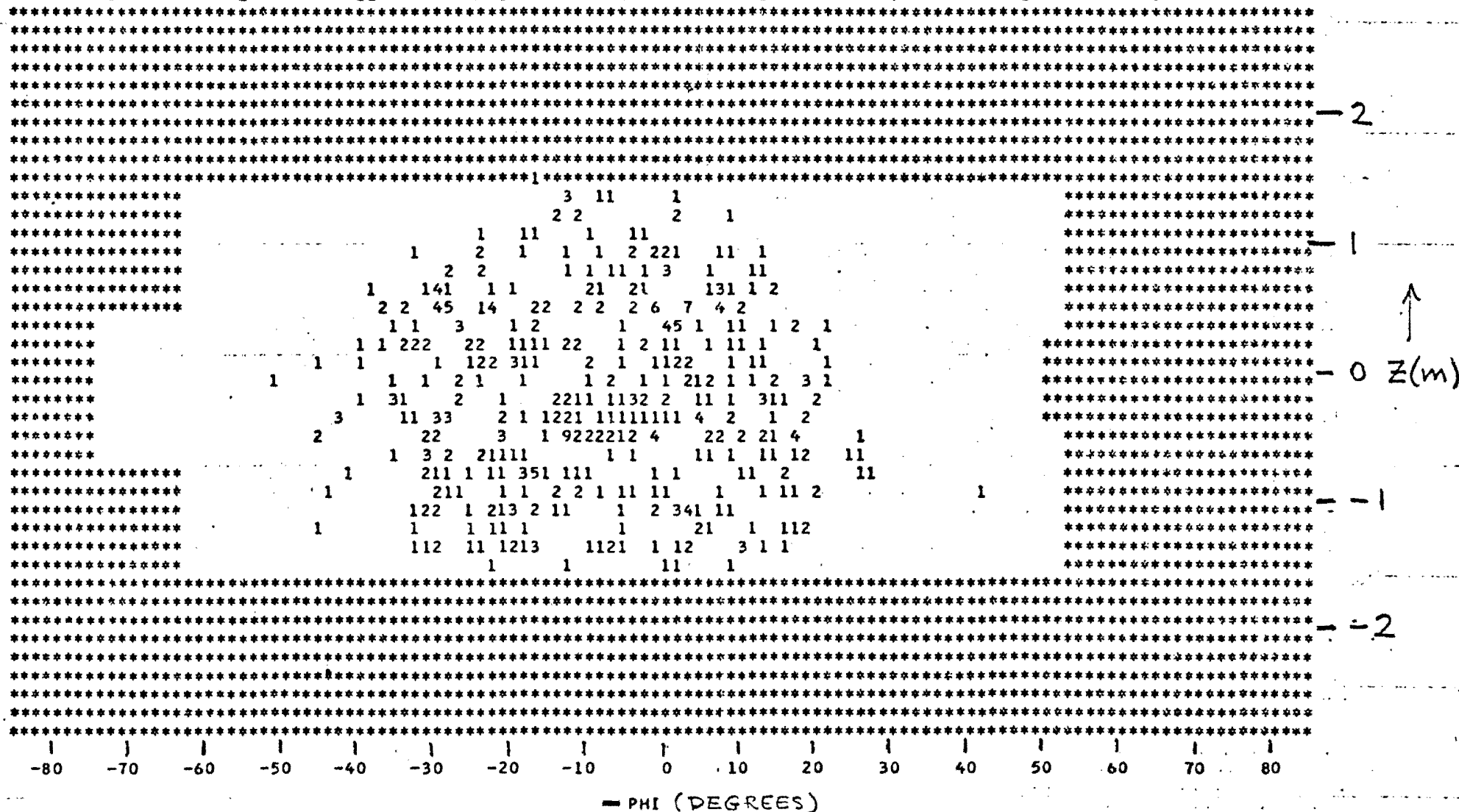
$y \equiv \dfrac{E - E'}{E}$

Distribution of 2500 events

$$\frac{d^2\sigma}{dx\,dy} \approx \frac{G^2 ME}{\pi} \frac{Q^2}{2\pi}(1-x)\left\{ \sigma_L + (1-y)\sigma_S + (1-y)^2\sigma_R \right\}$$

with $\underline{\sigma_L = \sigma_S = 0}$. $\sigma_{L,S,R}$ ARE HELICITY CROSS SECTIONS

Fig 4

CHAMBER NUMBERS

0	25	20	9	17	21	19	18	0
16	14	4	22	2	15	3	23	0
0	11	8	5	10	7	13	12	0

NUMBER OF HITS

| $|p| > 5 \text{GeV}/c$

0	0	10	26	46	20	0	0	0
0	4	31	48	68	47	11	0	0
0	2	22	61	49	41	9	1	0

(Scatter plot: Z(m) vertical axis from −2 to 2, PHI (DEGREES) horizontal axis from −80 to 80)

— PHI (DEGREES)

AT END OF INPUT TAPE READING, ELAPSED CP TIME IS   84.463 SEC.

Fig 5

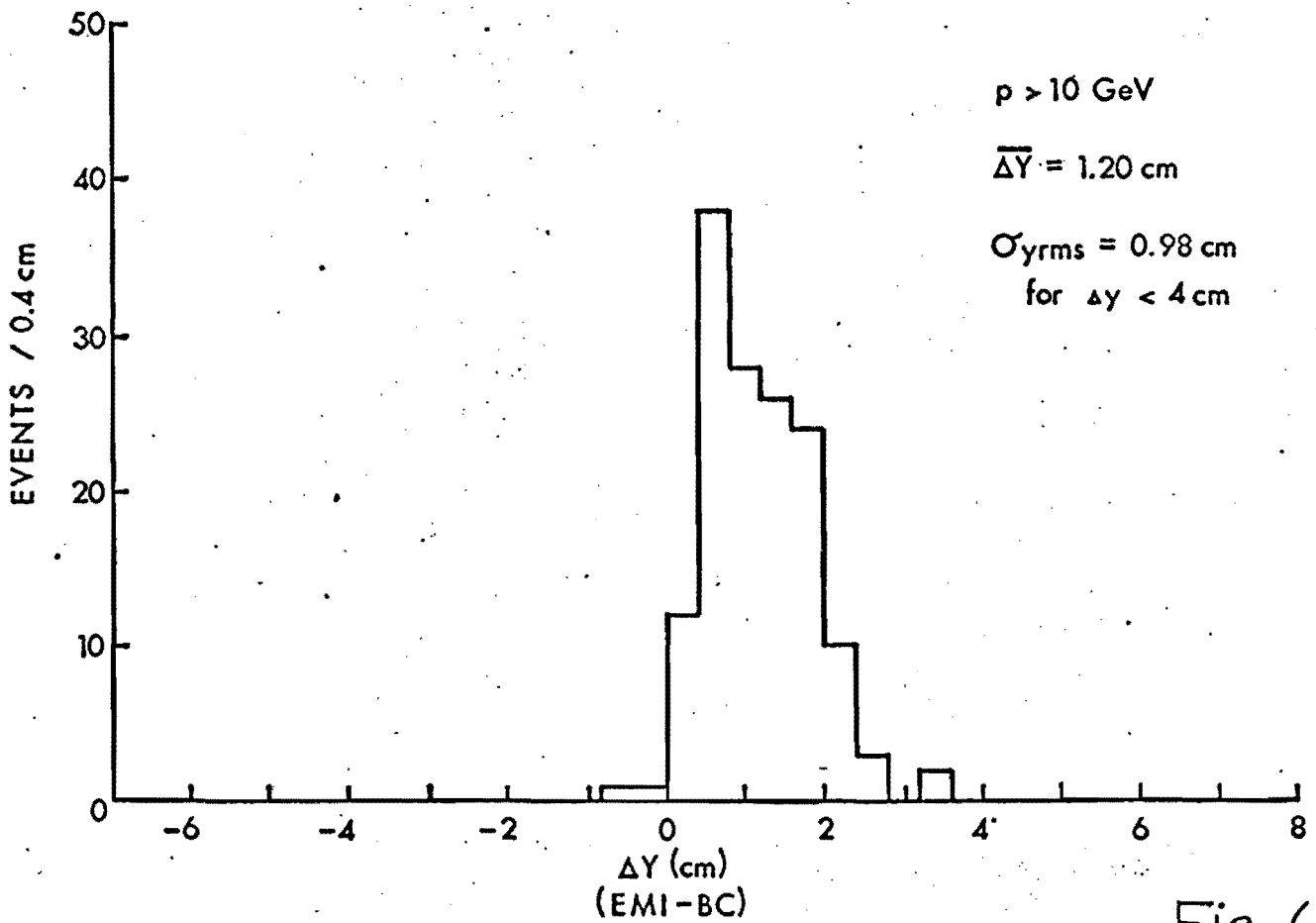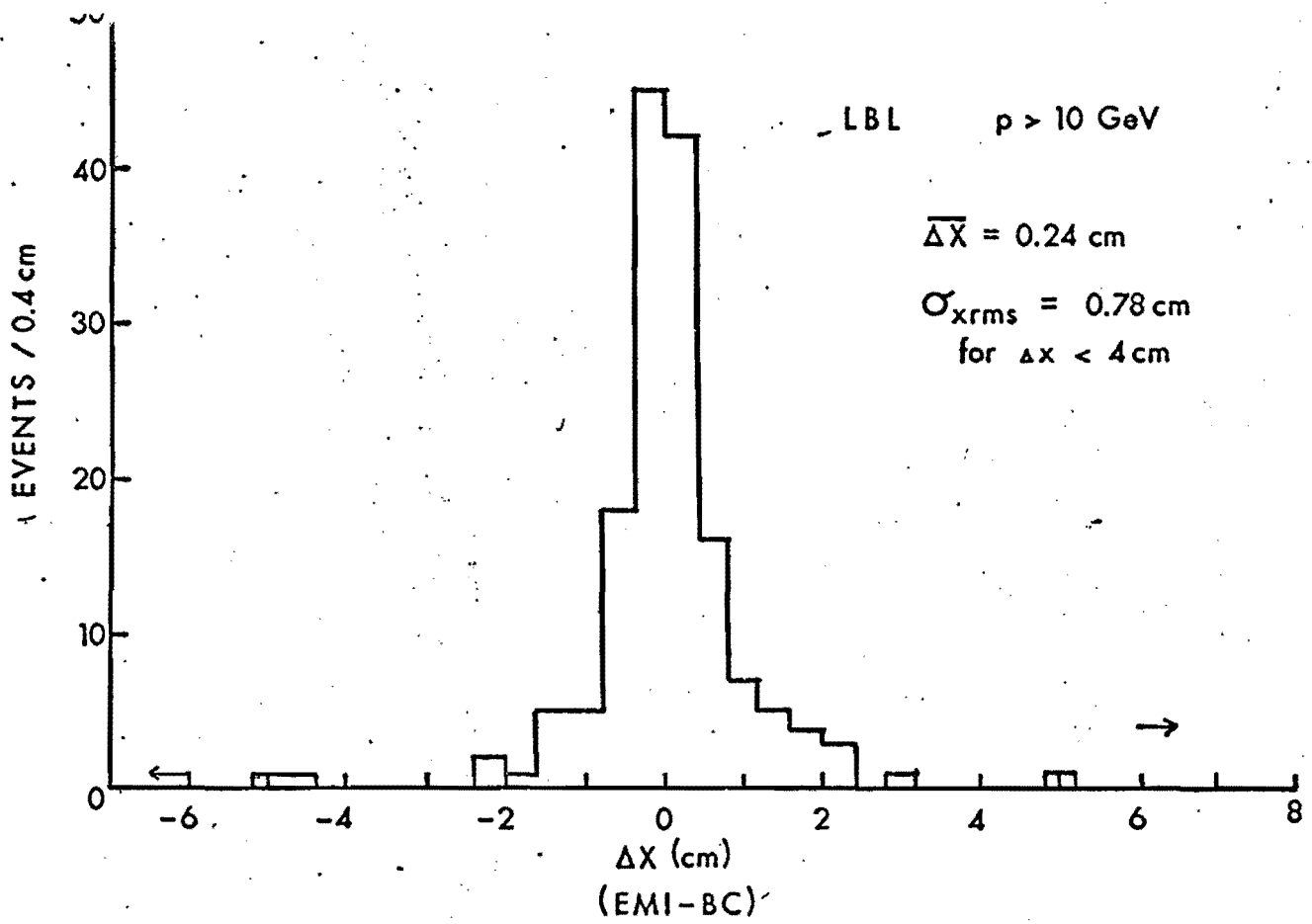END OF DATA INPUT PHASE. KIOWA HAS PROCESSED A TOTAL OF   492 EVENTS FROM GETUM.1

LBL   p > 10 GeV

$\overline{\Delta X}$ = 0.24 cm

σ_{xrms} = 0.78 cm
for Δx < 4 cm

p > 10 GeV

$\overline{\Delta Y}$ = 1.20 cm

σ_{yrms} = 0.98 cm
for Δy < 4 cm

Fig. 6

Figure 3a